Late Cretaceous seasonal palaeoclimatology and diatom palaeoecology from laminated sediments.

Full reference: Davies, A. & Kemp, A. E. S. (2016) Late Cretaceous seasonal palaeoclimatology and diatom palaeoecology from laminated sediments. Cretaceous Research 65, 82-111.

Andrew Davies[1]
Alan E S Kemp (corresponding author)

National Oceanography Centre, Southampton,
University of Southampton
European Way
SO14 3ZH
UK
Tel: 02380592788
Email: aesk@noc.soton.ac.uk

1 present address:
Halliburton,
97 Jubilee Avenue
Milton Park
Abingdon
Oxfordshire
OX14 4RW
Tel: 01235 443601
Email: Andrew.Davies@halliburton.com

Accepted for publication: 24th April 2016
Available online: 30th April 2016
Final version published online: 10th May 2016
Full bibliographic details: Cretaceous Research 65, (2016), pp. 82-111
DOI: 10.1016/j.cretres.2016.04.014

ABSTRACT

Laminated diatom-rich marine sediments from California and the Arctic Ocean provide a window into the seasonal climate and oceanography of the mid- and high-latitude Late Cretaceous. These remarkable shallow-buried sediments constitute palaeo-sediment traps that record exceptionally well-preserved sequential biogenic and lithogenic flux events. Many of the diatom laminae are composed of a few dominant taxa, and we use a species-based approach for palaeoecological interpretation. Contrary to many earlier interpretations, results indicate that both sites preserve a major flux of taxa adapted to exploit a strongly stratified ocean. The uppermost Maastrichtian Marca Shale of California records a seasonal cycle initiated with a spring bloom flux of diatom resting spores followed by a summer lithogenic sediment input likely driven by monsoonal storms providing river runoff and aeolian input. This is followed by a dominant diatom flux of species that thrived in the summer stratification in deep chlorophyll maxima and were sedimented in the fall when this stratification broke down. Dominant taxa comprising this group include *Hemiaulus*, *Stephanopyxis*, *Stellarima* and *Rhizosolenia*. The uppermost Campanian CESAR 6 core from the Arctic Alpha Ridge, records a spring bloom flux of resting spores followed by a more dominant summer and fall flux of diatom vegetative cells which were likely concentrated in subsurface summer blooms that generated a “summer export pulse” and by the breakdown of stratification in the fall that gave massive flux of deep chlorophyll maxima species in the fall dump. The dominance and diversity of *Hemiaulus* in the CESAR 6 core together with widespread evidence of N_2-fixation may indicate that some diatom blooms were powered by intracellular N_2-fixing cyanobacteria as in the modern oligotrophic ocean. Thin lenses of fine lithogenic sediment that occur mostly in the spring layer represent rafting by winter sea ice and support other evidence that suggests intermittent winter freezing in the Late Cretaceous Arctic.

Keywords: Late Cretaceous; Diatom blooms; Paleoecology; California; Arctic; Sea Ice

1. Introduction

Laminated pelagic and hemipelagic marine sediments often constitute "palaeo-sediment traps" that preserve sequential flux events from which the ancient seasonal flux cycle may be reconstructed. They commonly preserve both the biogenic flux events from surface ocean productivity and also the terrigenous sediment input common in hemipelagic or marginal settings. Within rare, exceptionally well-preserved Cretaceous sediments, fossil diatom algae record the seasonal cycle of marine production and flux to the sea bed. In the modern ocean diatom algae are the dominant, bloom-forming phytoplankton in many environments and are key players in the marine biological carbon pump. The relative contribution of diatoms to total primary production has been estimated to range from 35% in the oligotrophic oceans to 75% in the coastal zone and in the Antarctic (Nelson et al., 1995), while their contribution to export production (the downward flux of organic carbon from the euphotic zone) is proportionately even greater, due to their propensity for rapid sinking (Smetacek, 1999; Smetacek, 2000; Agusti et al., 2015). Ecological studies of diatoms, developed primarily from the coastal zone, have conventionally associated diatom blooms and subsequent export with the spring bloom or with upwelling environments (Guillard and Kilham, 1978; Margalef, 1978). Palaeoenvironmental interpretations have commonly followed this maxim and ascribed an upwelling origin to ancient diatomaceous sediment (Kitchell and Clark, 1982). However, new insights from water column and sediment trap sampling and from ancient laminated sediments, have demonstrated that key diatom species that are adapted to stratified conditions may contribute significantly to production and export (Sancetta et al., 1991; Kemp et al., 2000; Davies et al., 2009; Villareal et al., 2011; Karl et al., 2012). There is now, therefore, an opportunity, using a species-based approach, to develop new perspectives on the palaeoecology of ancient diatomaceous deposits and their palaeoceanographic and palaeoclimatic significance. In this paper we report the analysis of two laminated diatomites of Late Cretaceous age. The analysis of around 6,400 years of palaeo-sediment trap data is reported from two contrasting Late Cretaceous palaeoenvironments, the mid-latitude Marca Shale of California and the CESAR 6 core from the Alpha Ridge of the Arctic Ocean (Fig. 1).

The Cretaceous period saw the burgeoning of the diatom fossil record from isolated windows of preservation in early Cretaceous clastic deposits to the first significant diatomites in the Late Cretaceous. Following a major diatom radiation after the Cenomanian-Turonian anoxic event (Harwood and Nikolaev, 1995; Sinninghe Damsté et al., 2004), the development of the first extensive diatomites after 90 Ma provides the earliest widespread geological evidence for the rise to prominence of diatoms in ocean biogeochemistry (Harwood et al., 2007). Studies of Earth system behaviour in the greenhouse Cretaceous climates are especially topical since such warm, high CO_2 periods of the past are often invoked as potential analogues for present warming trends. In this context, the development of an enhanced understanding of the dominant phytoplankton that operate the marine biological carbon pump in warm stratified waters analogous to future projections is especially important. In earlier publications we reported the main elements of the Late Cretaceous seasonal cycle and the results of time series analysis of inter-annual to decadal scale climate variability (Davies et al., 2009; Davies et al., 2011; Davies et al., 2012). In this contribution we report the complete floral compositions of the two sections together with more detailed species-based diatom ecological interpretations and place these in a palaeoceanographic and palaeoclimatic context that complements recent palaeoecological studies of the Late Cretaceous from shallower coastal water environments of the Canadian Arctic (Chin et al., 2008; Witkowski et al., 2011).

2. Palaeogeographic settings and biostratigraphy

Two sites containing some of the best preserved Late Cretaceous diatoms are analysed in this study; that of the mid-latitude upper Maastrichtian Marca Shale and the high-latitude upper Campanian CESAR 6 Core from the Alpha Ridge, Arctic Ocean (Figs 1, 2).

2.1. *Marca Shale of California*

The Marca Shale member of the Moreno Formation, crops out along the Panoche Hills, on the western flank of the San Joaquin valley, central California, and represents the topmost unit of the Cretaceous Great Valley Sequence of California (Fig. 3A and Supplementary Fig. 1). Palaeontological data from planktonic and benthic foraminifers, dinoflagellates and radiolarians place the Marca Shale in the uppermost Maastrichtian stage and the top of the unit is marked by the Cretaceous-Tertiary boundary (Fonseca, 1997). The diatom floras are indicative of the topmost Cretaceous *Azpeitia morenoensis* diatom zone of Tapia and Harwood (2002), (Nikolaev et al., 2001) (Fig.2). Deposition of the Marca Shale occurred at a palaeolatitude of around 43°N, in a silled, forearc basin bounded to the east by the Sierra Nevada volcanic arc and to the west by the Franciscan complex as an emergent trench-slope break (Ingersoll, 1978; Bartow and Nilsen, 1990; Kodama and Ward, 2001). The trench-slope break may have been archipelagic or partly peninsular (Mitchell et al., 2010; Blakey, 2011). Sedimentary facies of laminated diatomites with a variable detrital component and phosphorites indicate an upper slope/ outer shelf environment and benthic foraminifera assemblages suggest deposition at palaeo water depths of between 200-500m (McGuire, 1988; Fonseca, 2000). The laminations within the Marca Shale were interpreted to represent varves and the diatomites and phosphorites to indicate the presence of a strong coastal upwelling regime (McGuire, 1988; Fonseca, 2000). Here, we report the study of nineteen sample sets and five early diagenetic nodules, all obtained from the Dosados Canyon section (36°39.5′N, 120°42.0′W), directly from surface outcrops.

2.2. *CESAR 6 core from the Alpha Ridge*

The CESAR 6 core was collected in 1983 from the Alpha Ridge of the Arctic Ocean (85°49.8′N, 109°09.2′W) at a water depth of 1365 m. It contains ~176 cm of biosiliceous sediment comprised of almost pure, unconsolidated, superbly preserved diatom ooze (Mudie and Blasco, 1985; Barron, 1985), with distinct millimetre-scale colour laminations (Fig. 3B). The CESAR 6 biosiliceous unit is almost identical in lithology, diatom composition and age to well-laminated Upper Cretaceous diatom ooze, recovered some 160 km away, also on the Alpha Ridge, from core Fl-437 (Kitchell and Clark, 1982). The lack of shallow water (benthic) diatoms, and the absence of coarser terrigenous material, led Barron (1985) to suggest that deposition of the CESAR 6 diatom ooze occurred near a shelf or bank edge, distal from the shoreline and Dell'Agnese and Clark (1994) similarly interpreted Core Fl-437 to have been deposited in deep water in an off-shelf environment, based on the same observations. Conflicting interpretations of the origins of lamination in the two cores (Kitchell et al., 1986; Stoffyn-Egli, 1987) have now been resolved by scanning electron microscope (SEM) studies, and a strongly seasonal flux sequence is present in both cores (Davies et al., 2009). The preservation of lamination is consistent with the anoxic bottom waters of a silled Arctic basin with only shallow water connections to the world ocean through the Turgay Strait, the Fram Strait and the narrowing Western Interior Seaway (Hay, 2008). The slightly older, shallower water, coastal and shelf sequences in Canadian Arctic Islands show evidence for widespread diatom productivity and the presence of a vigorous marine ecosystem (Chin et al., 2008; Witkowski et al., 2011). The Late Cretaceous Arctic summers were temperate, but there is widespread evidence for freezing winter temperatures from fossil leaf analysis (Spicer and Herman, 2010; Tomsich et al., 2010) possible frosts from tree rings (Falcon-Lang et al., 2004) and vertebrate enamels (Amiot et al., 2004). These contradict the postulated 15 °C mean annual sea surface temperature derived from TEX86 (Jenkyns et al., 2004). In fact, the presence of intermittent winter sea ice in the Arctic Ocean is indicated by the presence of thin lenses of terrigenous sediment within the Alpha Ridge diatom ooze laminae (Davies et al., 2009) and this is discussed in more detail below.

Biostratigraphically, the CESAR 6 floras closely resemble those of the early late Campanian *Trinacria indefinita* and late late Campanian *Stephanopyxis simonseni* zones established in the sequences of the Canadian Arctic continental margin and Arctic archipelago (Tapia and Harwood, 2002; Fig. 2). However, neither of the zone fossils, *T. indefinita* or *S. simonseni* is present in the CESAR 6 core. Numerous CESAR 6 taxa are present in both zones (e.g. *Actinoptychus tenuis, Goniothecium rogersii, Hemiaulus altus, H. kittonii, Proboscia cretacea, Stellarima steinyi, Stephanopyxis turris, Thalassiosiropsis wittiana, cf. Triceratium planum*, *T. acutangulum* and *Trochosira polychaeta*). However, *T. polychaeta* which is abundant in CESAR 6 is rare in the *Trinacria indefinita* zone and appears more characteristic of the *Stephanopyxis simonseni* zone. *Hemiaulus tumidicornis* that is abundant in CESAR 6, is also only found in the *S. simonseni* zone, whilst *A. sibiricus*, also abundant in CESAR 6 is more abundant in this zone, indicating that the CESAR 6 diatoms have most affinity with the late Campanian *Stephanopyxis simonseni* Zone. A similar late Campanian age was inferred for the Fl-437 core (Dell'Agnese and Clark, 1994). Previous age estimates based on silicoflagellates were interpreted to represent a Maastrichtian age (Bukry, 1985) but a more recent study advocates a late Campanian age (McCartney et al., 2010). Dinoflagellates from the nearby Fl-533 core suggest a Maastrichtian ages (Mudie, 1985; Firth and Clark, 1998), but this organic-rich core contains no biosilica. A late Campanian age therefore seems most likely. The additional potential complication is that the absence of the topmost Cretaceous zone fossil (*A. morenoensis*) from the Arctic sequences may be due to biogeographical limitations.

3. Materials and Methods

Sediment from the CESAR 6 core, interval 134-305 cm, is comprised of unconsolidated diatom ooze resembling a near-surface core from the modern Southern Ocean. This was sampled with a cookie-cutter slab-sampler (Dean et al., 1999). Samples from the Marca Shale were taken from the Dosados Canyon section where fresh diatomite was excavated from the subsurface. The CESAR 6 material was embedded using fluid displacive embedding (Pike and Kemp, 1996a; Kemp et al., 1998). The Marca Shale samples were cut to size with a pull saw and vacuum resin embedded. SEM analysis was conducted on polished thin sections (PTS) of resin embedded material and topographic stubs and peel slides, using a LEO 1450VP SEM. For the CESAR 6, topographic stubs were prepared by detaching the unconsolidated sediment from the counterparts to the resin-embedded blocks and mounting directly on stubs. The variable pressure SEM facilitates imaging of uncoated material. For the Marca Shale, topographic stubs were prepared by breaking pieces of diatomite from the counterparts to the resin-embedded blocks. These were then mounted on stubs and gold-coated. Analysis of the PTS was conducted using backscattered electron imagery (BSEI), whilst stubs and peel slides were analysed using topographic BSEI and secondary electron imagery. Low resolution (60×) BSEI base maps were created from overlapping images for each of the PTS, and higher resolution microscopy was used to identify any sub-layering within laminae. Lamina composition was verified by analysis of topographic stubs and peel slides of counterparts of resin-embedded sections and from individually sub-sampled detached laminae.

For diatom identification and estimation of relative abundances, both optical microscopy and SEM methods were used. Optical strew slides were prepared following an adapted version (Claire S. Allen, British Antarctic Survey, personal communication) of the method of Scherer (1994) (and see Supplementary Figure 2). Strew slides and strew stubs were prepared from 19 samples from the CESAR 6, comprised of material homogenised from 1 cm of the core, and from each sample level (Fig. 3A), including diagenetic nodules, from the Marca Shale. For the CESAR 6 samples, quantitative analyses were performed at 500×, with identifications checked at 1000×. Over 300 counts were made for each slide along several traverses of the cover slips. Diatoms were identified to at least the generic level using a number of key texts (Hanna, 1927; Long et al., 1946; Hajós and Stradner, 1975; Strelnikova, 1975; Barron, 1985; Harwood, 1988; Round et al., 1990; Dell'Agnese and Clark, 1994; Nikolaev et al., 2001; Tapia and Harwood, 2002). The results of the CESAR 6 counts have been previously published (Davies et al., 2009) and are reproduced with updated nomenclature in the Supplementary material (Supplementary Tables 2 and 3).

For the CESAR 6, abundances (Table 1) are based primarily on the quantitative strew slide counts (Supplementary Tables 2 and 3). Within the Marca Shale, however, many diatoms were fragmented, making strew slide counts problematic. Estimates for the Marca Shale are therefore based primarily on the frequency that individual specimens were encountered in analyses of topographic stubs or PTS. The estimates for the Marca Shale take into account the abundance of fragments, which can be more easily ascribed to a specific genus or species using SEM techniques. Early diagenetic nodules taken from the Marca Shale were found to exhibit better preservation of diatom valves and strew slides processed from these nodules were taken into account when estimating abundances.

Samples from the Marca Shale were located by measuring the section from the start of the lower pale brown laminated diatomaceous shale (Fig. 3A). In the figures the designation in metres corresponds to the distance above this horizon. Samples from CESAR 6 (Fig. 3B) were designated by the depth in core, given in centimetres in the figure captions. The samples are held at the Scanning Electron Microscope Facility of the National Oceanography Centre, Southampton and full sample designations are given in Supplementary Table 1. The CESAR 6 core is held at the core repository of the Bedford Institute of Oceanography, Canada.

4. Taphonomy

The state of diatom preservation varies between the two sites. Diatoms in the CESAR 6 are excellently preserved, with little evident dissolution or fragmentation of the frustules and show preservation of delicate features such as fine (<1 μm) setae. This is consistent with the appearance of the fresh CESAR 6 core as an unconsolidated diatom ooze, outwardly typical of the top tens of metres or so, of, for example, the modern deep sea diatom ooze. The almost total lack of fragmentation and pelletisation further indicates direct settling from surface blooms or concentrations, mainly unmediated by zooplankton ingestion and pelletisation. Only at the finest level is there evidence for variable preservation of some of the most delicate structures in different laminae, for example cingula and the processes that link chains, and this is attributed to dissolution in the water column related to varying levels of dissolved silica (Kemp et al., 2015). The preservation of laminae suggests an anoxic environment devoid of epifaunal or infaunal activity and there is no evidence of post-depositional disruption.

Diatoms in the Marca Shale have good preservation, but do suffer from extensive fragmentation and minor dissolution and basal samples show some recrystallisation to opal C-T. In early diagenetic carbonate nodules, diatoms show better preservation and are more intact (Fig. 4) with 32% of frustules counted as intact valves, in contrast to just 4% of frustules intact in the normal sediment suggesting that at least some of the observed fragmentation is due to post-depositional burial compaction (Fig. 4). This enhanced preservation of biosilica in early diagenetic carbonate nodules is typical and reported elsewhere in Upper Cretaceous marine deposits (El Albani et al., 2001). Some of the fragmentation of the diatom frustules may be the result of ingestion by zooplankton and there is also evidence for variable disruption of the laminae. This suggests an alternation between fully anoxic and dysaerobic conditions that may have permitted some reworking and fragmentation by epifaunal and infaunal activity. This is further supported by the remains of agglutinating foraminifera and moulds of calcite tests of other benthic species which have been reported elsewhere (Fonseca, 2000).

A key preservational feature of these sediments, particularly the CESAR 6 section is the presence of near-intact chains of diatoms (Figs 5, 6). This underscores the lack of post-depositional disruption. Furthermore, this feature is common to genera ranging from neritic (*Paralia*) to fully pelagic (*Hemiaulus*). The excellent preservation of linking structures has also facilitated an appraisal of their evolution (Kemp et al., 2015).

5. Lamina composition and diatom occurrence

We first provide an overview of the overall lamina composition and the diatom occurrence and distribution in the different distinct laminae of the two locations. Thereafter an account of the inferred palaeoecology of the main species is presented followed by detailed reconstructions of the seasonal cycles. An overall list of the main species identified from both the CESAR 6 and Marca Shale is given in Table 1. For the Marca Shale 10,300 laminae were examined and these were interpreted to represent 4,699 annual sedimentation packets or varves and for the CESAR 6 a total of 3,622 laminae representing 1,693 varves were examined.

5.1. CESAR 6 - Alpha Ridge: lamina composition and diatom occurrence

The CESAR 6 laminated fabric consists primarily of laminae of diatom resting spores alternating with laminae of diatom vegetative cells. Thinner laminae of mixed diatom setae and silicoflagellates are also common. Thin lenses and discontinuous laminae of terrigenous sediment are locally present. Diatom assemblage counts from the CESAR 6 are given in Davies et al. (2009) and are reproduced with updated nomenclature in Supplementary Tables 2 and 3.

5.1.1. *CESAR 6 - Diatom resting spore laminae*

Three distinct types of diatom resting spore laminae occur: near-monospecific laminae of "*Chaetoceros* type" Spore '1'; *Hemiaulus tumidicornis* laminae and mixed spore assemblage laminae (Figs 7, 8). The most common are the mixed assemblage spore laminae, which are composed of a combination of "*Chaetoceros* type" Spore '1', *H. tumidicornis* and a minor component of Spore '3' and *Skeletonema subantarctica*. Preservation of the valves in resting spore laminae is exceptional, with delicate ornamentation intact (e.g. the long filaments branching from valves of *S. subantarctica*) (Fig. 8 F – H). The least common are those of near-monospecific *H. tumidicornis*. There also occur rarer laminae composed of near-monospecific *Hemiaulus* sp. 1 (Fig. 8 A-C). Chrysophyte cysts are often present within all types of resting spore laminae, although they are most common in near-monospecific "*Chaetoceros* type" Spore '1' laminae along with variable amounts of vegetative cells. Very rarely, near-monospecific laminae of the chrysophyte cyst *Acanthosphaeridium reticulatum* are observed. Occasionally, multiple resting spore laminae occur instead of the normal vegetative/resting spore laminae alternation and are recognised by a succession of different resting spore laminae types, often separated by silicoflagellate/setae-rich laminae (see 5.1.3 - below).

5.1.2. *CESAR 6 - Diatom vegetative cell laminae*

Diatom vegetative cell laminae are dominated by *Hemiaulus* spp. (mainly *H. cf. antiquus* and *H. cf. gleseri* and to a lesser extent *H. danicus* and *H. cf. elegans*), *Trochosira polychaeta* and *Anaulus sibiricus*, all of which may form near-monogeneric (in the case of *Hemiaulus*) or near-monospecific laminae (Figs 5, 9, 10). Other less common forms are present, in variable amounts, within the mixed assemblage vegetative laminae, including other *Hemiaulus* spp. *Actinoptychus* spp., *Coscinodiscus* spp., *Skeletonemopsis crawfordii, Stellarima* spp., S*tephanopyxis turris, Thalassiosiropsis wittiana,* cf. *Triceratium* spp., *Trinacria* spp. and occasional pennate diatoms (primarily *Sceptroneis* spp.) (Figs 5, 11 – 13). Preservation of valves is generally exceptional, with a general lack of fragmentation or signs of dissolution except with the most delicate structures. Valves often possess intact girdle bands and delicate ornamentation (e.g. the long, fragile processes of *S. turris* and branching marginal spines of *S. crawfordii*). Although vegetative laminae may contain scattered valves of *Rhizosolenia*, valves of *Rhizosolenia* (thick and thin form) are often observed to form near-monospecific concentrations along the upper margin of vegetative laminae, which are occasionally sufficiently thick and continuous to form discrete laminae (Fig. 14). Small quantities of *Hemiaulus* sp. 1, *Hemiaulus tumidicornis* and other resting spores may also be present.

5.1.3. CESAR 6 - Silicoflagellate/setae-rich laminae

Laminae rich in silicoflagellates and setae of various origins may occur along the top of vegetative cell laminae and the base of spore laminae and commonly contain a significant but variable resting spore component. They therefore have an association with resting spore laminae but are distinguished by the silicoflagellate and setae component. Unlike all other lamina types, they may also contain a component of fragmented diatom valves, which occasionally forms a diatomaceous hash matrix. The most abundant component are extremely fine setae (<1 µm in diameter) that tend to form intertwined masses. Although the origin of these setae is unknown, they bear a striking resemblance to modern *Chaetoceros* spp. setae, which are often found associated with resting spores (e.g. Bull et al., 2000; Dean et al., 2001), and may be the setae of the vegetative cell of "*Chaetoceros* type" Spore '1'. A small proportion of the setae originate from the detached tips of the silicoflagellate skeletons, which are easily identified by means of their heavily silicified nature, tubular shape and relatively large size. Sponge spicules of differing morphologies may also be common. Valves of *P. cretacea*, recognised by their hexagonal cross-section, alternate columns of perforations and curved shape, are relatively abundant. The disarticulated horns of *Hemiaulus* and valves of *Gladiopsis* spp. also comprise a small proportion of the setae. Setae are occasionally observed forming pelletal aggregates in topographic stubs with inclusions of fragmented diatoms.

5.1.4. CESAR 6 – Lithogenic occurrences

Lithogenic material occurs sparsely but persistently in about 30% of the lamina couplets examined in the CESAR 6 core (Fig. 15). This generally takes the form of discontinuous elongate lenses of poorly sorted silt and clay but including small amounts up to a maximum of fine sand grade. Grains are generally angular with a mean longest and shortest diameter (in BSEI cross section) of 87.5 µm and 47 µm respectively. Occasional more laterally persistent thin laminae occur (Fig. 15A). but with average thickness of only 37 µm. The silt and fine sand grains are dominantly composed of quartz and feldspar with minor volcanic glass. These occur dominantly in the resting spore laminae (63%) with lesser concentrations in the silicoflagellate/ setae laminae (15.5%) and vegetative cell laminae (19.5%).

5.2. Marca Shale lamina composition and diatom occurrence

The Marca Shale may be broadly divided into darker and paler laminated intervals (Fig. 3). The darker intervals are richer in terrigenous sediment and there are common bioturbated intervals showing variable disruption of laminae. In the paler intervals, diatomaceous laminae are relatively thicker and bioturbated intervals are less common. The laminated fabric in the Marca Shale is predominantly composed of a diatomaceous and terrigenous laminae couplets.

5.2.1. Marca Shale – diatomaceous laminae

The diatom flora is dominated by the fragments and intact valves of three dominant taxa; *Hemiaulus polymorphus*, *Stephanopyxis spp.* (*S. appendiculata*, *S. barbadensis*, *S. discrepans* and *S. grunowii*), and *Stellarima* spp. *(S. distincta* and *S. steinyi*). Other common forms include the large (>200 μm) *Azpeitiopsis morenoensis*, *Chaetoceros*-type resting spores (remarkably similar to recent forms), *Chasea bicornis*, *Gladiopsis speciosa*, *Kentrodiscus* spp., *Medlinia deciusii, Paralia crenulata, Pseudopyxilla russica*, *Pterotheca* spp., *Proboscia cretacea* and *Trinacria* spp. (*T. aries and T. insipiens*). Other species are present (Hanna, 1927; Long et al., 1946; Nikolaev et al., 2001) but in low abundance and do not constitute a significant component of diatomaceous laminae. Rare near monospecific laminae of *Stephanopyxis* spp. (Figs 5B, 13 B-D), *Stellarima* spp. (Fig. 11 B, F), *H. polymorphus* (Fig. 10 L, M), *A. morenoensis,* (Fig. 11 D, E) *Chaetoceros*-type resting spores and *Gladiopsis speciosa* occur.

Occasional near monospecific laminae composed of intact *Chaetoceros*-type resting spores or *A. morenoensis* are observed (Fig. 17). *Chaetoceros*-type resting spore laminae consistently occur along the top of diatomaceous laminae, whilst *A. morenoensis* laminae only occur along their base and above terrigenous laminae, creating a definite three part diatomaceous succession. Although *A. morenoensis* may form discrete laminae, it more generally forms concentrations along the contact between terrigenous laminae and the main mixed assemblage diatomaceous laminae. High resolution imagery of sample sets comprising around 1000 laminae identified 110 laminae of *Chaetoceros*-type spores, of which 80.0% occurred at the top of diatomaceous laminae, 1.8% along the base, 15.5% were scattered throughout the laminae and 2.7% were towards the centre of the laminae. Over the same interval, 101 laminae contained concentrations of *A. morenoensis*, all of which occurred along the base of diatomaceous laminae. Terrigenous laminae immediately below concentrations of *A. morenoensis* are often observed to contain a coarser silt/ fine sand fraction than adjacent laminae..

5.2.2. Marca Shale –Lithogenic laminae

Lithogenic laminae are predominantly composed of arkosic silt to rare fine sand, held in a clay matrix, averaging between 140-586 µm in thickness, with absolute values ranging from 41-1935 µm. Silt content varies from 10% to 80%, estimated from BSEI, with grains moderately/poorly sorted, angular and averaging ~ 10 μm in diameter. Semi quantitative EDS analysis of grains and the results of XRD confirm that the silt is arkosic, comprised mainly of quartz, K feldspar and plagioclase. Sub-layering and grading is generally absent. A diatomaceous component is also present, including a few of the more common species of the diatomaceous laminae but a few species are relatively enriched, especially *Paralia crenulata* which is nine times more abundant in terrigenous, than in diatomaceous laminae, from BSEI mosaic counts. *Medlinia deciusii* also appears more abundant with respect to diatomaceous laminae. Relatively high proportions of *A. morenoensis* are also present.

6. Palaeoecology of key diatom genera and species

6.1. The bases for palaeoecological interpretation.

In order to assign palaeoecological preferences we use a number of criteria. Using the laminated sediments as “palaeo-sediment traps” we determine 1) the diatoms that form near-monospecific or near-monogeneric concentrations in individual laminae. This is taken to indicate that such diatoms have formed blooms or have been concentrated by other means in the water column (e.g. accumulation on a density interface), and that the laminae record flux from such blooms or concentration scenarios. 2) The position of individual lamina types relative to others is recorded and a dominant recurring pattern is taken to represent the annual cycle of flux (Figs 16. 17). 3) The annual/ seasonal flux cycle is reconstructed and the occurrence of monospecific laminae is fitted into this reconstruction. 4) Less abundant species are fitted, by association with lamina type, into the annual flux cycle and their palaeoecological preference deduced. 5) Where individual genera or species are extant, the affinities of modern examples are taken into consideration, and other supporting evidence is sought (e.g. evidence for N-fixation, presence of symbionts etc.). 6) Related microfossil palaeoecological evidence is used, preferentially from other "palaeo-sediment trap" laminated sediment sequences where available, as well as from conventional studies involving samples that do not resolve individual flux associations. Such interpretations are also complemented by judgements based on morphological features, (e.g. chain formation), sedimentary facies associations and geographic distribution as well as palaeontological and palaeoecological data from other groups (for example in the studies of Chin et al., 2008; Witkowski et al., 2011).

6.2. Planktonic and probable planktonic taxa

6.2.1. Hemiaulus Ehrenberg

Hemiaulus is a lamina-forming genus in both the Marca Shale and CESAR 6. The vegetative cell laminae of which *Hemiaulus* spp. are a component are distinct from the resting spore laminae in both settings. Cells of this genus form long chains by interlocking spines found at the summits of polar elevations and intact or near-intact chains are observed in both the Marca Shale and CESAR 6 (Fig. 5). The presence of still-intact chains and presence of near-monospecific to near monogeneric concentrations of intact frustules evidences rapid settling directly from blooms.

In the CESAR 6 *Hemiaulus* is the dominant genus in the vegetative cell laminae that alternates with the resting spore laminae interpreted to represent spring deposition and flux (Davies et al., 2009). The *Hemiaulus* production was within the stratified Arctic summer water column with flux events either during the summer and/ or on the end-summer breakdown of stratification following the fall dump model. In the Marca Shale, the position of *Hemiaulus* indicates flux following the terrigenous sediment lamina deposition. The terrigenous flux is interpreted to represent run-off and possible aeolian contribution derived from summer storms driven by a palaeo- North American monsoon (Davies et al., 2012). This is similar to the climate and flux cycle in the modern Gulf of California (Douglas et al., 2007) where abundant large diatom vegetative cells are sedimented in late summer/ early winter in the fall dump (Sancetta, 1995; Kemp et al., 2000). In both locations, the position of *Hemiaulus* spp. in the flux sequence, following flux from the spring bloom, is consistent with growth during the summer period of water column stratification. *Hemiaulus* was a dominant genus in the late Cretaceous through Eocene with 40 or more species (Sims, 1986). The late Cretaceous and Eocene species were generally more heavily silicified than the more delicate four remaining modern species, following a trend toward more lightly silicified planktonic diatoms through the Cenozoic (Round et al., 1990).

In the modern ocean, *Hemiaulus* spp. were previously regarded as typical of the sparse flora of oligotrophic regions (Guillard and Kilham, 1978), and as biogeochemically insignificant. However, substantial summer blooms and significant export of *Hemiaulus hauckii* are increasingly documented in the North Pacific Subtropical Gyre (NPSG) (Scharek et al., 1999; Villareal et al., 2011; Karl et al., 2012), where blooms occur in the near subsurface (20-25 m) and are thought to aggregate following mechanisms similar to the spring bloom, settling rapidly in a "summer export pulse" (Karl et al., 2012). Substantial *Hemiaulus* blooms also occur in association with distal oceanic river plumes, for example the Amazon (Subramaniam et al., 2008), Congo (Foster et al., 2009) and Mekong (Grosse et al., 2010). In all these cases, *Hemiaulus* blooms are, in part, fuelled by a non-obligate symbiosis with the nitrogen fixing cyanobacterial symbiont *Richelia intracellularis* in Diatom Diazotroph Associations (DDAs). Laminae of *Hemiaulus hauckii* are also a component of the Mediterranean sapropels (Kemp et al., 1999) and there is biomarker evidence of the abundant presence of N_2-fixing cyanobacteria during sapropel formation (Bauersachs et al., 2010). Although there is no direct evidence from the Cretaceous, there is widespread isotopic evidence for contemporaneous N-fixation (Meyers et al., 2009) and biomarker evidence for the presence of cyanobacteria (Kuypers et al., 2004; Wagner et al., 2004).

In summary, Upper Cretaceous sequences demonstrate substantial growth of *Hemiaulus* spp. during summer stratified conditions and flux during the summer or the late summer and fall. There are other adaptations that will allow growth in stratified settings (e.g. growth in low light in a deep chlorophyll maximum) but the most likely mechanism to support the Late Cretaceous *Hemiaulus* blooms, is symbiosis with a nitrogen fixing symbiont, analogous to the modern *Richelia –Hemiaulus* association. This is supported, at least circumstantially, by widespread isotopic and biomarker evidence for N-fixation by cyanobacteria in Upper Cretaceous sequences. The co-occurrence of several *Hemiaulus* species in the Cretaceous laminae is also consistent with observations of modern blooms where *Hemiaulus hauckii* is generally the dominant species but where other *Hemiaulus* species are present in subordinate amounts (Villareal, 1991; Scharek et al., 1999).

6.2.2. Trinacria Heiberg

Trinacria is a poorly studied, extinct genus that has a generally accepted age range of Cretaceous-Eocene, although it likely extends into the Miocene (Round *et al.*, 1990; Sims and Ross, 1988). Cells are tri-/quadripolar, forming chains through interlocking extended apices, which are encountered on topographic stubs (Fig. 6). Valve morphology places the genus within the Hemiaulaceae, and consequently, *Trinacria* is often grouped with *Hemiaulus* when analysing the ecology of fossil assemblages (e.g. Harwood, 1988). *Trinacria* has been generally considered to be a marine planktonic genus, occupying an offshore or oceanic niche (e.g. Stickley *et al.*, 2004). On the basis of the abundance of *Trinacria* spp. in the Horton River section from the Canadian Arctic (Tapia and Harwood, 2002) it has been regarded as indicative of an outer neritic (outer shelf) setting. The co-occurrence of *Trinacria* with *Hemiaulus* spp. in the mixed diatomaceous laminae of the Marca Shale and the vegetative cell laminae in CESAR 6, respectively, suggests that *Trinacria* was similarly adapted to stratified conditions and bloomed and sedimented in association with the “summer export pulse” and/or fall dump flux scenarios of the hemiaulids. Its relatively rare presence is however consistent with earlier interpretations of its occurrence in otherwise oceanic assemblages in that its primary niche is an outer neritic one but that it is capable of migrating to open ocean settings.

6.2.3. Stephanopyxis Ehrenberg

Stephanopyxis is a lamina-forming genus in the Marca Shale and occurs more rarely as a component of vegetative cell laminae in CESAR 6. In both settings it may occur in chains (Fig. 5, A & B). It is a fairly common planktonic genus in the present oceans capable of forming long chains by interlocking processes with sibling valves (Round *et al.*, 1990). These intertwined chains can aggregate into large flocculent masses (T.A. Villareal pers comm.). In the modern, valves of *Stephanopyxis* are heavily silicified and robust and are often a component of reworked diatom associations (Sjunneskog and Scherer, 2005) – however, the intact delicate chains preserved in the CESAR 6 and Marca sections, together with lack of other evidence of reworking indicate that the observed concentrations result from water column blooms. *Stephanopyxis* is also distinguished by its long stratigraphic range from the Albian (Gersonde and Harwood, 1990; Girard et al., 2009) to modern.

Modern forms are most commonly found in tropical or warm water regions (Round *et al.*, 1990) although *Stephanopyxis turris* shows a wide temperature tolerance range (Ren et al. 2014). *Stephanopyxis palmeriana* has been sampled at a depth of 100 m in the Sargasso Sea and cultures were found to grow at ~2% light levels (Goldman, 1993) and it was suggested that substantial production could be maintained through the sustained exploitation of nutrients periodically injected at depth. Recently, the doming of isopycnals under the influence of mesoscale eddies has become regarded as an important mechanism for stimulating *Stephanopyxis* blooms (Goldman and McGillicuddy, 2003). BSEI of Holocene laminated sediments from the Gulf of California show that the greatest flux of *S. palmeriana* occurs in the autumn, whilst sediment traps in the Santa Barbara Basin show peak flux during the winter (Pike and Kemp, 1996b; Pike and Kemp, 1997; Kemp et al., 2000) . These observations led Kemp *et al*. (2000) to include *Stephanopyxis* as a key player in the fall dump mode of export flux with growth in a deep chlorophyll maximum during the summer followed by sedimentation on the seasonal disruption of water column stratification. The occurrence of *Stephanopyxis* spp. within the late summer/ autumn laminae from the Marca and CESAR 6 argue for a similar ecological adaptation during the Cretaceous, and their co-occurrence with *Hemiaulus* in both localities is supportive of this.

6.2.4. Stellarima Hasle & Sims

Stellarima, an extant genus first appearing in the Late Cretaceous (Sims and Hasle, 1987), is a lamina-forming genus in the Marca Shale. Formerly placed in the genus *Coscinodiscus*, valves of *Stellarima* are discoid and modern species occupy a solitary, marine, planktonic niche (Round *et al.*, 1990). Sediment trap studies have shown that the modern form *S. stellaris*, a warm-temperate water species (Hasle and Syvertsen, 1996), is found concentrated in the water column during the autumn and winter in the Baltic Sea, suggesting it too may be a species characteristic of the fall dump. The other well known extant species, *S. microtrias*, is an abundant part of the plankton around Antarctica and is known to form endogenous resting spores, which are similar in morphology to the vegetative cells (Syvertsen, 1985). The distribution of *Stellarima* spp. in the Late Cretaceous indicates that at this time the genus was cosmopolitan, consistent with a planktonic mode of life (Sims and Hasle, 1987; Harwood, 1988; Tapia and Harwood, 2002). Sims and Hasle (1987) described both a resting stage and vegetative cell of *S. steinyi* in a study of Upper Cretaceous material from Siberia, Arctic Ocean and the Marca Shale. Both the resting stages and vegetative cells were identified in this study and were found to have been sedimented concurrently (Fig. 4A). The large, robust valves of the *S. steinyi* and *S. distincta* and their occurrence in the flux cycle with *Hemiaulus* and *Stephanopyxis* suggests they were fall dump forms characterised by growth in stratified waters during the summer and flux in the autumn on the breakdown of stratification. On the other hand, in the CESAR 6, *Stellarima* sp.1 is observed to form rare near-monospecific laminae within the resting spore varve couplet. Valves of *Stellarima* sp.1 are lightly silicified, in sharp contrast to the other Cretaceous species of *Stellarima* (*S. distincta* and *S. steinyi*) and is inferred to reflect spring bloom flux, analogous to some species of *Coscinodiscus*.

6.2.5. Trochosira Gleser

Trochosira is a fossil genus, ranging from the Campanian to Paleogene (Harwood, 1988; Harwood and Nikolaev, 1995). *T. polychaeta* is geographically widespread (Strelnikova, 1971; Hajós and Stradner, 1975; Harwood, 1988; Dell'Agnese and Clark, 1994; Tapia and Harwood, 2002), suggesting it is likely to have been a planktonic species. Valves are commonly linked with robust central linking spines (Sims, 1988), but also with complex marginal structures (Kemp et al., 2015) allowing the formation of chains (Fig. 5F). It is a lamina-forming genus in the CESAR 6. Unusually for the CESAR 6 diatoms, *T. polychaeta* shows a range of wide range of preservation that is interpreted to result from dissolution within the water column, and not post depositionally (Kemp et al., 2015). The relatively robust appearance of *T. polychaeta* in some states of preservation led some authors to interpret it as a resting spore (e.g. Kitchell et al., 1986; Dell'Agnese and Clark, 1994). However the range of delicate features and occurrence in chains clearly indicate a vegetative cell status (see Kemp, et al. 2015 for a full discussion). Its concurrent sedimentation with *Hemiaulus* within the vegetative laminae of the CESAR 6 suggests it is likely that they shared the same ecological niche of adaptation to growth during the summer stratification.

6.2.6. Anaulus Ehrenberg

Anaulus is a lamina-forming genus in the CESAR 6. The valves of this extant genus possess two conspicuous psuedosepta that cross the valve. Cells in all studied samples in this study occur singularly, although modern forms are capable of forming short chains (Round *et al.*, 1990) and have an areolate valve surface, apart from the regions around the pseudosepta, which are hyaline. Based on the dominance of *A. sibiricus* in resting spore laminae and *Hemiaulus cf. elegans* in vegetative laminae in core Fl-437 from the Arctic Ocean (Kitchell *et al.*, 1986), Harwood (1988) suggested that *A. sibiricus* is a resting spore of *H. cf. elegans*. However, the presence of areolae, girdle bands and the similarity to extant vegetative *Anaulus* cells, casts doubt on this interpretation. Extant species of *Anaulus* have a clear ecological preference for littoral environments and the genus is commonly referred to as a surf-zone diatom (Talbot and Bate, 1988; Hewson et al., 2001). However, *Anaulus sibiricus* displays a wide geographical distribution, (Barron, 1985; Harwood, 1988) and is also a major lamina-forming species in the CESAR 6, indicating it was not restricted to the littoral zone. It is possible that *A. sibiricus* is a vegetative cell, reflecting fall dump export flux or may alternatively represent a resting spore of *Hemiaulus*, produced in response to environmental stress (see section 6.4 on resting spores – below).

6.2.7. Rhizosolenia Brightwell

The fossil form of *Rhizosolenia* observed in this study has been interpreted as a resting spore, and occurs in two forms; a thin and a thick form, identical in morphology except in respect to the cell diameters (Barron, 1985; Kitchell *et al.*, 1986). It is a lamina-forming genus in the CESAR 6. Analysis of both cell morphologies under optical and electron microscopy has revealed that cells possess a non-ornamented, cylindrical hyaline portion, to which the ribbed conical section, identified as *Rhizosolenia*, is connected by a fine girdle band (Fig. 14A,B). In most specimens, the two valve segments have become disconnected. The two valve segments may be connected in a straight line along the central axis of the cylindrical valve section (Fig. 14B), or the two valve segments may be joined at an angle (Fig. 14F). The cylindrical, hyaline portion of the valve has not hitherto been associated with the *Rhizosolenia* valve segment, and when unconnected resembles valves of *Pseudopyxilla*.

Although superficially resembling *Rhizosolenia*, the CESAR 6 species differs in a number of important respects. Firstly there appears to be no groove in the valve surface to accommodate the spine of adjacent valves, seen in modern *Rhizosolenia*. The heavily ribbed valves also contrast with modern forms, which also possess numerous scale-like girdle bands, unlike the hyaline valves shown here. The relatively heavily silicified nature of the hyaline valve suggests that the cells are likely to be resting spores, consistent with the conclusions of earlier studies (Kitchell *et al.*, 1986). Valves of this species occur in concentrations and near-monospecific laminae above vegetative cell laminae and below resting spore laminae, consistent with sporulation at the end of the summer/ autumn. Alternatively, the Arctic *Rhizosolenia* may be a heavily silicified ‘winter’ stage, by analogy with observations of the modern Antarctic diatom *Eucampia antarctica* (Fryxell and Prasad, 1990), sedimented after the initial summer/autumn fall dump of *Hemiaulus* and *Trochosira*. This fossil is only known from the Cretaceous/Eocene Arctic cores CESAR 6, Fl-437 and Fl-422 (Barron, 1985; Dell'Agnese and Clark, 1994) and may therefore have been an endemic Arctic species.

Modern rhizosolenid species are characteristic of stratified marine settings ranging from the expanses of the subtropical gyres to the summer stratification of coastal and shelf seas. They show a range of adaptations to the stratified environment. Some form multi-species mats that regulate their buoyancy, mining nutrients from nutricline depths and returning to the surface (Villareal et al., 1999), not only supporting mat growth but also providing up to 27% of the surface nitrate pool through nitrate release (Singler and Villareal, 2005). Other rhizosolenid species such as *Pseudoguinardia recta* thrive in deep chlorophyll maxima where they may grow at 1.12 divisions /day at the 2% light level at depths of 100 m (Goldman, 1993). A further adaptation, like that of *Hemiaulus* is symbiosis with the nitrogen-fixer *Richelia intracellularis* in diatom-diazotroph associations (Villareal and Carpenter, 1989). Extensive sediment trap studies show major fluxes of rhizosolenid diatoms in the late summer to early winter period (Takahashi et al., 1989; Sancetta et al., 1991; Sancetta, 1992; Sancetta, 1995; Lange et al., 2000) and it is regarded as a key player in the fall dump flux when stratification breaks down at the end of the summer (Kemp et al., 2000). On the other hand rhizosolenid species with *Richelia*-type endosymbionts formed part of the "Summer export pulse" at the ALOHA site together with *Hemiaulus hauckii* (Scharek et al., 1999) demonstrating a propensity for summer as well as fall export. The position of the Late Cretaceous *Rhizosolenia* in the Alpha Ridge flux cycle is consistent with the late summer/ fall flux and general ecology of its modern descendents.

6.2.8. Azpeitiopsis Sims

Valves of the fossil genus *Azpeitiopsis* are large, solitary, discoidal and robustly silicified and form laminae in the Marca Shale. *A. morenoensis* is an important biostratigraphic index fossil appearing in the Lower Maastrichtian and possesses a global distribution (Hanna, 1927; Strelnikova, 1975; Shipboard-Scientific-Party, 1989; Tapia and Harwood, 2002). The closest extant relative of *Azpeitiopsis* is the genus *Azpeitia*, with which *Azpeitiopsis* shares many morphological similarities, a species of which, *Azpetia nodulifera*, is particularly important in palaeoceanographic studies in the Gulf of California. *A. nodulifera* is generally rare in coastal settings, but is common in subtropical/tropical gyres (Fryxell *et al.*, 1986; Schrader *et al.*, 1993) and its presence in the Gulf of California can be correlated with the warmer, more oceanic conditions of El Niño events (Sancetta, 1995; Barron et al., 2004). Sediment traps deployed at the Namibia upwelling mooring site (central Benguela System) reveal *Azpeitia* spp. has a peak flux in the summer, with a smaller secondary peak in flux in the winter (Romero *et al.*, 2002). Sediment traps off the coast of northern Chile record a peak flux of *Azpeitia* spp. during the late spring, with higher flux over all seasons during El Niño years (Romero *et al.*, 2001). The intermittent occurrence of *A. morenoensis* in the Marca Shale is consistent with a more oceanic affinity, with higher abundances in the Marca Basin relating to "palaeo" El Niño-like events, analogous to *A. nodulifera*.

6.2.9. Coscinodiscus Ehrenberg

First appearing in the Late Cretaceous (Harwood and Nikolaev, 1995), *Coscinodiscus* is widespread in the fossil record. Modern representatives of *Coscinodiscus* occupy a free-living, solitary, marine planktonic niche, often with a cosmopolitan distribution (Round *et al.*, 1990). The Santa Barbara Basin trap experiment (August 1993 to July 1996) demonstrated that several large *Coscinodiscus* spp. (*C. centralis, C. perforatus, C. granii, C. oculus-iridis* and *C. wailesii*) are important components of the early winter and winter flux (Lange et al., 2000). Similarly, Sancetta (1995) noted high fluxes of *Coscinodiscus* during the late autumn in the Gulf of California. High flux of large *Coscinodiscus* spp. during the late autumn/early winter has been documented in laminated sediments from the Gulf of California (Pike and Kemp, 1996b; Kemp et al., 2000). *Coscinodiscus* spp., especially larger forms, are key species involved in fall dump export flux . The occurrence of *Coscinodiscus* spp. within the mixed vegetative laminae in the CESAR 6 suggests that some species of this genus were representatives of the fall dump taxa at this time.

6.2.10.Ârerataulina Pergallo

Valves of *Cerataulina* are elongate with a long cylindrical and shorter conical apex, from which numerous long filaments branch. Valves are generally hyaline, although some may possess a finely perforated section near the lower part of the cylindrical part of the valve wall. The lower apex of *Cerataulina*, from which the long filaments emanate, appear to be related to specimens of *Skeletonema subantarctica*, valves of which are often found intertwined with specimens of *Cerataulina* (Fig. 8 F-H). It therefore appears that these two diatoms are part of the same valve. Hajós and Stradner (1975) interpreted *C. cretacea* to be a permanent spore from a non-identified planktonic diatom, consistent with their occurrence in the resting spore laminae.

6.3 Tychoplanktonic and near-shore taxa

6.3.1. Paralia Heiberg

Paralia occurs in both the modern and fossil realms ~~with~~ and is characterised by robust frustules that link to form straight chains. It is commonly found in both the plankton and benthos of modern temperate coastal environments (McQuoid and Nordberg, 2003) and so may be regarded as tychoplanktonic. The extant form *P. sulcata*, has been associated with a wide variety of environmental factors, including high salinity, low light and strong winds (McQuoid and Nordberg, 2003), although it is most commonly associated with the high primary productivity coastal upwelling zones (e.g. Abrantes, 1991). The species can be found in a range of salinities but is generally thought to be indicative of marine environments. Primarily growing in the benthos (McQuoid and Hobson, 1998), with an affinity for arenaceous sediments (Round et al., 1990), strong physical mixing may play a crucial role in transporting cells into the plankton. There is also a correlation with increased storminess and wind-mixing and the enhanced presence of *P. sulcata* in more pelagic environments (Gebühr et al., 2009). More recent taxonomic studies demonstrate that P. sulcata is actually a species complex such that new species are now being defined by SEM and molecular methods although these are collectively referred to as *Paralia sulcata* (*sensu lato*) (MacGillivary and Kaczmarska, 2015). In fact, *Paralia sulcata* (*sensu lato*) is remarkably similar in morphology to the fossil species *Paralia crenulata. P. crenulata* is concentrated within terrigenous laminae in the Marca Shale suggesting that it was also tychoplanktonic at this time and was transported offshore during strong physical mixing events, likely associated with the summer convective thunderstorms. Notably, *Paralia* is not found in the CESAR 6 sequence, reinforcing the latter's distal pelagic setting although it is a dominant taxon in the coastal and shelf sequences of the Canadian high Arctic and Islands (Witkowski et al., 2011).

6.3.2. Actinoptychus Ehrenberg

Actinoptychus is an extant neritic genus that possesses characteristic valves that are sectored into alternate elevated and depressed sectors. In the present oceans, *Actinoptychus* primarily occupies a benthic (epilithic or epiphytic) niche (Round *et al.*, 1990). Valves are robust and heavily silicified, consistent with an ecological preference to high energy environments, and as such are often preserved in sediments and common in the geological record. In the Gulf of California, Sancetta (1995) regards this genus as a shelf dwelling form that is advected into the pelagic realm during summer storms. After valves have been advected into the plankton, they may be transported hundreds of miles offshore (e.g. Lange and Berger, 1993). *Actinoptychus* is rare in both the Marca and CESAR 6 while its presence in the latter suggests similar potential for long range transport.

6.3.3. Medlinia Sims

Medlinia is only known from the fossil record, with a range from the Late Cretaceous (Campanian) to the Oligocene and little ecological information exists for this genus. Valves are tripolar and possess linking mechanisms at the three marginal apices and/or the central area of the valve. Using the linking mechanisms, frustules are capable of forming straight chains with very narrow or no intercellular spaces. The two species discussed in this study possess restricted geographical distributions with *M. deciusii* only from the Marca Shale, whilst *M. mucronata* is known from the Marca Shale and Palaeocene of Arkhangelsk, Russia

(Schmidt, 1873-1959). In view of the robust nature of the valves of this genus, which are likely to be preserved in the fossil record, the restricted geographical extent suggests that *Medlinia* may have been confined to the near-shore, neritic environment, supported by its concentration in terrigenous laminae in the Marca Shale that suggests a common niche with *Paralia crenulata*.

6.3.4. Triceratium Ehrenberg

Although many studies of fossil assemblages group this genera with the holoplankton (e.g. Stickley *et al.*, 2004), modern forms occupy a free-living or attached, coastal marine niche (Round *et al.*, 1990). In a study of large, living epiphytic and epilithic diatoms in southern California, *T. pentacrinus* was found to be one of the most commonly observed marine species, forming long filaments attached to rocks or macroalgae (Tiffany and Lange, 2002). It occurs rarely in CESAR 6 suggesting a similar potential to *Actinoptychus* for long distance advection. *Triceratium* is an extant genus that is commonly represented in the fossil record and is well described from the Cretaceous (e.g. Tapia and Harwood, 2002). However, recent investigations have highlighted the need for a thorough evaluation of multipolar diatom genera (Witkowski et al., 2015). *Triceratium sensu stricto* first appears in the Eocene and it seems likely that the forms described as *Triceratium* here will be reclassified in future.

6.3.5. Gladiopsis Gersonde & Harwood

Gladiopsis is a fossil genus that was separated from the genus *Gladius* during a study of some exceptionally well preserved lower Cretaceous diatoms (Gersonde and Harwood, 1990), and is one of the most distinctive Cretaceous diatoms, with characteristic long and cylindrical frustules. The ecology of *Gladiopsis* is unknown, although the genus was initially described from a nearshore, shallow marine assemblage (Gersonde and Harwood, 1990). However, individual species of *Gladiopsis*, for example *G. speciosus*, displays a cosmopolitan distribution (Strelnikova, 1974; Hajós and Stradner, 1975; Harwood, 1988; Tapia and Harwood, 2002), suggesting that it may not have been restricted solely to nearshore environments. In the Marca Shale, *Gladiopsis* forms rare near-monospecific laminae within the terrigenous varve component, indicating it may have been benthic or tychoplanktonic, washed into the basin during physical mixing.

6.4. Resting Spores

Resting spore development is generally associated with the onset of unfavourable environmental conditions and sporulation generally occurs in response to a sudden change in one or more environmental factors (Davis *et al.*, 1980). These include nutrient levels, irradiance, hours of sunshine, pH, temperature and salinity (McQuoid and Hobson, 1996). Nitrogen- and iron (Fe)-limitation, in particular, have been shown to be key triggers of spore formation (Hargraves and French, 1983; Sugie et al., 2010). Resting spore formation is a routine part of the life cycle in spore-forming species and facilitates re-seeding of populations on seasonal and sub-seasonal time scales. Resting spores have been conventionally thought to occur mostly in species that occupy a coastal or shelf niche (Hargraves, 1986) with the exception of species that inhabit a “pseudo-benthic” environment at the base of the thermocline in oceanic waters (Bienfang and Szyper, 1981), such as *Hemiaulus*, *Rhizosolenia* and *Stephanopyxis*. However recent studies also highlight the importance of resting spore formation and associated carbon flux from open ocean diatoms including some *Chaetoceros* subgenus *Hyalochaete* species (Rynearson et al. 2013).

6.4.1. Chaetoceros spp.-type spores

Chaetoceros-type spores form laminae in both the Marca Shale and CESAR 6. These spores bear a striking resemblance to modern Hyalochaete *Chaetoceros* resting spores, which currently comprise the bulk of biosiliceous sediments underlying zones of coastal upwelling and are indicative of highly productive environments (Bull and Kemp, 1995; Pike and Kemp, 1996b; Thunell, 1998; Koning et al., 2001). In a multidisciplinary study in the southern Benguela Current system, vegetative cells of *Chaetoceros* spp. were found to dominate the upper water column, whilst resting spores dominated the sediments and water column below the thermocline (Pitcher, 1986). The heavy silicification of the resting spores in contrast to the lightly silicified frustules of the vegetative cells ensures *Chaetoceros* spores are preferentially preserved in the sediments. *Chaetoceros* spores are overwhelmingly deposited following the spring bloom when sporulation occurs in response to the reduction of nutrient levels (Kemp, 1995; Sancetta, 1995). Rapid sedimentation is achieved by the expulsion of transparent exopolymer particles (TEP), which allow cells to form flocculating aggregates, which rapidly sink, bypassing the effects of dissolution and grazing in the upper water column (Alldredge et al., 1993; Bull and Kemp, 1995; Grimm et al., 1997). Spore 1 and *Chaetoceros*-type spores in the CESAR 6 and Marca Shale are therefore taken to relate to spring bloom flux, consistent with their position in each annual flux cycle. The intermittent occurrence of *Chaetoceros*-type spores in the Marca Shale may relate to interannual variability. Along the modern Californian margin the abundance of *Chaetoceros* resting spores is strongly modulated by El Niño Southern Oscillation (ENSO). *Chaetoceros* spores dominate during non El Niño years whilst there is a marked drop in their abundance during El Niño years and an increased abundance of taxa with affinities for warm offshore waters (Lange et al., 1990; Lange et al., 1997). Although most commonly known from coastal and shelf settings large fluxes of near-monospecific *Chaetoceros* resting spores have been recently recorded from the open ocean spring bloom in the North Atlantic (Rynearson et al., 2013), an environment more analogous to the pelagic Alpha Ridge setting of the CESAR 6 core.

6.4.2. Hemiaulus tumidicornis

Hemiaulus tumidicornis forms discrete laminae in the CESAR 6. Although previously ascribed to the genus *Hemiaulus*, many authors have suggested that the fossil diatom *H. tumidicornis* is in fact a resting spore (e.g. Kitchell et al., 1986; Dell'Agnese and Clark, 1994). High-resolution BSEI conducted in this study provides clear support for this, showing it to be an endospore of an apparently weakly silicified species of *Hemiaulus* (Fig. 7 E-H). The vegetative stage is seldom preserved in the CESAR 6 sediments, and when it does occur it is only in conjunction with *H. tumidicornis*. Two morphologically distinct types of *H. tumidicornis* are observed; a generally smooth form and a form with numerous spiny projections emanating from near the polar elevations. Both these forms have been grouped as *H. tumidicornis* owing to the fact that they both appear to originate from the same vegetative cell (Fig 7 F). *H. tumidicornis* occurs within the resting spore varve segment, implying it represents spring bloom export flux.

6.4.3. Hemiaulus sp. 1

The fossil diatom *Hemiaulus* sp. 1 forms discrete laminae in the CESAR 6. It is morphologically very similar to *Hemiaulus* vegetative cells, being lanceolate, with transverse folds and associated internal costae and possessing two polar elevations with a single labiate process situated near the centre of the valve face, through which extends an external conical tube. The valves are hyaline and exhibit a range of size and morphologies, none of which have been observed to possess a girdle band (Fig. 8 A-C). In most specimens the tips of the fragile polar elevations are fractured off, although they are present in a few samples (Fig. 8C). These specimens show that the polar elevations possess a spine, akin to the linking apparatus found on vegetative cells. Despite this no specimens could be found linked in any of the material studied. These observations may suggest that *Hemiaulus* sp. 1 is a resting spore, consistent with earlier conclusions (Barron, 1985; Kitchell *et al.*, 1986), probably originating from one of the many *Hemiaulus* species. Alternatively, by analogy with observations of the modern Antarctic diatom *Eucampia antarctica*, *Hemiaulus* sp.1 may be a heavily silicified ‘winter’ stage (Fryxell and Prasad, 1990). *Hemiaulus* sp.1 forms rare near-monospecific laminae above resting spore laminae and below vegetative cell laminae in the CESAR 6, indicating it was sedimented after the spring bloom and prior to the fall dump hinting it is likely to be a resting spore.

6.4.4. Spore ‘3’

Valves of Spore ‘3’ superficially resemble those of *H. tumidicornis*, both of which are small, hyaline, possessing polar elevations, and a single process situated in the centre of the valve face, however, the valves are distinct in several ways. The polar elevations of Spore ‘3’ are much straighter, cylindrical and elongate than those of *H. tumidicornis* and also possess a ring of projections along their apex (Fig. 8D,E). The valve face of Spore ‘3’ is also much smoother than that of *H. tumidicornis*, which have crenulated valve face, often with many spiny projections. Based on the similarities of Spore ‘3’ with those of *H. tumidicornis* and its occurrence within the resting spore varve segment, Spore ‘3’ is interpreted to be a resting spore of an unidentified *Hemiaulus* species deposited following the spring bloom.

6.4.5. Skeletonema subantarctica

In a study of fossil species of the genus *Skeletonema*, Sims (1994) examined specimens of both the species *S. subantarctica* and *S. penicillus*. It was noted that both forms possess similar, if not identical, structures, suggesting that the two forms may be conspecific. Girdle bands attached to these valves were found not to be typical of either *Skeletonema* or *Skeletonemopsis*, which along with other valve characteristics (including the fact that the valves are hyaline) led to the conclusion that the specimens were resting spores (Sims, 1994). This conclusion is further supported in this study with the recognition that valves of “*S. subantarctica*” appear to be associated with valves of *Cerataulina* (Fig. 8 F-H) and occur within resting spore laminae in the CESAR 6.

7. Origins and palaeoclimatic significance of lithogenic sediment within the CESAR 6 core

The absence of any size-sorting together with a complete lack of evidence for any current structures such as scouring, cross or parallel lamination in CESAR 6 rules out bottom current activity as a mechanism for introducing the lithogenic sediment. Aeolian contributions would be expected to have strong modes in the medium to coarse silt grade without the abundant clay and also lacking the coarser sand grains (Holz et al., 2004). Furthermore, the humid, forested land areas surrounding the Late Cretaceous Arctic lacked the necessary arid or desert areas to supply dust (Otto-Bliesner and Upchurch, 1997; Spicer and Herman, 2010). Although organic rafting of marine sediment may be locally important, the high frequency of the Alpha Ridge rafting events together with the lack of material coarser than fine sand makes this an unlikely agent (Emery, 1963). Distal hemipelagic deposition would dominantly involve sediment less than 15 μm with an expected mode less than 7 μm (Holz et al., 2004) and even in modern high latitudes does not exceed 40 μm (Hebbeln, 2000). The absence of sorting does suggest a rafting origin. Ice might be a candidate, but if there was a component of glacial ice supply one would expect to see particles much coarser than just fine sand grade (medium and coarse sand, granules and larger drop stones) but there is no evidence of *any* such clasts in either the CESAR 6 or the Fl-437 core. Similarly, sea ice formed from anchor ice flotation or by seabed freezing in shallow water with subsequent flotation would also be expected to have a much coarser size range (Kempema et al., 1989). The largest sand grain long axis measured in the CESAR 6 is 290 μm and the sand grade material is dominantly in the very fine (63-125 μm) with some in the fine (125-250 μm) size fractions.

In fact, the process that uniquely produces this size distribution is the formation of turbid ice by suspension freezing and subsequent sediment entrainment (Smedsrud, 2001). In this process, thin frazil ice crystals form in turbulent supercooled water, typically during autumn or early winter storms (Kempema et al., 1989; Smedsrud, 2001) (Fig. 18). These crystals then scavenge suspended sediment and rise to the surface to form sediment-laden granular ice or slush ice that may ultimately completely freeze to form turbid ice. Experimental evidence demonstrates that no grains with diameters larger than 250 µm are suspended by frazil ice with larger particles settling with the ice crystals to the sea bed (Smedsrud, 2001). This distinctive grain size cut-off together with the small proportion of sand (typically less than 5-10%) found in turbid ice (Kempema et al., 1989; Nürnberg et al., 1994) matches the textural characteristics of the lithogenic sediment in the Alpha Ridge cores. The newly formed slush ice is highly mobile and is capable of rafting sediment many hundreds of kilometres from its source (Meese et al., 1997; Sherwood, 2000) thus explaining why the Alpha Ridge site has lithogenic sediment but lay some 500 km distant from the nearest land. Further to this, it has been shown that protist communities in sea-ice meltwater ponds in the modern Arctic are dominated by chrysophytes (Kilias et al., 2014) and their presence has been used to infer sea-ice in Eocene sediments (Stickley et al., 2008). The fact that chrysophytes in the CESAR 6 material are most commonly found within monospecific "Chaetoceros type" and Spore '1' laminae is consistent with a sea-ice origin.

The inference of freezing winter sea surface temperatures has significant implications. A mean annual SST of 15°C was proposed for the Late Cretaceous Arctic Ocean on the basis of the TEX86 method from a different Alpha Ridge core (FL-533) (Jenkyns et al., 2004). However subsequent papers now propose that the TEX86 method yields a summer SST maximum rather than an annual average (Sluijs et al., 2006) so that significantly colder winter temperatures may have occurred. The evidence from the CESAR 6 core for the presence of intermittent winter sea ice is consistent with wider evidence for cold winters (Spicer and Herman, 2010), that includes estimates of polar temperatures down to –10°C from late Campanian-Maastrichtian Alaskan vertebrate enamels (Amiot et al., 2004), evidence for possible frosts from Campanian-Maastrichtian age tree rings from Ellesmere Island (Falcon-Lang et al., 2004), CLAMP estimates of cold month mean temperatures of -2.7°C from the Campanian-Maastrichtian of central Alaska (Tomsich et al., 2010) as well as models of the Late Cretaceous ocean that suggest the formation of seasonal sea ice (Otto-Bliesner et al., 2002).

8. The seasonal cycle of marine production and biogenic and lithogenic flux

On the basis of the "palaeo-sediment trap" data summarised above, it is possible to reconstruct the respective seasonal-scale palaeoceanographic and palaeoclimatic histories of the two study areas.

8.1. The Arctic Ocean seasonal sequence

In its simplest form the Alpha Ridge lamina sequence is a couplet showing an alternation between resting spore flux and vegetative cell flux. Superimposed on this are the occurrence of laminae or concentrations of diatom setae and silicoflagellates at the base of the resting spore lamina and near monospecific concentrations and occasional laminae of *Rhizosolenia* spp. at the top of the vegetative cell lamina. In the simple couplet, the resting spore flux is ascribed to the spring bloom and the vegetative cell flux to result from production during the summer (Figs. 16, 18) (Davies et al., 2009). The summer production and flux may be closely associated temporally and analogous to the "Summer Export Pulse" identified in modern *Hemiaulus* spp. from the North Pacific Subtropical Gyre (Karl et al., 2012). Alternatively, flux may have been generated by mixing, either during storms, or more likely associated with the onset of the Arctic winter in a fall dump. The presence of concentrations and occasional discrete laminae of *Rhizosolenia* spp.at the top of the vegetative cell lamina are consistent with flux at the end of the growth period triggered by the onset of winter mixing analogous to the typical fall dump flux of modern rhizosolenids (Sancetta et al., 1991; Kemp et al., 2000) and other fossil rhizosolenid occurrences in laminated sediment, including in the Holocene of the Gulf of California and in the Pliocene – to Pleistocene Mediterranean sapropels . The laminae of silicoflagellates and diatom setae intermittently present at the base of the resting spore laminae suggest periodic flux of the vegetative stage of the *Chaetoceros*-type spore prior to spore formation and flux. Similar *Chaetoceros* vegetative cell flux and preservation of setae and rare vegetative cells is known from Pleistocene sediments of the Santa Barbara Basin (Bull et al., 2000) . Seventy-eight percent of the discontinuous lenses and concentrations of terrigenous material in the CESAR 6, interpreted to represent rafting by slush ice, occur within the setae or resting spore laminae, and so are also consistent with a spring melting of the ice, in part concurrent with the spring bloom. However, sea ice diatoms are not present and are not recognized in the Arctic until the Eocene (Stickley et al., 2009; 2012), suggesting that diatoms had not yet evolved to exploit this developing niche.

8.2. The mid latitude western North America seasonal cycle

The dominant Marca shale lamina sequence is a couplet with an alternation between a diatomaceous lamina and a terrigenous lamina (Fig. 17). The presence of *Chaetoceros*-type resting spores along the top, and concentrations of *Azpeitiopsis morenoensis* along the base of the diatom lamina closely resembles the flux sequence of the Holocene sediments of the Gulf of California, which record a late summer to autumn fall dump flux that includes large species followed by mixed species and spring *Chaetoceros* flux (Kemp et al., 2000). This is consistent with the operation of a Late Cretaceous North American Monsoon during the Late Cretaceous (Fricke et al., 2010) in which summer storms delivered terrigenous sediment through a combination of localised runoff, reworking and mobilisation of shelf sediment and eolian input (Fig. 19). The relative concentration of *Paralia crenulata* and sponge remains within the terrigenous lamina further supports a reworked, coastal or shelf origin. The species *Stephanopyxis appendiculata*, *S. discrepans* and *Hemiaulus polymorphus* commonly form near-monospecific concentrations in laminae and are members of modern genera that are characterised by growth in summer stratified waters and summer or fall dump flux patterns.

9. Comparisons of the diatom flora of the Marca Shale and CESAR 6

Of the 46 species in the Marca Shale and 57 in the CESAR 6, only 8 are present in both. The Marca Shale contains a more diverse assemblage, with 30 diatom genera identified in this study, whilst the CESAR 6 contains 22. Although some differences between the two floras may be due to age difference, ecological factors are likely also influential. The principal differences between the two floras are summarised in Table 3.3. The CESAR 6 is characterised by a greater diversity and abundance of *Hemiaulus*, with over 20 morphotypes recognised (although some are spores). The CESAR 6 also has a greater abundance of *Anaulus*, *Chaetoceros*-type spores and other resting spores (e.g. Spore '3', *H.* spore 1, *H. tumidicornis* and *Skeletonema subantarctica*), a lower abundance and diversity of *Stephanopyxis*, *Stellarima* and benthic/neritic species (*Paralia*, *Medlinia, Actinoptychus, Gladiopsis, Glorioptychus* and *cf. Triceratium*) and the presence of *Rhizosolenia* and *Trochosira*.

The lower abundance and diversity of benthic species in the CESAR 6 is an indication that it was deposited in an environment more distal from shore than that of the Marca Shale (see also Fig. 15 of Witkowski et al, 2011). A more oceanic setting for the CESAR 6 can be corroborated with the greater diversity and abundance of *Hemiaulus*, which currently dominates blooms in oligotrophic oceanic settings (e.g. central North Pacific and tropical Atlantic). *Stephanopyxis* is currently part of the diatom export flux in coastal settings (e.g. the Gulf of California and Santa Barbara Basin) and the greater abundance and diversity of this genus in the Marca Shale probably relates to a more coastal setting than the CESAR 6. Alternatively, in the modern oceans *Stephanopyxis* has an affinity for warm/tropical regions (Goldman and McGillicuddy, 2003) and the greater abundance/diversity in the Marca Shale may relate to its lower palaeolatitude. The species of *Rhizosolenia* discussed in this study is only known from Arctic cores, suggesting it may have been an endemic Arctic species. The lack of this form in the Marca Shale may therefore also be an artefact of the differing palaeolatitudes of the two sites. Likewise, although *T. polychaeta* has been identified from numerous sites, all occur at high palaeolatitudes (DSDP Site 275 at a current latitude of 50°26'S is the lowest), which may suggest that *T. polychaeta* had an affinity for cooler conditions, providing an explanation for its absence from the Marca Shale.

The greater abundance of *Chaetoceros*-type spores in the CESAR 6, along with other spores present in the resting spore laminae, suggests a greater influence of diatoms with a "bloom and bust" mode of life, indicative of spring bloom assemblages in the modern ocean (Brodie and Kemp, 1994; Bull and Kemp, 1995; Grimm et al., 1996; Lange et al., 2000). Such diatoms are adapted to rapidly exploit available nutrients when conditions are favourable, generally with the onset of stratification and when irradiance levels are sufficient for growth in the spring. The vegetative cells of these diatoms are characteristically lightly silicified (e.g. Treppke *et al.*, 1996) and are rarely preserved in sediments. There is also a greater abundance of possible "pseudo benthic" spores in the CESAR 6, including *A. sibiricus*, *Rhizosolenia* and *Hemiaulus* sp. 1, which may relate to more stressful environmental conditions compared to the Marca Shale. That the CESAR 6 was deposited well within the Arctic Circle suggests irradiance and hours of sunshine may have been important environmental factors forcing sporulation.

A major portion of the preserved diatom export flux in both assemblages is comprised of taxa adapted to exploit stratified conditions that were sedimented from episodic blooms or in a fall dump. This observation contrasts with the traditional interpretation of the formation of diatom-rich deposits, such as the Marca Shale and CESAR 6, which calls for upwelling-fuelled spring bloom export flux (Kitchell and Clark, 1982; Kitchell et al., 1986; Fonseca, 1997).

10. Comparisons between Late Cretaceous and Modern diatom ecology: implications for our changing oceans

While the modern oceans might seem vastly different from those of the Cretaceous, we live in a period of rapid change in which increasing levels of atmospheric CO_2 are leading to warming (IPCC, 2014). In this context, warming of the present surface ocean (Levitus et al., 2009; Lyman et al., 2010) and local freshening (Bindoff et al., 2007) are leading to increased stratification in both hemispheres in the surface 300 m (Bindoff et al., 2007; Lyman et al., 2010; Capotondi et al., 2012). Based on traditional views of diatom ecology, it is held that future increased ocean stratification will lead to decreased diatom production and a reduced effectiveness of the marine biological carbon pump, that, in turn will lead to reduced CO_2 draw down to the oceans, thus acting as a positive feedback to global warming (Bopp et al., 2005; Steinacher et al., 2010). Counter to this orthodoxy, new oceanographic surveys are documenting major diatom production and flux events in stratified settings such as the subtropical gyres (McGillicuddy et al., 2007; Dore et al., 2008; Karl et al., 2012). Importantly, the key diatom genera and groups in these blooms including *Hemiaulus* and rhizosolenids that were previously regarded as unimportant for production (Guillard and Kilham, 1978) represent some of the core taxa of the Late Cretaceous. Indeed while there are only 4 extant species of *Hemiaulus* in the modern ocean, it was a dominant and diverse genus in the Late Cretaceous with over 40 species recognised (Harwood and Nikolaev, 1995). The increasing evidence from the modern ocean of the significance for production and flux of stratified-adapted diatoms including *Hemiaulus*, *Stephanopyxis* and the rhizosolenids together with our records of their importance in the stratified seas of the Late Cretaceous, suggests that increased stratification may lead to increased rather than decreased diatom production and export. This would then result in a negative- rather than positive feedback to global warming (Kemp and Villareal, 2013).

11. Conclusions

Analysis of the laminated microfabric of the mid latitude Marca Shale and high latitude CESAR 6 core from the Alpha Ridge has shown that both preserve a robust annual flux cycle with seasonal sedimentation of different diatom groups. The floral composition of each lamina allows inferences to be made on the ecology of Cretaceous diatoms. Contrary to many earlier interpretations, results indicate that both sites preserve a major flux of taxa adapted to exploit a strongly stratified ocean. These stratified-adapted diatoms were likely deposited during the summer in a “summer export pulse” or at the onset of autumn/ winter mixing in a fall dump. Dominant taxa comprising this group include *Hemiaulus*, *Stephanopyxis*, *Stellarima* and *Rhizosolenia*. A spring bloom signal of production and flux is also be observed at both sites, characterised by *Chaetoceros*-type spores, *Hemiaulus tumidicornis* and some forms of *Stellarima* and *Coscinodiscus*. The dominance and diversity of *Hemiaulus* in the CESAR 6 core may provide evidence for diatom blooms powered by N_2-fixing cyanobacteria in the Late Cretaceous. In the Marca shale laminae, lithogenic sediment influx occurred during the summer monsoon, likely driven by runoff that also transported neritic diatoms to the deep basin. A minor but persistent lithogenic sediment component in the Alpha ridge laminae evidences intermittent winter freezing in the Arctic Ocean. The high production and export generated by diatoms in the stratified seas of the Late Cretaceous suggests that future predictions of reduced diatom production and a weakening of the biological carbon pump with increasing stratification of the modern ocean may be erroneous.

Acknowledgements

The research was funded by a NERC research studentship (Davies) and NERC research grant (Kemp). We are grateful to P. Mudie for facilitating sampling of the CESAR 6 core. We gratefully acknowledge discussions with Jenny Pike, Pat Simms, John Barron and Jakub Witkowski. The manuscript was improved by the comments of three anonymous referees. We thank Richard Pearce for assistance with electron microscopy and K. Davis for expertise in drafting.

Figure Captions

Figure 1
Late Cretaceous palaeogeography showing settings of the Alpha Ridge Cesar Core location and of the Marca Shale forearc basin. Palaeogeography adapted from Blakey (2011).

Figure 2
Stratigraphic position of the Marca Shale and CESAR 6 sections with respect to the Late Cretaceous diatom zonation of Tapia and Harwood (2002). Diatom zones indicated are the *Azpeitiopsis morenoensis* Concurrent Zone, the *Stephanopyxis simonseni* Partial Range Zone, the *Trinarcia indefinita* Interval Zone, the *Costopyxis antiqua* Partial Range Zone and the *Gladius antiquus* Concurrent Zone. Also shown is the estimated range of the interval of the Kanguk Formation on Devon Island reported in Witkowski et al. (2011).

Figure 3
Left panel (Fig. 3a) shows location of Marca Shale outcrop in relation to the Great Valley and the stratigraphy with main lithological subdivisions. The location of the sample sets taken is indicated to the right of the stratigraphic column. Right panel (Fig. 3b) shows a schematic log of the CESAR 6 core after Mudie and Blasco (1985). The location of discrete samples and the resin-embedded, continuously imaged sequence is shown to the left. The diatom ooze is Unit 4. Units 3 and 2 are a silty muds and clays of Paleogene age; Unit 1 a silty to clayey mud of Neogene age.

Figure 4
Contrasting preservation in carbonate nodules of the Marca Shale (level - 35.5 m). Scale bars = 50 µm (A); 20 µm (B, C). A: Back scattered electron image (BSEI) of a polished thin section (PTS), prepared from an early diagenetic nodule from the Marca Shale showing excellent preservation of the cell walls. This shows both a vegetative cell (VC) and more heavily silicified (thicker in cross section) resting stages of *Stellarima steinyi*, demonstrating that deposition occurred concurrently. The pale grey material is carbonate and a broken diatom hash matrix is seen in the darker zones. B: Detail of *Stellarima steinyi* showing intact preservation in contrast to adjacent fragmented diatom material (arrowed). C: Contrasting preservation in normal sediment with typical compacted valves of *Stellarima* sp.

Figure 5
Scanning Electron Microscope (SEM) and light microscope (LM) photomicrographs of chain-forming diatoms. Scale bars = 10 µm except A, C, F (20 µm). A. Chain of *Stephanopyxis turris* from the CESAR 6 (core depth - 258 cm), B. Chain of *Stephanopyxis discrepans* from the Marca Shale (level - 68 m). C. Chain of *Hemiaulus cf. gleseri* from CESAR 6 (core depth - 208 cm). D. LM image of a chain of *Hemiaulus polymorphus* from a carbonate nodule from the Marca Shale (level 35.5 m). E. Chain of *Paralia crenulata* from the Marca Shale (level - 68 m). F. Chain of *Trochosira polychaeta* from CESAR 6 (core depth - 278 cm).

Figure 6
SEM photomicrograph of chain of *Trinacria acutangulum* from CESAR 6 (core depth - 221 cm). Scale bar = 20 µm.

Figure 7
Photomicrographs of diatom resting spores. Scale bars = 10 µm except A, (25 µm); B (2 µm); G, H, (5 µm). A and B – Overview and detail of *Chaetoceros* type spores (spore 1) CESAR 6 (core depth - 188 cm). C and D SEM and LM of *Chaetoceros*-type resting spores from the Marca Shale (level - 53 m and 35.5 m respectively). E-H – *Hemiaulus tumidicornis* spores in CESAR 6: Overview (E) and detail (F) of laminae including rarer (porous) vegetative stages

(core depth - 248 cm). Detail of spiny form (G) and smooth form (H) (core depths - 188 cm and 288 cm respectively).

Figure 8
Photomicrographs of diatom resting spores from CESAR 6 (SEM unless indicated). Scale bars = 5 µm except F, G, H, I, (10 µm); J, K (20 µm). A-C – *Hemiaulus* sp. 1 showing variation in hyaline frustule (A,B) and detail of terminal spine at the end of the polar elevation (C) (all core depth - 188 cm). D and E – Spore '3' (core depths - 188 cm and 208 cm respectively). F – *Skeletonema subantarctica* (core depth - 305 cm). G – Complete valve of *Cerataulina*. H – *Ceratualina* – showing detachment to form *S. subantarctica* and a hyaline valve segment (both core depth - 258 cm). I and J (optical photomicrograph) – *Goniothecium rogersii*. (core depths - 178 cm and 305 cm respectively) K – *Odontotropsis cristata*. (core depth - 288 cm).

Figure 9
Photomicrographs of *Hemiaulus* from CESAR 6 (SEM unless indicated). Scale bars = 10 µm except A, B, G (5 µm). A and B - *H. cf. antiquus*. (core depths - 288 cm and 198 cm respectively). C and D – *H. cf. elegans* . (core depths - 188 cm and 288 cm respectively). E and F – *H. danicus* (core depths - 188 cm and 238 cm respectively). G and H – *H. cf. gleseri* (core depths - 188 cm and 288 cm respectively). I and J (LM) – *H. hostilis* (core depths - 188 cm and 278 cm respectively).

Figure 10
Photomicrographs of *Hemiaulus* (A – G and L-M - SEM; H - K – LM). Scale bars = 10 µm except B, E, F (5 µm). From CESAR 6: A and B – *H. rossicus*. C and D – *H. kittonii*. E – *Hemiaulus* 'G'. F – *Hemiaulus* '2'. (all core depth - 278 cm). G – *Hemiaulus* '6' (core depth - 268 cm). H and I – *H. cf. includens* (both core depth - 228 cm). From the Marca Shale: J and K - *H. curvulatus*. L and M – *H. polymorphous* (all level - 61 m).

Figure 11
SEM photomicrographs of centric diatoms. Scale bars = 20 µm except B, I, (10 µm); C, D (20 µm); E (10 µm); F. G, H, J, K (5 µm). A – *Thalassiosiropsis wittiana* (CESAR 6, core depth - 278 cm). B and C – *Stellarima steinyi* from Marca Shale (level - 62 m) (B) and CESAR 6 (core depth - 278 cm) (C). D and E – *Azpeitiopsis morenoensis* (Marca Shale) (level - 60 m and 62 m respectively). F – *Stellarima distincta* and G – *Paralia crenulata* (both Marca Shale) (level - 60 m and 68 m respectively). H - *Skeletonemopsis crawfordii* (CESAR 6, core depth - 298 cm). I – K *Aptinoptychus*: I - *A. packii* (Marca Shale, level - 53 m). J – *A. tenuis* and K – *A. simbirskianus* (both CESAR 6, core depth - 278 cm).

Figure 12
SEM and LM photomicrographs of *Trinacria* (A-F and I-K), cf. *Triceratium* (G-H) and *Medlinia* (L and M). Scale bars = 10 µm except L (5 µm). A and B – *T. acutangulum* (CESAR 6, core depths 134 and 278 cm respectively). C and D (LM) – *T. insipiens* (Marca Shale, levels - 19 m and 35.5 m respectively). E and F – *T. tessela* G and H – *T. indefinitum* (all CESAR 6, E and F – both core depth - 178 cm; G and H – both core depth 305 cm). All from Marca: I and J – low and high focus LM of *T. aires*. K – LM of *T. tristictia* (all from level 35.5 m). L and M - *M. deciusii* (both level 61 m).

Figure 13
SEM and LM photomicrographs of *Stephanopyxis* (A-D) and *Anaulus* (E-G). Scale bars = 5 µm except A (10 µm); D (20 µm); E (50 µm). A – *S. turris* (CESAR 6, core depth 188 cm). B – *S. discrepans*. C and D (LM) - *S. appendiculata* (Marca Shale, level 68 m (B and C) and

level 60 m (D)). E - G – *A. sibiricus* – E – shows lamina concentration (CESAR 6, E and G from 278 cm; F – 188 cm).

Figure 14
SEM and LM photomicrographs of *Rhizosolenia* sp. from CESAR (A-F). Scale bars = 10 µm except H (20 µm); J (50 µm); E (10 µm). Overview (A) and detail (B) of lamina concentration of "thick" form showing ribbed polar - and hyaline central segment, C (LM) and D showing "thin" form. E – LM showing junction between ribbed and hyaline sections, E – showing hyaline segment attached at angle (A, C, D from core depth 268 cm; B – 198 cm; E and F from 278 cm). G and H *Proboscia cretacea* from Marca Shale – level 61 m (G) and LM from CESAR 6 – 305 cm (H). I and J – *Gladiopsis speciosa* (I – LM), from CESAR 6 – core depth - 305 cm and 178 cm respectively).

Figure 15
SEM images of lithogenic material within the CESAR 6 laminae. All from core depth 215.7 cm. Scale bars = 50 µm except C (20 µm). A – Thin lamina of silt and clay with rare fine sand grains. B – Isolated quartz grain of fine sand grade. C – Detail of lens with clay and very fine silt grade sediment.

Figure 16
Schematic showing a reconstruction of the annual flux cycle from the CESAR-6 Alpha Ridge. Left panel shows BSEI of polished thin section distinguishing paler, resting spore laminae and darker (more porous) laminae mainly of vegetative cells. Cartoon to the right shows a reconstruction of the annual flux cycle including typical diatom species, with position of more minor components indicated. Key shows major species components.

Figure 17
Schematic showing a reconstruction of the annual flux cycle from the Marca Shale. Left panel shows BSEI of polished thin section distinguishing pale terrigenous mud (white quartz silt grains clearly visible) and dark diatomaceous laminae. Cartoon in centre shows a reconstruction of the annual flux cycle including typical diatom species, with position of more minor components indicated. Note the presence of tychopelagic/ benthic diatoms within the summer terrigenous flux (see Fig. 19). Right panel shows images of typical diatom components: bottom – *Chaetoceros*-type resting spores indicative of spring bloom flux; middle – *Azpeitiopsis morenoensis* indicative of late summer or "fall dump" flux; top – near-monospecific concentration of *Stephanopyxis discrepans* within the vegetative cell lamina indicative of summer production and "fall dump" flux. Key shows major species components.

Figure 18
Reconstruction of the Late Cretaceous seasonal flux cycle in the Arctic Ocean (CESAR 6). Top (early Winter) shows the mechanism of formation of the turbid slush ice (after Sherwood, 2000; Smedsrud, 2001; 2002). Frazil ice crystals form in turbulent supercooled water during early winter storms. The same storms suspend sediment that the frazil ice then scavenges and may lift particles up to about 250 µm in diameter. The resultant slush ice then undergoes long distance rafting. Spring panel shows the rapid development of the spring diatom bloom dominated by *Chaetoceros* - type species and resulting in rapid flux of resting spores together with lithogenic material from the melting ice. Summer panel shows the development of strong stratification with production dominated by species growing in deep chlorophyll maxima and possibly by N-fixation-driven blooms that may have resulted in a summer export pulse. Late summer/ fall panel shows the breakdown of stratification with onset of storms and mixing resulting in a fall dump of remaining diatoms.

Figure 19
Reconstruction of the Late Cretaceous seasonal flux cycle of the Marca Shale. Spring panel shows the spring bloom with rapid flux of Chaetoceros type resting spores. Summer panel shows development of stratification with species in a deep chlorophyll maxima. Monsoonal storms drive input of lithogenic sediment by run-off and aeolian flux and also input to deep basin of reworked neritic benthic diatoms (*Paralia*). Autumn brings breakdown in stratification and mass sedimentation of diatoms in the fall dump.

References

Abrantes, F., 1991. Increased upwelling off Portugal during the last Glaciation: diatom evidence. Marine Micropaleontology, 17 285-310.
Agusti, S., Gonzalez-Gordillo, J.I., Vaque, D., Estrada, M., Cerezo, M.I., Salazar, G., Gasol, J.M., Duarte, C.M., 2015. Ubiquitous healthy diatoms in the deep sea confirm deep carbon injection by the biological pump. Nature Communications, 6 doi:10.1038/ncomms8608.
Alldredge, A.L., Passow, U., Logan, B.E., 1993. The abundance and significance of a class of large, transparent organic particles in the ocean. Deep-Sea Research Part I, 40 1131-1140.
Amiot, R., Lecuyer, C., Buffetaut, E., Fluteau, F., Legendre, S., Martineau, F., 2004. Latitudinal temperature gradient during the Cretaceous Upper Campanian-Middle Maastrichtian: delta O-18 record of continental vertebrates. Earth and Planetary Science Letters, 226 (1-2) 255-272.
Barron, J.A., 1985. Diatom Biostratigraphy of the CESAR 6 Core, Alpha Ridge. In H.R. Jackson, P.J. Mudie, S.M. Blasco (Eds.), Initial Geological Report on CESAR-the Canadian Expedition to Study the Alpha Ridge Geological Survey of Canada, Paper 84-22, Report 10. pp. 137-148.
Barron, J.A., Bukry, D., Bischoff, J.L., 2004. High resolution palaeoceanography of the Guaymas Basin, Gulf of California, during the past 15 000 years. Marine Micropaleontology, 50 185-207.
Bartow, A.J., Nilsen, T.H., 1990. Review of the Great Valley Sequence, Eastern Diablo Range and Northern San Joaquin Valley, Central California. In J.G. Kuespert, S.A. Reid (Eds.), Structure, Stratigraphy and Hydrocarbon Occurrences of the San Joaquin Basin, California: Tulsa Society for Sedimentary Geology (SEPM)-Pacific Section. pp. 253-265.
Bauersachs, T., Speelman, E.N., Hopmans, E.C., Reichart, G.J., Schouten, S., Damste, J.S.S., 2010. Fossilized glycolipids reveal past oceanic N-2 fixation by heterocystous cyanobacteria. Proceedings of the National Academy of Sciences of the United States of America, 107 (45) 19190-19194.
Bienfang, P.K., Szyper, J.P., 1981. Phytoplankton dynamics in the subtropical Pacific Ocean off Hawaii. Deep-Sea Research Part I, 28 981-1000.
Bindoff, N.L., Willebrand, J., Artale, V., Cazenave, A., Gregory, J., Gulev, S., Hanawa, K., Le Quere, C., Levitus, S., Nojiri, Y., Shum, C.K., Talley, L.D., Unnikrishnan, A., 2007. Observations: Ocean Climate Change and Sea Level. In S. Solomon, D. Qin, M. Manning, Z. Chen, M. Marquis, K.B. Averyt, M. Tignor, H.L. Miller (Eds.), Climate Change 2007: The Physical Science Basis CUP. Cambridge.
Blakey, R. 2011, North American Paleogeographic Maps. https://www2.nau.edu/rcb7/globaltext2.html (August 2011).
Bopp, L., Aumont, O., Cadule, P., Alvain, S., Gehlen, M., 2005. Response of diatoms distribution to global warming and potential implications: A global model study. Geophysical Research Letters, 32 (19) L19606. doi:19610.11029/12005GL023653.
Brodie, I., Kemp, A.E.S., 1994. Variation in biogenic and detrital fluxes and formation of laminae in late Quaternary sediments from the Peruvian coastal upwelling zone. Marine Geology, 116 385-398.
Bukry, D., 1985. Correlation of Late Cretaceous silicoflagellates from Alpha Ridge. In H.R. Jackson, P.J. Mudie, S.M. Blasco (Eds.), Initial Geological Report on CESAR - the Canadian Expedition to Study the Alpha Ridge, Arctic Ocean Geological Survey of Canada, Paper 84-22, Report 9. pp. 125-135.
Bull, D., Kemp, A.E.S., 1995. Composition and origins of laminae in late Quaternary and Holocene sediments from the Santa Barbara Basin. In J.P. Kennett, J.G. Baldauf, M. Lyle (Eds.), Proceedings of the Ocean Drilling Program, Scientific Results. Leg146 (Pt. 2) College Station, TX (Ocean Drilling Program). pp. 77-87.

Bull, D., Kemp, A.E.S., Weedon, G.P., 2000. A 160-k.y.-old record of El Nino - Southern Oscillation in marine production and coastal runoff from Santa Barbara Basin, California, USA. Geology, 28 (11) 1007-1010.

Capotondi, A., Alexander, M.A., Bond, N.A., Curchitser, E.N., Scott, J.D., 2012. Enhanced upper ocean stratification with climate change in the CMIP3 models. Journal of Geophysical Research-Oceans, 117.

Chin, K., Bloch, J., Sweet, A., Tweet, J., Eberle, J., Cumbaa, S., Witkowski, J., Harwood, D., 2008. Life in a temperate Polar sea: a unique taphonomic window on the structure of a Late Cretaceous Arctic marine ecosystem. Proceedings of the Royal Society B-Biological Sciences, 275 (1652) 2675-2685.

Davies, A., Kemp, A.E.S., Pike, J., 2009. Late Cretaceous seasonal ocean variability from the Arctic. Nature, 460 254-258.

Davies, A., Kemp, A.E.S., Palike, H., 2011. Tropical ocean-atmosphere controls on inter-annual climate variability in the Cretaceous Arctic. Geophysical Research Letters, 38 L03706. doi:03710.01029/02010GL046151.

Davies, A., Kemp, A.E.S., Weedon, G.P., Barron, J.A., 2012. El Niño-Southern Oscillation variability from the Cretaceous Marca Shale of California. Geology, 40 15-18.

Davis, C.O., Hollibaugh, J.T., Seibert, D.L.R., Thomas, W.H., Harrison, P.J., 1980. Formation of resting spores by *Leptocylindricus danicus* (Bacillariophyceae) in a controlled experimental ecosystem. Journal of Phycology, 16 296-302.

Dean, J.M., Kemp, A.E.S., Pearce, R.B. 2001. Palaeo-flux records from electron microscope studies of Holocene laminated sediments, Saanich Inlet, British Columbia. Marine Geology, 174 139-158.

Dean, J.M., Kemp, A.E.S., Bull, D., Pike, J., Patterson, G., Zolitschka, B., 1999. Taking varves to bits: Scanning electron microscopy in the study of laminated sediments and varves. Journal of Paleolimnology, 22 (2) 121-136.

Dell'Agnese, D.J., Clark, D.L., 1994. Siliceous microfossils from the warm Late Cretaceous and Early Cenozoic Arctic Ocean. Journal of Paleontology, 68 (1) 31-47.

Dore, J.E., Letelier, R.M., Church, M.J., Lukas, R., Karl, D.M., 2008. Summer phytoplankton blooms in the oligotrophic North Pacific Subtropical Gyre: Historical perspective and recent observations. Progress in Oceanography, 76 (1) 2-38.

Douglas, R., Gonzalez-Yajimovich, O., Ledesma-Vazquez, J., Staines-Urias, F., 2007. Climate forcing, primary production and the distribution of Holocene biogenic sediments in the Gulf of California. Quaternary Science Reviews, 26 (1-2) 115-129.

El Albani, A., Vachard, D., Kuhnt, W., Thurow, J., 2001. The role of diagenetic carbonate concretions in the preservation of the original sedimentary record. Sedimentology, 48 (4) 875-886.

Emery, K.O., 1963. Organic transportation of marine sediments. In M.N. Hill (Ed.), The Sea, 3 Interscience Publishers. New York. pp. 776-793.

Falcon-Lang, H.J., MacRae, R.A., Csank, A.Z., 2004. Palaeoecology of Late Cretaceous polar vegetation preserved in the Hansen Point volcanics, NW Ellesmere Island, Canada. Palaeogeography Palaeoclimatology Palaeoecology, 212 (1-2) 45-64.

Firth, J.V., Clark, D.L., 1998. An early Maastrichtian organic-walled phytoplankton cyst assemblage from an organic-rich black mud in Core Fl-533, Alpha Ridge: evidence for upwelling conditions in the Cretaceous Arctic Ocean. Marine Micropaleontology, 34 1-27.

Fonseca, C., 1997. Late Cretaceous-Early Tertiary paleoceanography and cyclic sedimentation along the Californian Margin: Evidence from the Moreno Formation. Unpublished PhD Thesis, Stanford University.

Fonseca, C., 2000. Upwelling, sedimentation and anoxia control on deposition of phosphates in the Late Cretaceous California margin. In L.P. C.R. Glenn (Ed.), Marine Authigenesis: From Global to Microbial, Special Publication No. 66 SEPM. pp. 455-480.

Foster, R.A., Subramaniam, A., Zehr, J.P., 2009. Distribution and activity of diazotrophs in the Eastern Equatorial Atlantic. Environmental Microbiology, 11 (4) 741-750.

Fricke, H.C., Foreman, B.Z., Sewall, J.O., 2010. Integrated climate model-oxygen isotope evidence for a North American monsoon during the Late Cretaceous. Earth and Planetary Science Letters, 289 (1-2) 11-21.

Fryxell, G.A., Prasad, A.K.S.K., 1990. *Eucampia antarctica* var. *recta* (Mangin) stat. nov. (Biddulphiaceae, Bacillarophyceae): life stages at the Weddell Sea ice edge. Phycologia, 29 (1) 27-38.

Fryxell, G.A., Sims, P.A., Watkins, T.P., 1986. *Azpeitia* (Bacillariophyceae): Related genera and promorphology. Systematic Botany Monographs, 13 (1-74).

Gebühr, C., Wiltshire, K.H., Aberle, N., van Beusekom, J.E.E., Gerdts, G., 2009. Influence of nutrients, temperature, light and salinity on the occurrence of Paralia sulcata at Helgoland Roads. Aquatic Biology, 7 185-197.

Gersonde, R., Harwood, D.M., 1990. Lower Cretaceous diatoms from ODP Leg 113 Site 693 (Weddell Sea). Part 1: Vegetative cells. Proceedings of the Ocean Drilling Program, Scientific Results, 113 Ocean Drilling Program, College Station. Texas. pp. 365-402.

Girard, V., Saint Martin, S., Saint Martin, J.-P., Schmidt, A.R., Struwe, S., Perrichot, V., Breton, G., Neraudeau, D., 2009. Exceptional preservation of marine diatoms in upper Albian amber. Geology, 37 (1) 83-86.

Goldman, J.C., 1993. Potential role of large oceanic diatoms in new primary production. Deep-Sea Research, 40 159-168.

Goldman, J.C., McGillicuddy, D.J., 2003. Effect of large marine diatoms growing at low light on episodic new production. Limnology and Oceanography, 48 (3) 1176-1182.

Grimm, K.A., Lange, C.B., Gill, A.S., 1996. Biological forcing of hemipelagic sedimentary laminae: evidence from ODP Site 893, Santa Barbara Basin, California. Journal of Sedimentary Research, 66 (3) 613-624.

Grimm, K.A., Lange, C.B., Gill, A.S., 1997. Self-sedimentation of phytoplankton blooms in the geologic record. Sedimentary Geology, 110 (3-4) 151-161.

Grosse, J., Bombar, D., Hai, N.D., Lam, N.N., Voss, M., 2010. The Mekong River plume fuels nitrogen fixation and determines phytoplankton species distribution in the South China Sea during low- and high-discharge season. Limnology and Oceanography, 55 (4) 1668-1680.

Guillard, R.R.L., Kilham, P., 1978. The ecology of marine planktonic diatoms. In D. Werner (Ed.), The Biology of Diatoms. Botanical Monographs, 13, University of California Press. Berkeley. pp. 372-469.

Hajós, M., Stradner, H., 1975. Late Cretaceous Archaemonadaceae, Diatomaceae and Silicoflagellatae from the South Pacific Ocean, Deep Sea Drilling Project, Leg 29, Site 275. Initial Reports of the Deep Sea Drilling Project, 29. Washington D.C. pp. 913-1009.

Hanna, G.D., 1927. Cretaceous diatoms from California. Occasional Papers of the California Academy of Sciences, 13 5-49, 45 pls.

Hargraves, P.E., 1986. The relationship of some fossil diatom genera to resting spores. In M. Ricard (Ed.), Proceedings of the 8th International Diatom Symposium (pp. 67-80). Koenigstein: O. Koeltz.

Hargraves, P.E., French, F.W., 1983. Diatom resting spores: significances and strategies. In G.A. Fryxell (Ed.), Survival Strategies of the Algae Cambridge University Press. Cambridge. pp. 49-68.

Harwood, D.M., 1988. Upper Cretaceous and lower Paleocene diatom and silicoflagellate biostratigraphy of Seymour Island, eastern Antarctic Peninsula. In M.R. Feldmann, M.E. Woodburne (Eds.), Geology and Paleontology of Seymour Island, Antarctic Peninsula., 169 Geological Society of America Memoir. Boulder. pp. 55-129.

Harwood, D.M., Nikolaev, V.A., 1995. Cretaceous diatoms: morphology, taxonomy, biostratigraphy. In C.D. Blome, et al (convenors) (Ed.), Siliceous Microfossils, 8. pp. 81-106, pls 101-104.

Harwood, D.M., Nikolaev, V.A., Winter, D.M., 2007. Cretaceous Records of Diatom Evolution, Radiation, and Expansion. In S. Starratt (Ed.), Pond Scum to Carbon Sink:

Geological and Environmental Applications of the Diatoms The Paleontology Society Papers 13 Paleontological Society. pp. 33-59.
Hasle, G.R., Syvertsen, E.E., 1996. Marine diatoms. In C.R. Tomas (Ed.), Identifying Marine Diatoms and Dinoflagellates New York (Academic Press). pp. 5-386.
Hay, W.W., 2008. Evolving ideas about the Cretaceous climate and ocean circulation. Cretaceous Research, 29 (5-6) 725-753.
Hebbeln, D., 2000. Flux of ice-rafted detritus from sea ice in the Fram Strait. Deep-Sea Research Part II-Topical Studies in Oceanography, 47 (9-11) 1773-1790.
Hewson, I., O'Neil, J.M., Abal, E., 2001. A low-latitude bloom, of the surf-zone diatom, *Anaulus australis* (Centrales, Bacillariophyta) on the coast of Southern Queensland (Australia). Journal of Plankton Research, 23 (11) 1233-1236.
Holz, C., Stuut, J.B.W., Henrich, R., 2004. Terrigenous sedimentation processes along the continental margin off NW Africa: implications from grain-size analysis of seabed sediments. Sedimentology, 51 (5) 1145-1154.
Ingersoll, R.V., 1978. Paleogeography and paleotectonics of the Late Mesozoic forearc basin of northern and central California. In D.G. Howell, K.A. McDougall (Eds.), Mesozoic Palaeogeography of the Western United States: Tusla., 2 Society of Sedimentary Geology (SEPM)-Pacific Coast Paleogeography Symposium. pp. 471-482.
IPCC, 2014: Climate Change 2014: Synthesis Report. Contribution of Working Groups I, II and III to the Fifth Assessment Report of the Intergovernmental Panel on Climate Change [Core Writing Team, R.K. Pachauri and L.A. Meyer (eds.)]. IPCC, Geneva, Switzerland, 151 pp.
Jenkyns, H.C., Forster, A., Schouten, S., Damste, J.S.S., 2004. High temperatures in the Late Cretaceous Arctic Ocean. Nature, 432 (7019) 888-892.
Karl, D.M., Church, M.J., Dore, J.E., Letelier, R.M., Mahaffey, C., 2012. Predictable and efficient carbon sequestration in the North Pacific Ocean supported by symbiotic nitrogen fixation. Proceedings of the National Academy of Sciences, 109 (6) 1842-1849.
Kemp, A.E.S., 1995. Laminated sediments from coastal and open ocean upwelling systems: what variability do they record? In C.P. Summerhayes, K.-C. Emeis, M.V. Angel, R.L. Smith, B. Zeitzschel (Eds.), Upwelling in the Ocean: Modern Processes and Ancient Records. Dahlem Workshop Report, ES18. Wiley, Chichester. pp. 239-257.
Kemp, A.E.S., Davies, A., Pearce, R.B., 2015. *Trochosira polychaeta*: a colonial diatom from the Late Cretaceous exhibiting two contrasting chain-linking mechanisms and a wide range of preservation. Diatom Research, 30 (2) 151-162.
Kemp, A.E.S., Pearce, R.B., Koizumi, I., Pike, J., Rance, S.J., 1999. The role of mat-forming diatoms in the formation of Mediterranean sapropels. Nature, 398 57-61.
Kemp, A.E.S., Pearce, R.B., Pike, J., Marshall, J.E.A., 1998. Microfabric and microcompositional studies of Pliocene and Quaternary sapropels from the eastern Mediterranean. In A.H.F. Robertson, K.-C. Emeis, C. Richter, A. Camerlenghi (Eds.), Proceedings of the Ocean Drilling Program, Scientific Results, 160 College Station. TX. pp. 333-348.
Kemp, A.E.S., Pike, J., Pearce, R.B., Lange, C.B., 2000. The "Fall dump" - a new perspective on the role of a "shade flora" in the annual cycle of diatom production and export flux. Deep-Sea Research Part II-Topical Studies in Oceanography, 47 (9-11) 2129-2154.
Kemp, A.E.S., Villareal, T.A., 2013. High diatom production and export in stratified waters: a potential negative feedback to global warning. Progress in Oceanography, 119, 4-23.
Kempema, E.W., Reimnitz, E., Barnes, P.W., 1989. Sea Ice Sediment Entrainment and Rafting in the Arctic. Journal of Sedimentary Petrology, 59 (2) 308-317.
Kilias, E.S., Peeken, I., Metfies, K., 2014. Insight into protist diversity in Arctic sea ice and melt-pond aggregate obtained by pyrosequencing. Polar Research, 33 23466, http://dx.doi.org/10.3402/polar.v33.23466

Kitchell, J.A., Clark, D.L., 1982. Late Cretaceous-Paleogene paleogeography and paleocirculation: evidence of north polar upwelling. Palaeogeography, Palaeoclimatology, Palaeoecology, 40 135-165.

Kitchell, J.A., Clark, D.L., Gombos, A.M., 1986. Biological selectivity of extinction: A link between background and mass extinction. Palaios, 1 504-511.

Kodama, K.P., Ward, P.D., 2001. Compaction-corrected paleomagnetic paleolatitudes for Late Cretaceous rudists along the Cretaceous California margin: Evidence for less than 1500 km of post-Late Cretaceous offset for Baja British Columbia. Geological Society of America Bulletin, 113 1171-1178.

Koning, E., van Iperen, J.M., van Raaphorst, W., Helder, W., Brummer, G.-J.A., van Weering, T.C.E., 2001. Selective preservation of upwelling-indicating diatoms in sediments off Somalia, NW Indian Ocean. Deep-Sea Research Part I, 48 (11) 2473-2495.

Kuypers, M.M.M., van Breugel, Y., Schouten, S., Erba, E., Damste, J.S.S., 2004. N-2-fixing cyanobacteria supplied nutrient N for Cretaceous oceanic anoxic events. Geology, 32 (10) 853-856.

Lange, C.B., Berger, W.H., 1993. Diatom productivity and preservation in the western equatorial Pacific: the Quaternary record. Proceedings of the Ocean Drilling Program, Scientific Results. pp. 509-523.

Lange, C.B., Burke, S.K., Berger, W.H., 1990. Biological production off southern California is linked to climate change. Climatic Change, 16 319-329.

Lange, C.B., Weinheimer, A.L., Reid, F.M.H., Thunell, R.C., 1997. Temporal sedimentation patterns of diatoms, radiolarians, and silicoflagellates in Santa Barbara Basin, California. California Cooperative Oceanic Fisheries Investigations Reports, 38 161-170.

Lange, C.B., Weinheimer, A.L., Reid, F.M.H., Tappa, E., Thunell, R.C., 2000. Response of siliceous microplankton from the Santa Barbara Basin to the 1997-98 El Nino event. California Cooperative Oceanic Fisheries Investigations Reports, 41 186-193.

Levitus, S., Antonov, J.I., Boyer, T.P., Locarnini, R.A., Garcia, H.E., Mishonov, A.V., 2009. Global ocean heat content 1955-2008 in light of recently revealed instrumentation problems. Geophysical Research Letters, 36 L07608. doi 07610.01029/02008GL037155.

Long, J.A., Fuge, D.P., Smith, J., 1946. Diatoms of the Moreno Shale. Journal of Paleontology, 20 (2) 89-118.

Lyman, J.M., Good, S.A., Gouretski, V.V., Ishii, M., Johnson, G.C., Palmer, M.D., Smith, D.M., Willis, J.K., 2010. Robust warming of the global upper ocean. Nature, 465 (7296) 334-337.

Margalef, R., 1978. Life-forms of phytoplankton as survival alternatives in an unstable environment. Oceanologica Acta, 1 493-509.

MacGillivary, M.L., Kaczmarska, I., 2015. *Paralia* (Bacillariophyta) stowaways in ship ballas: implications for biogeography and diversity of the genus. Journal of Biological Research, 22:2 doi 10.1186/s40709-015-0024-5.

McCartney, K., Witkowski, J., Harwood, D.M., 2010. Early evolution of silicoflagellates during the Cretaceous. Marine Micropaleontology, 77 83-100.

McGillicuddy, D.J., Anderson, L.A., Bates, N.R., Bibby, T., Buesseler, K.O., Carlson, C.A., Davis, C.S., Ewart, C., Falkowski, P.G., Goldthwait, S.A., Hansell, D.A., Jenkins, W.J., Johnson, R., Kosnyrev, V.K., Ledwell, J.R., Li, Q.P., Siegel, D.A., Steinberg, D.K., 2007. Eddy/wind interactions stimulate extraordinary mid-ocean plankton blooms. Science (Washington, D.C.), 316 (5827) 1021-1026.

McGuire, D.J., 1988. Depositional Framework of the Upper Cretaceous-Lower Tertiary Moreno Formation, Central San Joaquin Basin, California. In S.A. Graham (Ed.), Studies of the Geology of the San Joaquin Basin., 60 Pacific Section S.E.P.M. pp. 173-188.

McQuoid, M.R., Hobson, L.A., 1996. Diatom resting stages. Journal of Phycology, 32 889-902.

McQuoid, M.R., Hobson, L.A., 1998. Assessment of paleoenvironmental conditions on southern Vancouver Island, British Columbia, Canada, using the tychoplankter *Paralia sulcata*. Diatom Research, 13 311-321.

McQuoid, M.R., Nordberg, K., 2003. The diatom *Paralia sulcata* as an environmental indicator species in coastal sediments. Estuarine, Coastal and Shelf Science, 56 339-354.

Meese, D.A., Reimnitz, E., Tucker, W.B., Gow, A.J., Bischof, J., Darby, D., 1997. Evidence for radionuclide transport by sea ice. Science of the Total Environment, 202 (1-3) 267-278.

Meyers, P.A., Bernasconi, S.M., Yum, J.G., 2009. 20 My of nitrogen fixation during deposition of mid-Cretaceous black shales on the Demerara Rise, equatorial Atlantic Ocean. Organic Geochemistry, 40 (2) 158-166.

Mitchell, C., Graham, S.A., Suek, D.H., 2010. Subduction complex uplift and exhumation and its influence on Maastrichtian forearc stratigraphy in the Great Valley Basin, northern San Joaquin Valley, California. Geological Society of America Bulletin, 122 (11-12) 2063-2078.

Mudie, P.J., 1985. Palynology of the CESAR cores, Alpha Ridge. In H.R. Jackson, P.J. Mudie, S.M. Blasco (Eds.), Initial Geological Report on CESAR - the Canadian Expedition to Study the Alpha Ridge, Arctic Ocean Geological Survey of Canada, Paper 84-22, report 11. pp. 149-174.

Mudie, P.J., Blasco, S.M., 1985. Lithostratigraphy of the CESAR Cores. In H.R. Jackson, P.J. Mudie, S.M. Blasco (Eds.), *Initial Geological Report on CESAR - the Canadian Expedition to Study the Alpha Ridge, Arctic Ocean* Geological Survey of Canada, Paper 84-22, report 6. pp. 59-99.

Nelson, D.M., Treguer, P., Brzezinski, M.A., Leynaert, A., Queguiner, B., 1995. Production and dissolution of biogenic silica in the ocean: Revised global estimates, comparison with regional data and relationship to biogenic sedimentation. Global Biogeochemical Cycles, 9 (3) 359-372.

Nikolaev, V.A., Kociolek, J.P., Fourtanier, E., Barron, J.A., Harwood, D.M., 2001. Late Cretaceous diatoms (Bacillariophyceae) from the Marca Shale member of the Moreno Formation, California., Occasional Papers of the California Academy of Sciences (pp. 1-119).

Nürnberg, D., Wollenburg, I., Dethleff, D., Eicken, H., Kassens, H., Letzig, T., Reimnitz, E., Thiede, J., 1994. Sediments in Arctic sea ice: implications for entrainment, transport and release. Marine Geology, 119 185-214.

Otto-Bliesner, B.L., Brady, E.C., Shields, C., 2002. Late Cretaceous ocean: Coupled simulations with the National Center for Atmospheric Research Climate System Model. Journal of Geophysical Research, 107 (D2) 10.1029/2001JD000821.

Otto-Bliesner, B.L., Upchurch, G.R., 1997. Vegetation-induced warming of high-latitude regions during the Late Cretaceous period. Nature, 385 804-807.

Pike, J., Kemp, A.E.S., 1996a. Preparation and analysis techniques for studies of laminated sediments. In A.E.S. Kemp (Ed.), Palaeoclimatology and Palaeoceanography from Laminated Sediments, 116 Geological Society of London Special Publications. pp. 37-48.

Pike, J., Kemp, A.E.S., 1996b. Records of seasonal flux in Holocene laminated sediments, Gulf of California. In A.E.S Kemp (Ed.), Palaeoclimatology and Palaeoceanography from Laminated Sediments, 116 Geological Society of London Special Publications. pp. 157-169.

Pike, J., Kemp, A.E.S., 1997. Early Holocene decadal-scale ocean variability recorded in Gulf of California laminated sediments. Paleoceanography, 12 (2) 227-238.

Pitcher, G.C., 1986. Sedimentary flux and the formation of resting spores of selected *Chaetoceros* species at two sites in the southern Benguela system. South African Journal of Marine Science, 4 231-244.

Ren, J., Gersonde, R., Esper, O., Sancetta, C., 2014. Diatom distributions in northern North Pacific surface sediments and their relationship to modern environmental variables. Palaeogeography, Palaeoclimatology, Palaeoecology, 402 81-103.

Romero, O.E., Hebbeln, D., Wefer, G., 2001. Temporal and spatial variability in export production in the SE Pacific Ocean: evidence from siliceous plankton fluxes and surface sediment assemblages. Deep-Sea Research Part I, 48 2673-2697.

Romero, O., Boeckel, B., Donner, B., Lavik, G., Fischer, G., Wefer, G., 2002. Seasonal productivity dynamics in the pelagic central Benguela System inferred from the flux of carbonate and silicate organisms. Journal of Marine Systems, 37 259-278.

Round, F.E., Crawford, R.M., Mann, D.G., 1990. The Diatoms: biology and morphology of the genera. Cambridge University Press.

Rynearson, T.A., Richardson, K., Lampitt, R.S., Sieracki, M.E., Poulton, A.J., Lyngsgaard, M.M., Perry, M.J., 2013. Major contribution of diatom resting spores to vertical flux in the sub-polar North Atlantic. Deep-Sea Research Part I-Oceanographic Research Papers, 82 60-71.

Sancetta, C., 1992. Comparison of phytoplankton in sediment trap time series and surface sediments along a productivity gradient. Paleoceanography, 7 183-194.

Sancetta, C., 1995. Diatoms in the Gulf of California: Seasonal flux patterns and the sediment record for the past 15,000 years. Paleoceanography, 10 67-84.

Sancetta, C., Villareal, T.A., Falkowski, P., 1991. Massive fluxes of rhizosolenid diatoms: a common occurrence? Limnology and Oceanography, 36 1452-1457.

Scharek, R., Tupas, L.M., Karl, D.M., 1999. Diatom fluxes to the deep sea in the oligotrophic North Pacific gyre at Station ALOHA. Marine Ecology-Progress Series, 182 55-67.

Scherer, R.P., 1994. A new method for the determination of absolute abundance of diatoms and other silt-sized sedimentary particles. Journal of Paleolimnology, 12 171-179.

Schmidt, A., Schmidt, M., Fricke, F., Muller, O., Heiden, H., Hustedt, F., 1875-1959. Atlas der Diatomaceenkunde. Leipzig, Berlin, 480 plates.

Schrader, H., Swanberg, N., Lycke, A., Paetzel, M., Schrader, T., 1993. Diatom inferred productivity changes in the eastern equatorial Pacific. The Quaternary record of ODP Leg 111, Site 677. Hydrobiologia, 269/270 137-151.

Sherwood, C.R., 2000. Numerical model of frazil ice and suspended sediment concentrations and formation of sediment laden ice in the Kara Sea. Journal of Geophysical Research-Oceans, 105 (C6) 14061-14080.

Shipboard-Scientific-Party, 1989. Site 748. In R. Schlich, S.W.Jr. Wise (Eds.), Proceedings of the Deep Sea Drilling Project Initial Reports, 120. pp. 157-233.

Sims, P.A., 1986. *Spynctolethus* Hanna, *Ailuretta* gen. nov. and evolutionary trends within the Hemiauloideae. Diatom Research, 1 241-269.

Sims, P.A., 1988. The fossil genus *Trochosira*, its morphology, taxonomy and systematics. Diatom Research, 3 245-257.

Sims, P.A., 1994. *Skeletonemopsis*, a new genus based on the fossil species *Skeletonema* Grev. Diatom Research, 9 (2) 387-410.

Sims, P. A., Ross, R., 1988. Some Cretaceous and Paleogene Trinacria (diatom) species. Bulletin of the British Museum (Natural History). Botany series, 18 (4) 275-322.

Sims, P.A., Hasle, G.R., 1987. Two Cretaceous *Stellarima* species: *S. steinyi* and *S. distincta*; their morphology, palaeogeography and phylogeny. Diatom Research, 2 (2) 229-240.

Singler, H.R., Villareal, T.A., 2005. Nitrogen inputs into the euphotic zone by vertically migrating *Rhizosolenia* mats. Journal of Plankton Research, 27 (6) 545-556.

Sinninghe Damsté, J.S.S., Muyzer, G., Abbas, B., Rampen, S.W., Masse, G., Allard, W.G., Belt, S.T., Robert, J.M., Rowland, S.J., Moldowan, J.M., Barbanti, S.M., Fago, F.J., Denisevich, P., Dahl, J., Trindade, L.A.F., Schouten, S., 2004. The rise of the rhizosolenid diatoms. Science, 304 (5670) 584-587.

Sjunneskog, C., Scherer, R.P., 2005. Mixed diatom assemblages in glacigenic sediment from the central Ross Sea, Antarctica. Palaeogeography Palaeoclimatology Palaeoecology, 218 (3-4) 287-300.

Sluijs, A., Schouten, S., Pagani, M., Woltering, M., Brinkhuis, H., Damste, J.S.S., Dickens, G.R., Huber, M., Reichart, G.J., Stein, R., Matthiessen, J., Lourens, L.J., Pedentchouk, N., Backman, J., Moran, K., 2006. Subtropical Arctic ocean temperatures during the Palaeocene/Eocene thermal maximum. Nature, 441 (7093) 610-613.

Smedsrud, L.H., 2001. Frazil-ice entrainment of sediment: large-tank laboratory experiments. Journal of Glaciology, 47 (158) 461-471.
Smedsrud, L.H., 2002. A model for entrainment of sediment into sea ice by aggregation between frazil-ice crystals and sediment grains. Journal of Glaciology, 48 (160) 51-61.
Smetacek, V., 1999. Diatoms and the ocean carbon cycle. Protist, 150 (1) 25-32.
Smetacek, V., 2000. The giant diatom dump. Nature, 406 574-575.
Spicer, R.A., Herman, A.B., 2010. The Late Cretaceous environment of the Arctic: A quantitative reassessment based on plant fossils. Palaeogeography, Palaeoclimatology, Palaeoecology, 295 (3-4) 423-442.
Steinacher, M., Joos, F., Frolicher, T.L., Bopp, L., Cadule, P., Cocco, V., Doney, S.C., Gehlen, M., Lindsay, K., Moore, J.K., Schneider, B., Segschneider, J., 2010. Projected 21st century decrease in marine productivity: a multi-model analysis. Biogeosciences, 7 (3) 979-1005.
Stickley, C.E., Brinkhuis, H., Schellenberg, S.A., Sluijs, A., Röhl, U., Fuller, M., Grauert, M., Huber, M., Wamaar, J., Williams, G.L., 2004. Timing and nature if the deepening of the Tasmanian Gateway. Paleoceanography, 19 PA4027, doi:4010.1029/2004PA001022.
Stickley, C.E., Koç, N., Brumsack, H-J., Jordan, R.W., Suto, I., 2008. A siliceous microfossil view of middle Eocene Arctic paleoenvironments: A window of biosilica production and preservation, Paleoceanography, 23, PAIS14, doi:10.1029/2007PA001485.
Stickley, C.E., St John, K., Koc, N., Jordan, R.W., Passchier, S., Pearce, R.B., Kearns, L.E., 2009. Evidence for middle Eocene Arctic sea ice from diatoms and ice-rafted debris. Nature, 460 (7253) 376-U388.
Stickley, C.E., Koc, N., Pearce, R.B., Kemp, A.E.S., Jordan, R.W., Sangiorgi, F., St John, K., 2012. Variability in the length of the sea ice season in the Middle Eocene Arctic. Geology, 40 (8) 727-730.
Stoffyn-Egli, P., 1987. Iron and manganese micro-precipitates within a Cretaceous biosiliceous ooze from the Arctic Ocean: possible hydrothermal source. Geo-Marine Letters, 7 223-231.
Strelnikova, N.I., 1971. Species novae bacillariophytorum e sedimentis cretae posterioris in declivate orientali partis polaris ac praepolaris Montium Uralensium. Novosti Systematiki Nizshikh Rastenii, Botanicheskii Institut, Akademia Nauk SSSR, 8 41-51.
Strelnikova, N.I., 1974. Late Cretaceous diatoms of western Siberia: Academie Nauk, SSSR, Roy. 8. 202 pp. (In Russian).
Strelnikova, N.I., 1975. Diatoms of the Cretaceous Period. Third symposium on Recent and Fossil Diatoms, Vol. 53 (pp. 311-321). Kiel: Nova Hedwigia, Beihefte.
Subramaniam, A., Yager, P.L., Carpenter, E.J., Mahaffey, C., Bjorkman, K., Cooley, S., Kustka, A.B., Montoya, J.P., Sanudo-Wilhelmy, S.A., Shipe, R., Capone, D.G., 2008. Amazon River enhances diazotrophy and carbon sequestration in the tropical North Atlantic Ocean. Proceedings of the National Academy of Sciences. 105 (30) 10460-10465.
Sugie, K., Kuma, K., Fujita, S., Ikeda, T., 2010. Increase in Si:N drawdown ratio due to resting spore formation by spring blom-forming diatoms unde Fe- and N-limited conditions in the Oyashio region. Journal of Experimental Marine Bology and Ecology, 383 108-116.
Syvertsen, E.E., 1985. Resting spore formation in the Antarctic diatoms *Coscinodiscus furcatus* Karsten and *Thalassiosira australis* Pergallo. Polar Biology, 4 113-119.
Takahashi, K., Honjo, S., Tabata, S., 1989. Siliceous phytoplankton flux: interannual variability and response to hydrographic changes in the northeastern Pacific. In D.H. Peterson (Ed.), Aspects of Climate Variabiliy in the Pacific and the Western Americas, Geophysical Monograph 55 American Geophysical Union. Washington DC. pp. 151-160.
Talbot, M.M.B., Bate, G.C., 1988. The relative quantities of live and detrital organic matter in a beach-surf ecosystem. Journal of Experimental Marine Biology and Ecology, 121 (3) 255-264.
Tapia, P.M., Harwood, D.M., 2002. Upper Cretaceous diatom biostratigraphy of the Arctic archipelago and northern continental margin, Canada. Micropaleontology, 48 (4) 303-342.

Thunell, R.C., 1998. Particle fluxes in a coastal upwelling zone: sediment trap results from Santa Barbara Basin, California. Deep-Sea Research II, 45 1863-1884.

Tiffany, M.A., Lange, C.B., 2002. Diatoms provide attachment sites for other diatoms: A natural history of epiphytism from southern California. Phycologia, 41 (2) 116-124.

Tomsich, C.S., McCarthy, P.J., Fowell, S.J., Sunderlin, D., 2010. Paleofloristic and paleoenvironmental information from a Late Cretaceous (Maastrichtian) flora of the lower Cantwell Formation near Sable Mountain, Denali National Park, Alaska. Palaeogeography Palaeoclimatology Palaeoecology, 295 (3-4) 389-408.

Treppke, U.F., Lange, C.B., Wefer, G., 1996. Vertical fluxes of diatoms and silicoflagellates in the eastern equatorial Atlantic, and their contribution to the sedimentary record. Marine Micropaleontology, 28 73-96.

Villareal, T.A., 1991. Nitrogen-Fixation by the Cyanobacterial Symbiont of the Diatom Genus *Hemiaulus*. Marine Ecology-Progress Series, 76 (2) 201-204.

Villareal, T.A., Adornato, L., Wilson, C., Schoenbaechler, C.A., 2011. Summer blooms of diatom-diazotroph assemblages and surface chlorophyll in the North Pacific gyre: A disconnect. Journal of Geophysical Research-Oceans, 116 C03001. doi:03010.01029/02010JC006268.

Villareal, T.A., Carpenter, E.J., 1989. Nitrogen fixation, suspension characteristics, and chemical composition of *Rhizosolenia* mats in the central North Pacific gyre. Biological Oceanography, 6 327-345.

Villareal, T.A., Pilskaln, C., Brzezinski, M., Lipschultz, F., Dennett, M., Gardner, G.B., 1999. Upward transport of oceanic nitrate by migrating diatom mats. Nature, 397 (6718) 423-425.

Wagner, T., Damste, J.S.S., Hofmann, P., Beckmann, B., 2004. Euxinia and primary production in Late Cretaceous eastern equatorial Atlantic surface waters fostered orbitally driven formation of marine black shales. Paleoceanography, 19 (4) doi:10.1029/2003PA000898.

Witkowski, J., Harwood, D.M., Chin, K.R., 2011. Taxonomic composition, paleoecology and biostratigraphy of Late Cretaceous diatoms from Devon Island, Nunavut, Canadian High Arctic. Cretaceous Research, 32 (3) 277-300.

Witkowski, J., Sims, P.A., Strelnikova, N.I., Williams, D.M., 2015. *Entogoniopsis* gen. nov. and *Trilamina* gen. nov. (Bacillariophyta): a survey of multipolar pseudocellate diatoms with internal costae, including comments on the genus *Sheshukovia* Gleser. Phytotaxa, 209 (1) 1-89.

Table 1. List of the main diatoms encountered in observations of the CESAR 6 and Marca Shale. A = abundant, C = common, F = fair, R = rare, VR = very rare. * = taxa observed to form near monospecific laminae. See also Supplementary Tables 2 and 3 for detailed CESAR 6 counts.

TABLE 1

Species	**CESAR 6**	**Marca Shale**
Acanthodiscus immaculatus	−	VR
Actinoptychus packii	−	R
A. simbirkianus	R	−
A. taffii	−	R
A. tenuis	R	−
Anaulus sibiricus	A*	−
A. undulatus	−	VR
A. sp 1	R	−
Aulacodiscus archangelskianus	−	VR
Azpeitiopsis morenoensis	−	F*
Cerataulina cretacea	−	R
C. sp1	F	−
Chaetoceros-type spore	−	C*
C.-type spore '1'	A*	−
Chasea bicornis	−	R
Coscinodiscus circumspectus	R	?
C. sibiricus	VR	−
C. symbolophorus	VR	−
Euodiella bicornigera	−	VR
Gladiopsis pacificus	R	−
G. speciosa	R	F*
Gloriopthychus callidus	−	VR
Goniothecium rogersii	R	−
Helminthopsis wornardti?	VR	VR?
Hemiaulus altus	R	−
H. ambiguus	VR	VR
H. andrewsi	−	VR
H. cf. antiquus	C*	−
H. curvulatus	−	VR
H. danicus	C	−
H. cf. elegans	F	−
H. cf. gleseri	C*	−
H. giganteus?	VR	−
H. hostilis	R	−
H. cf. includens	R	−
H. kittonii	R	−
H. oonki	VR	−
H. polymorphus	−	A*
H. polymorphus var. *morianus*	VR	−
H. rossicus	R	−
H. tumidicornis	A*	−
H. sp. Barron1	R	−
H. sp. 1	A*	−
H. sp. 2	R	−
H. sp. 3	VR	−

H. sp. 4	VR	−
H. sp. 5	VR	−
H. sp. 6	R	−
H. sp. G	VR	−
H. sp. 7	VR	−
Kentrodiscus aculeatus	−	R
K. blandus	−	R
Medlinia deciusii	−	F
M. mucronata	−	F
Micrampulla parvula	−	F
Odontotropis cristata	VR	−
O. galleonis	−	VR
Paralia crenulata	−	C
Porpeia sp.	−	VR
Proboscia cretacea	F	F
Pseudopyxilla americana	R	−
P. russica	F	R
P. sp Strelnikova	R	−
Pseudostictodiscus picus	−	R
Pterotheca crucifera	VR	VR
P. evermannii	−	F
P. of Strelnikova (1974)	VR	−
Rhizosolenia sp.	C*	−
Sceptroneis dimorpha	F	−
S. grunowii	−	VR
S. praecaducea?	−	VR
S. sp. A	−	VR
S. sp. B	R	−
Sheshukovia excavata	−	VR
Skeletonema subantarctica	F	−
Skeletonemopsis crawfordii	VR	−
S. morenoensis	−	VR
Spore '3'	C	−
Stellarima distincta	−	C *?
S. steinyi	R	A*
S. sp. 1	R*	−
S. sp. 2	R	−
Stephanopyxis appendiculata	−	A*
S. barbadensis	−	R
S. discrepans	−	A*
S. grunowii	−	R
S. turris	R	−
Thalassiosiropsis wittiana	VR	VR
Cf. Triceratium indefinitum	R	−
Cf. T. planum	R	−
Trinacria acutangulum	R	−
T. aires	−	F
T. insipiens	−	R
T. tessela	R	−
T. tristictia	−	VR
Trochosira polychaeta	A*	−
Xanthiopyxis grantii	−	VR
Unknown	F*	−

Figure 1

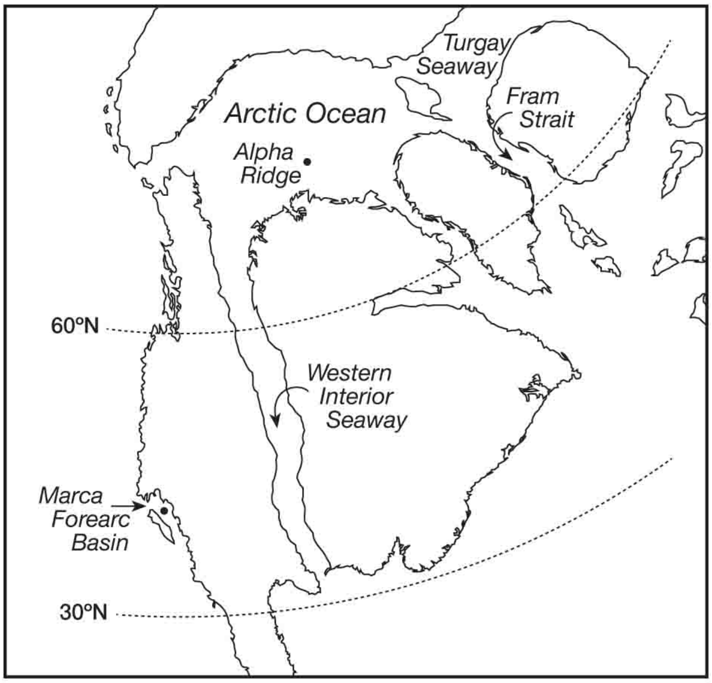

Figure 2

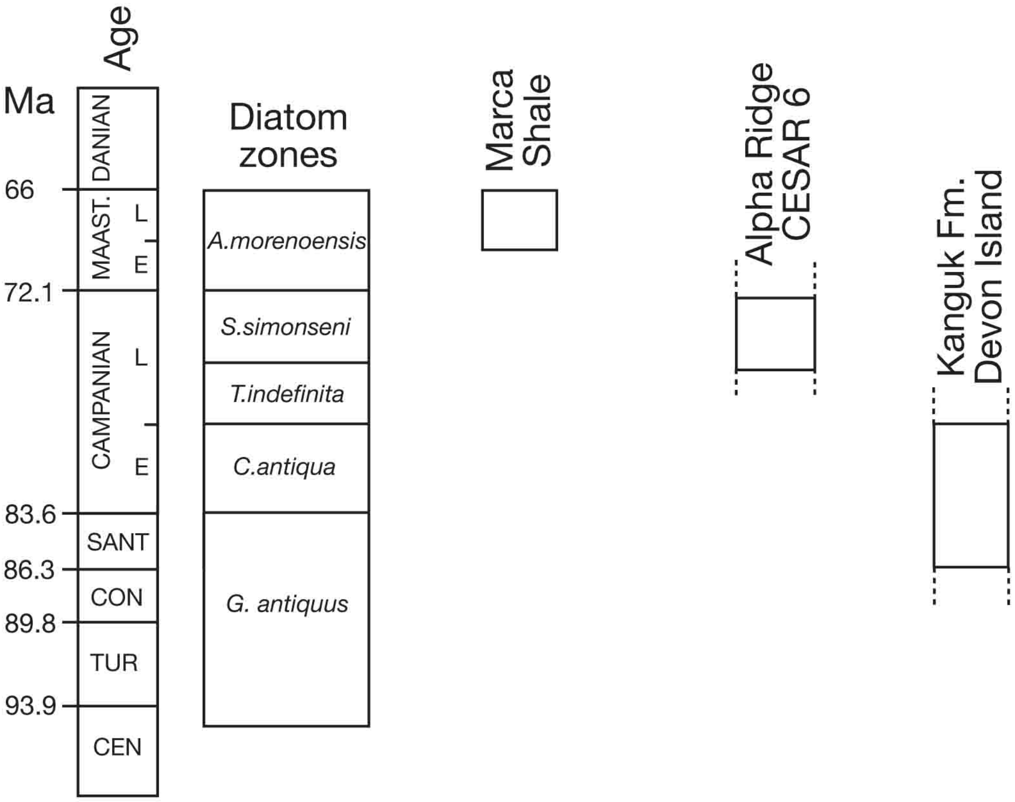

Fig. 2

Figure 3

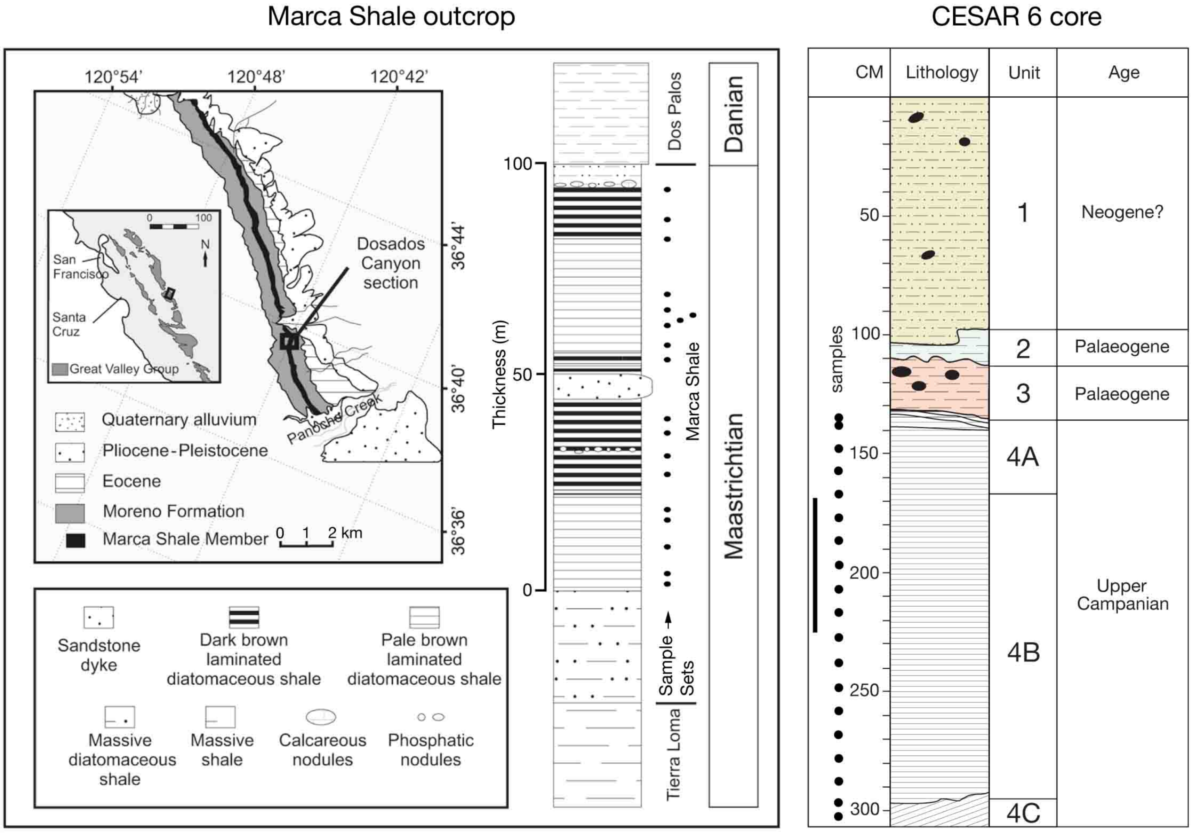

3a

3b

Figure 4

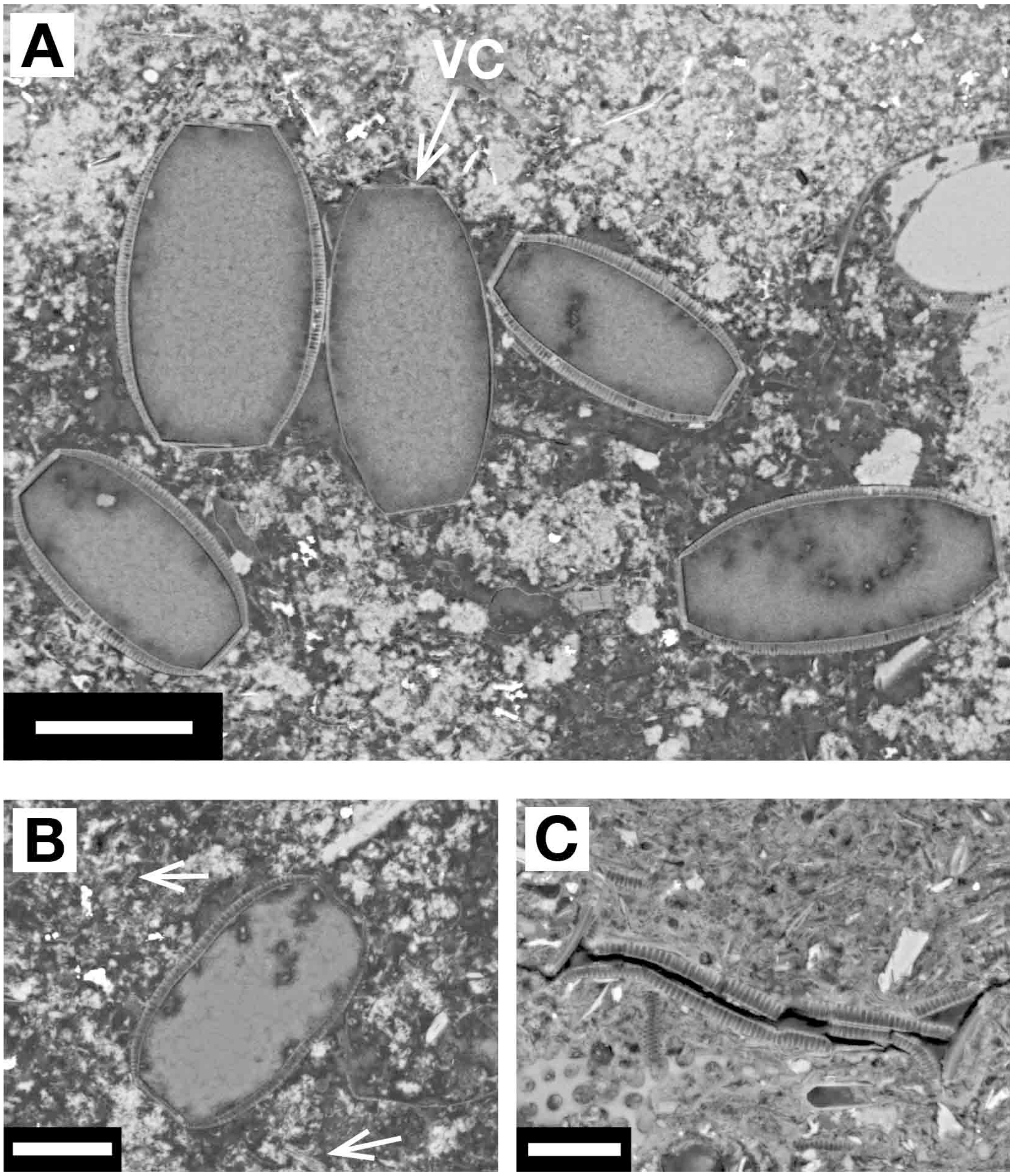

Figure 5

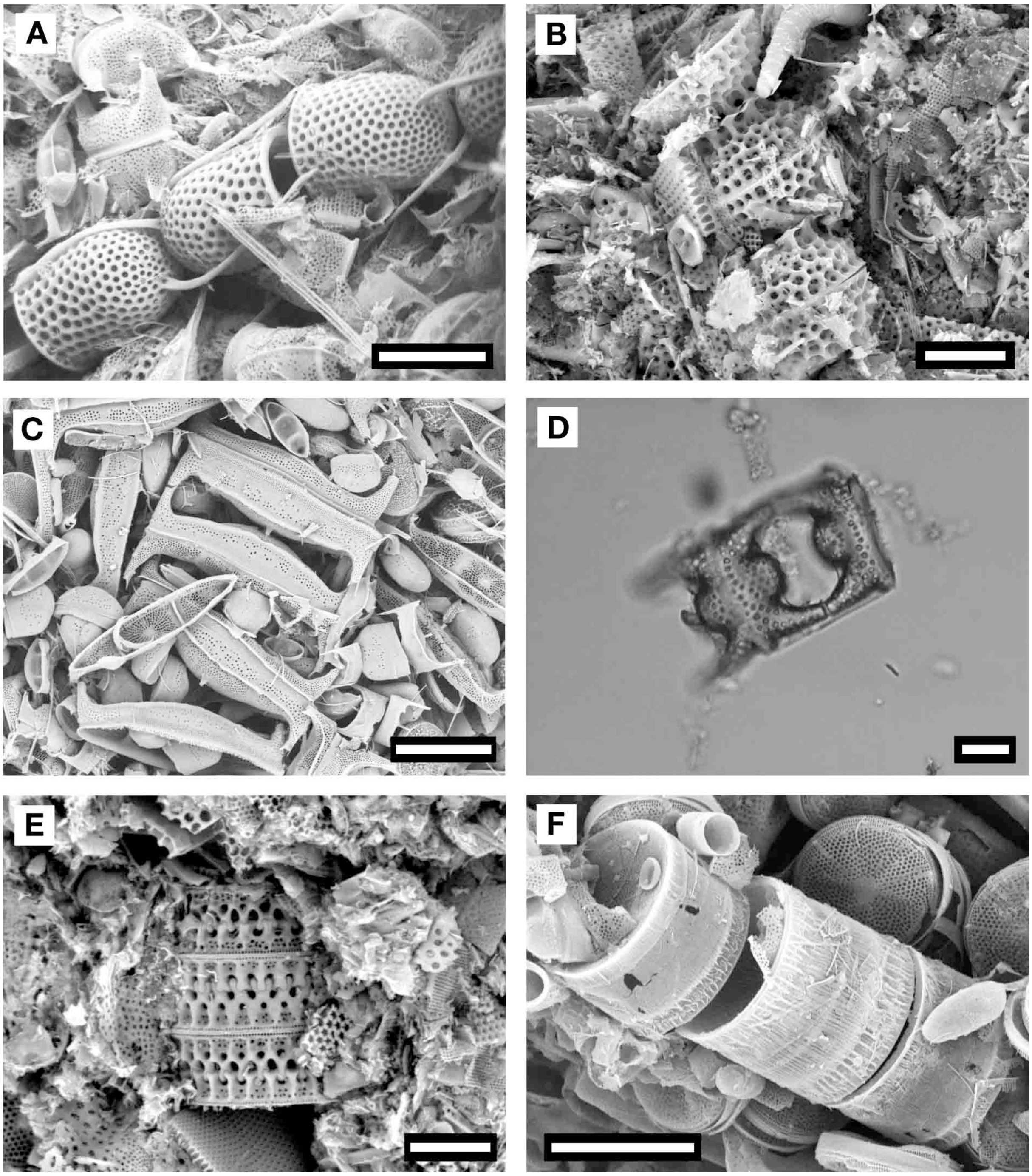

Figure 6

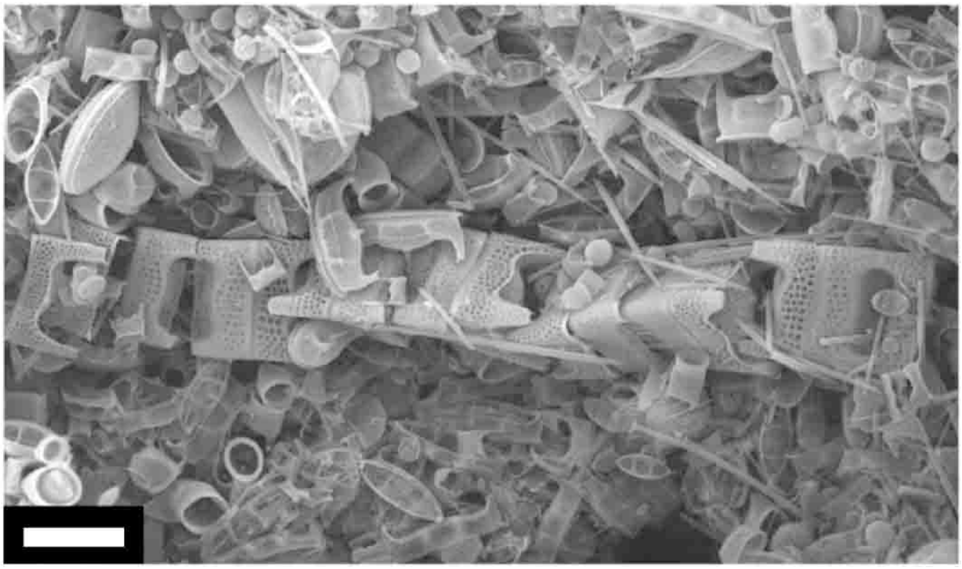

Figure 7

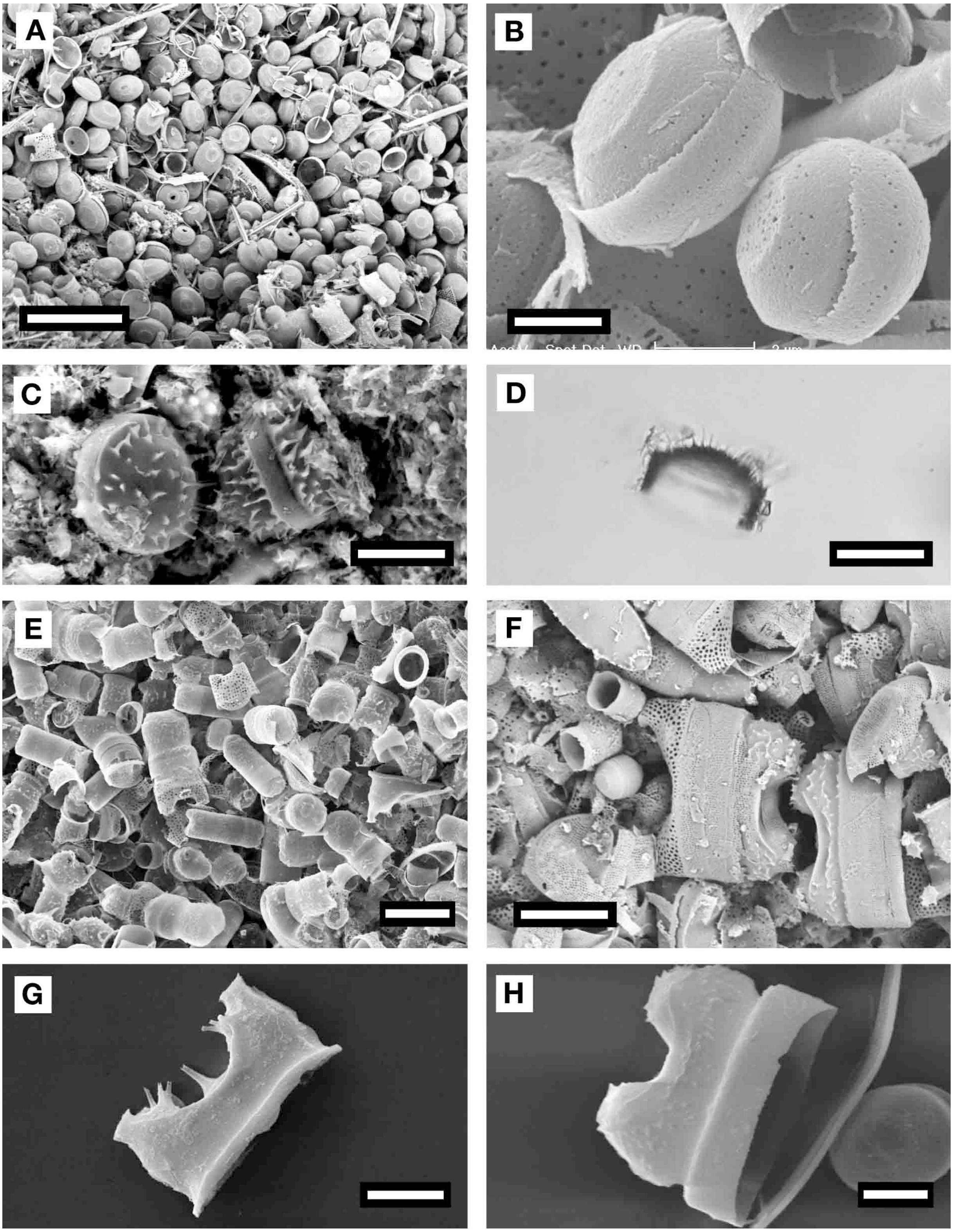

Figure 8

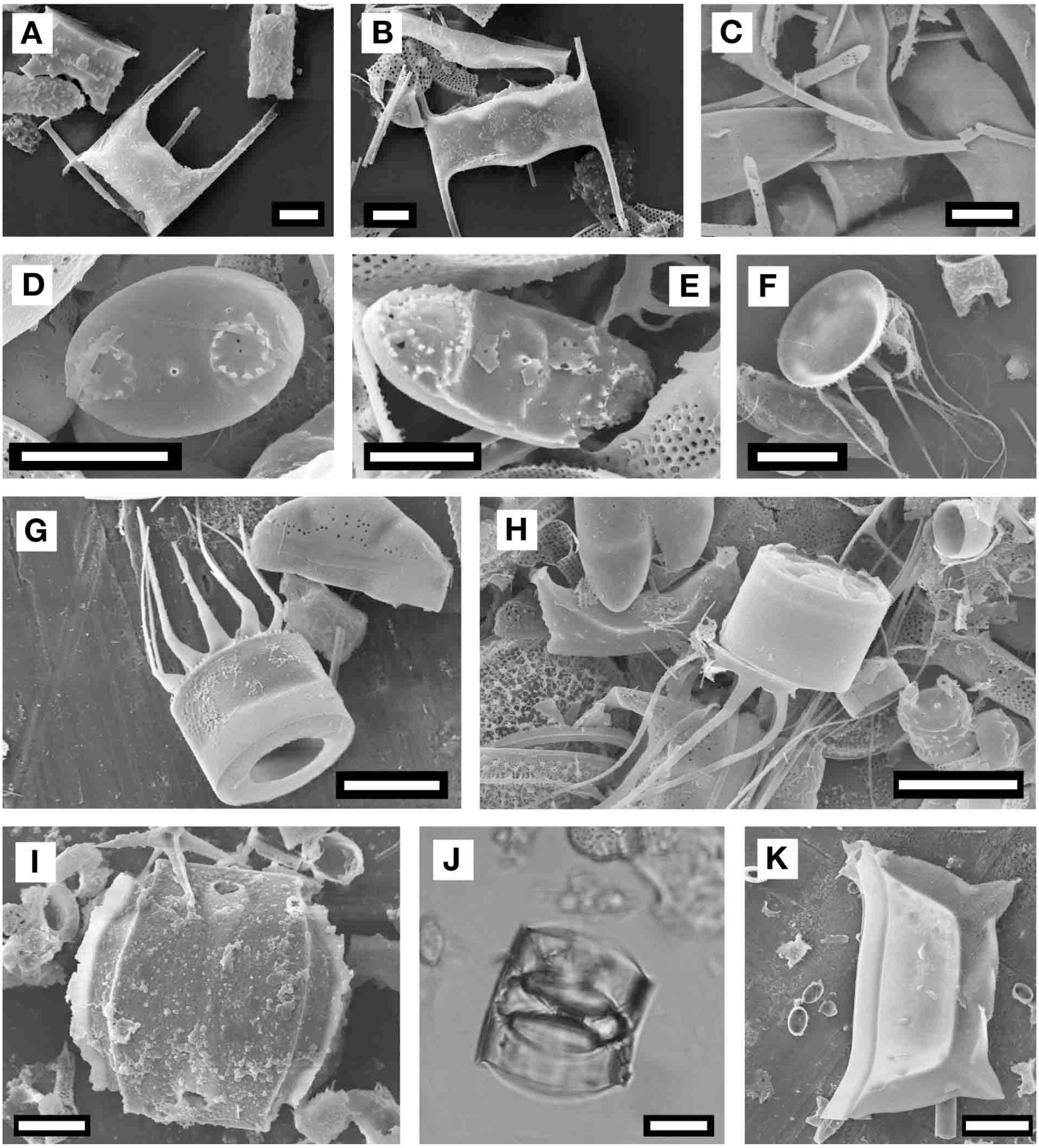

Figure 9

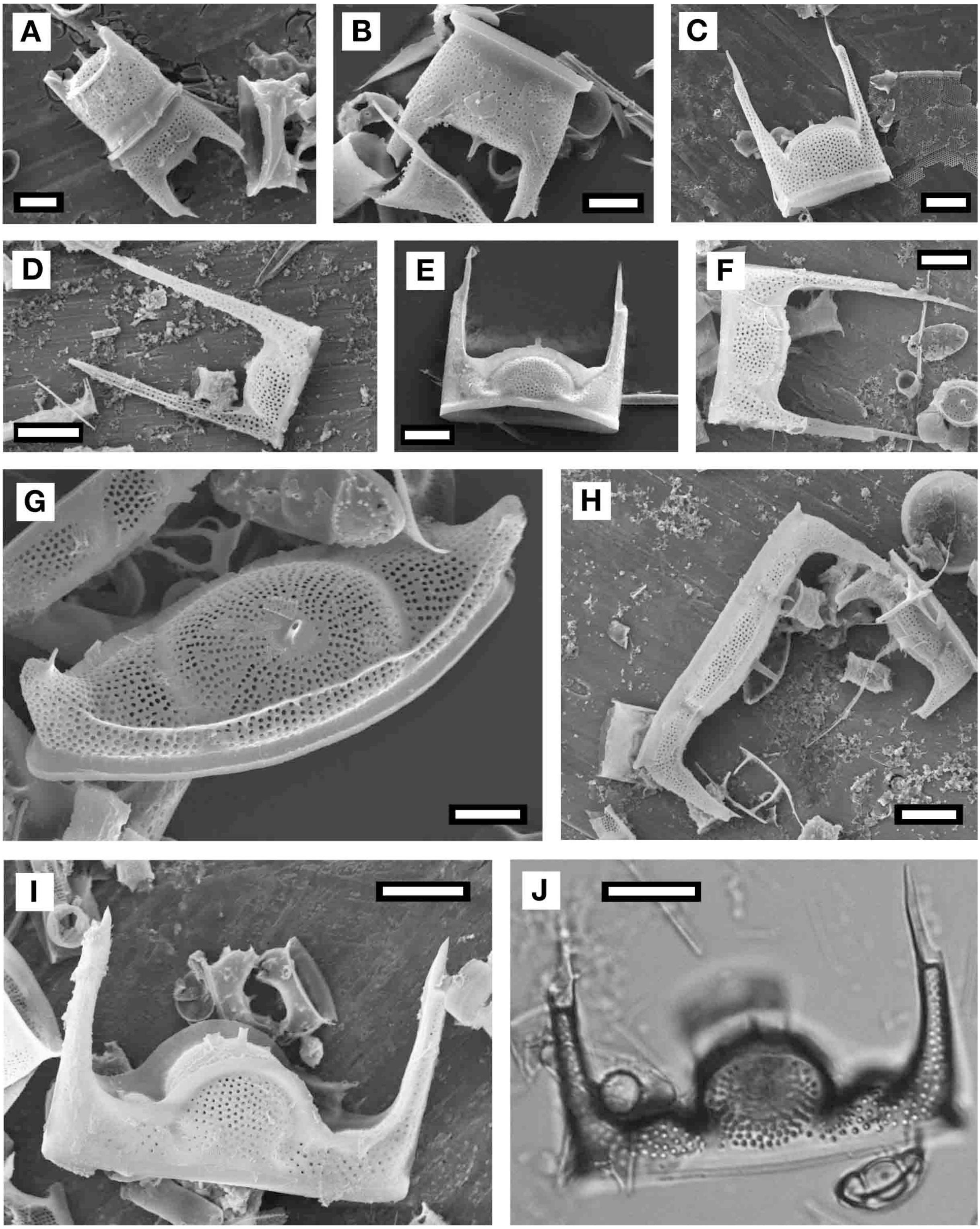

Figure 10

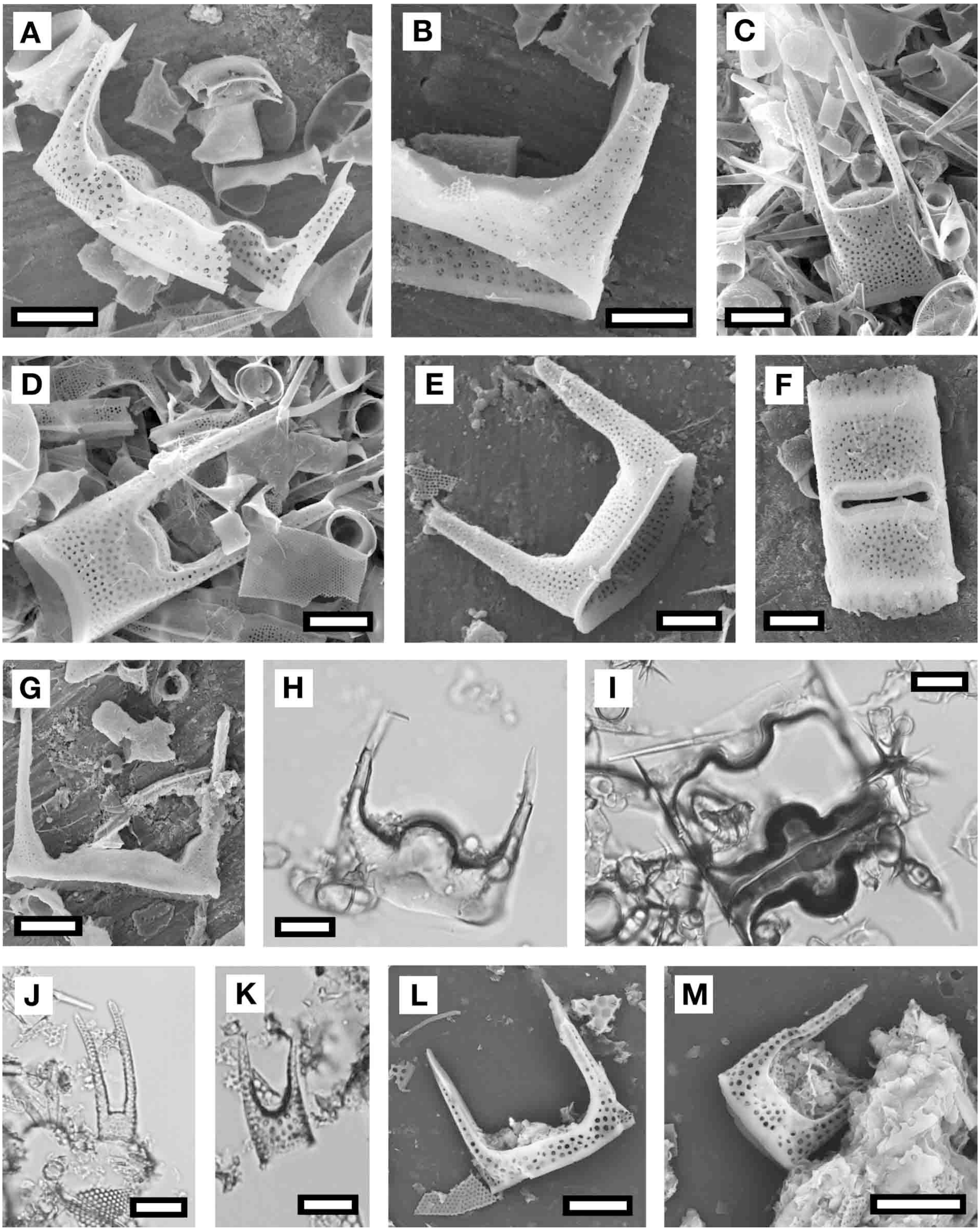

Figure 11

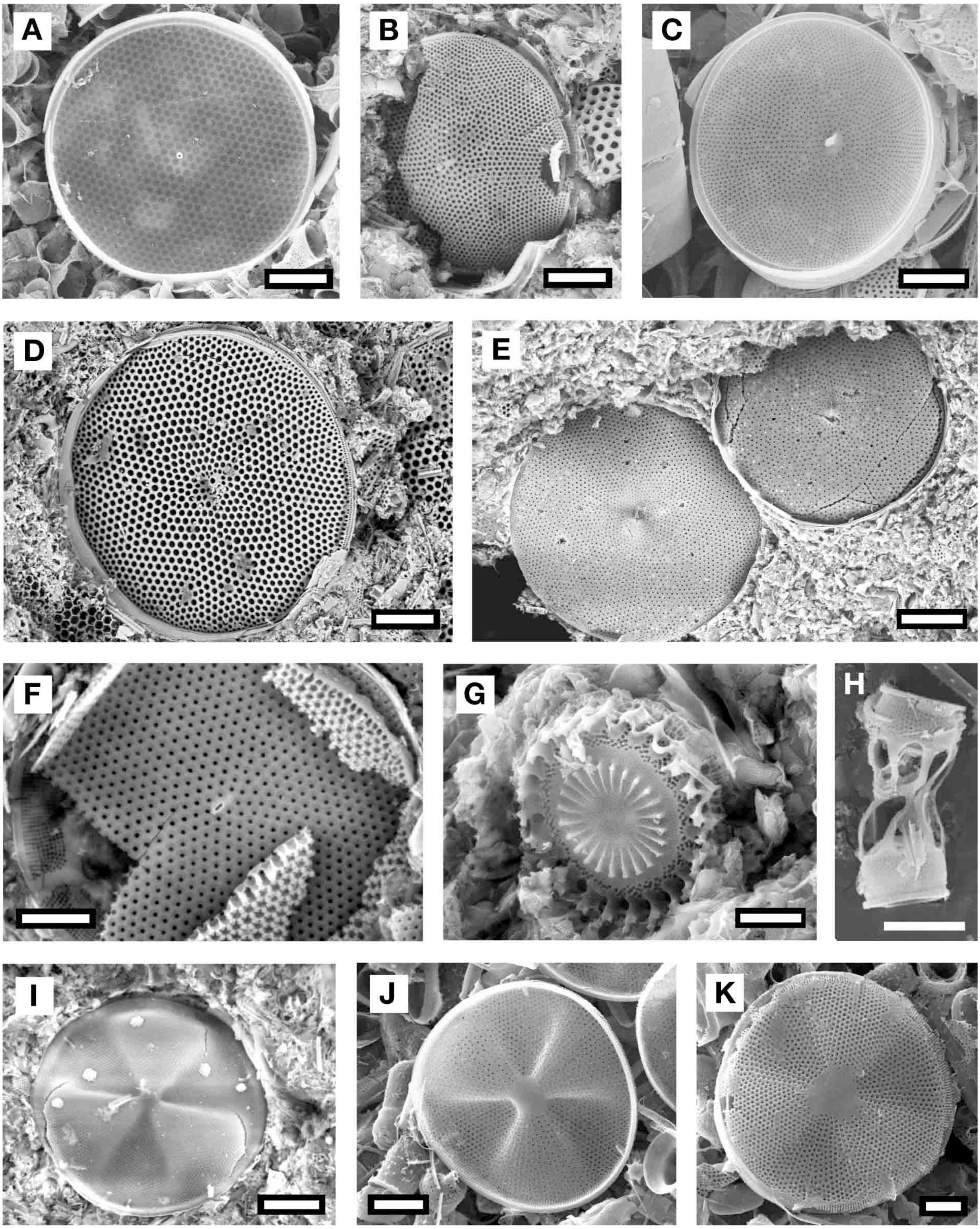

Figure 12

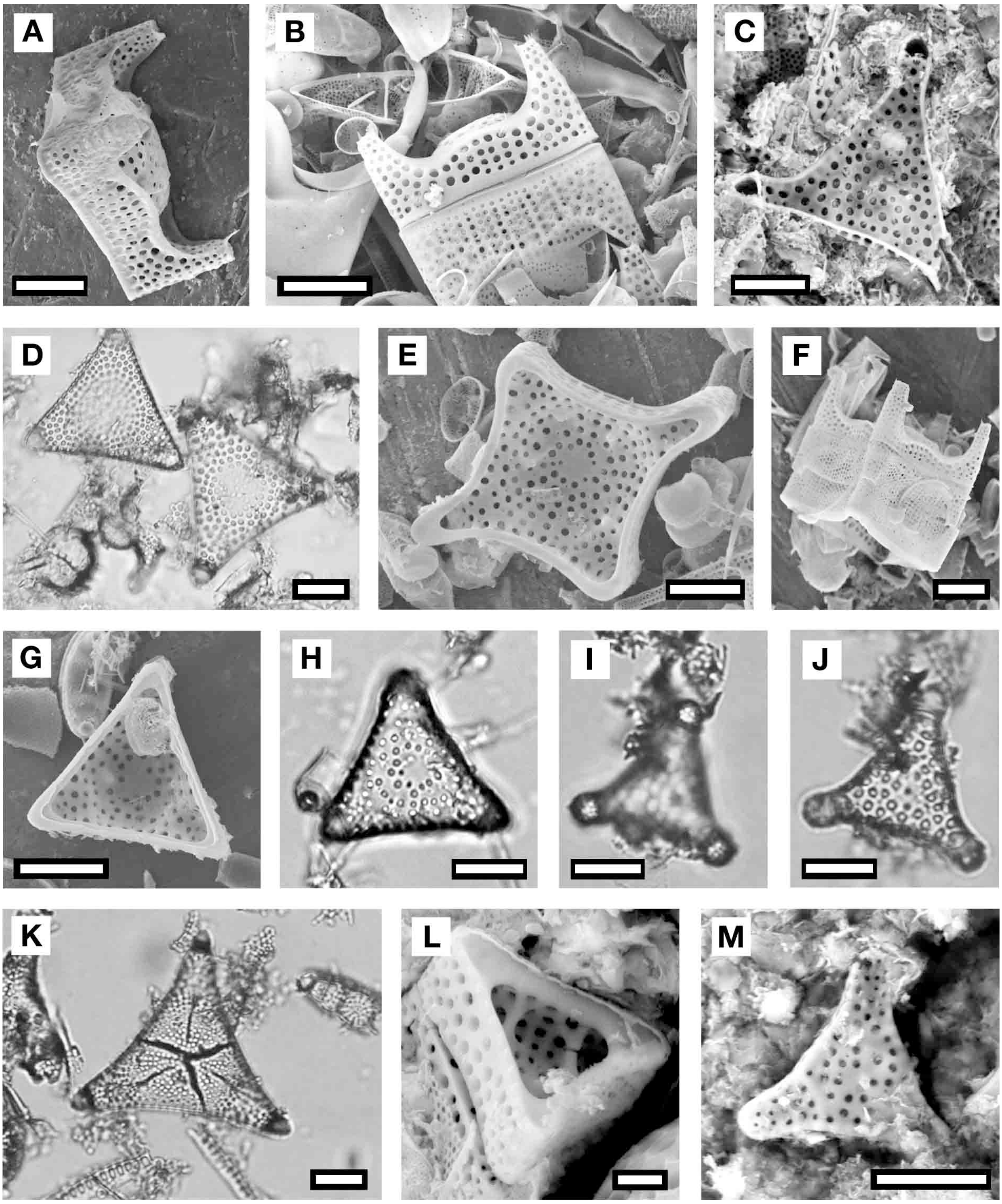

Figure 13

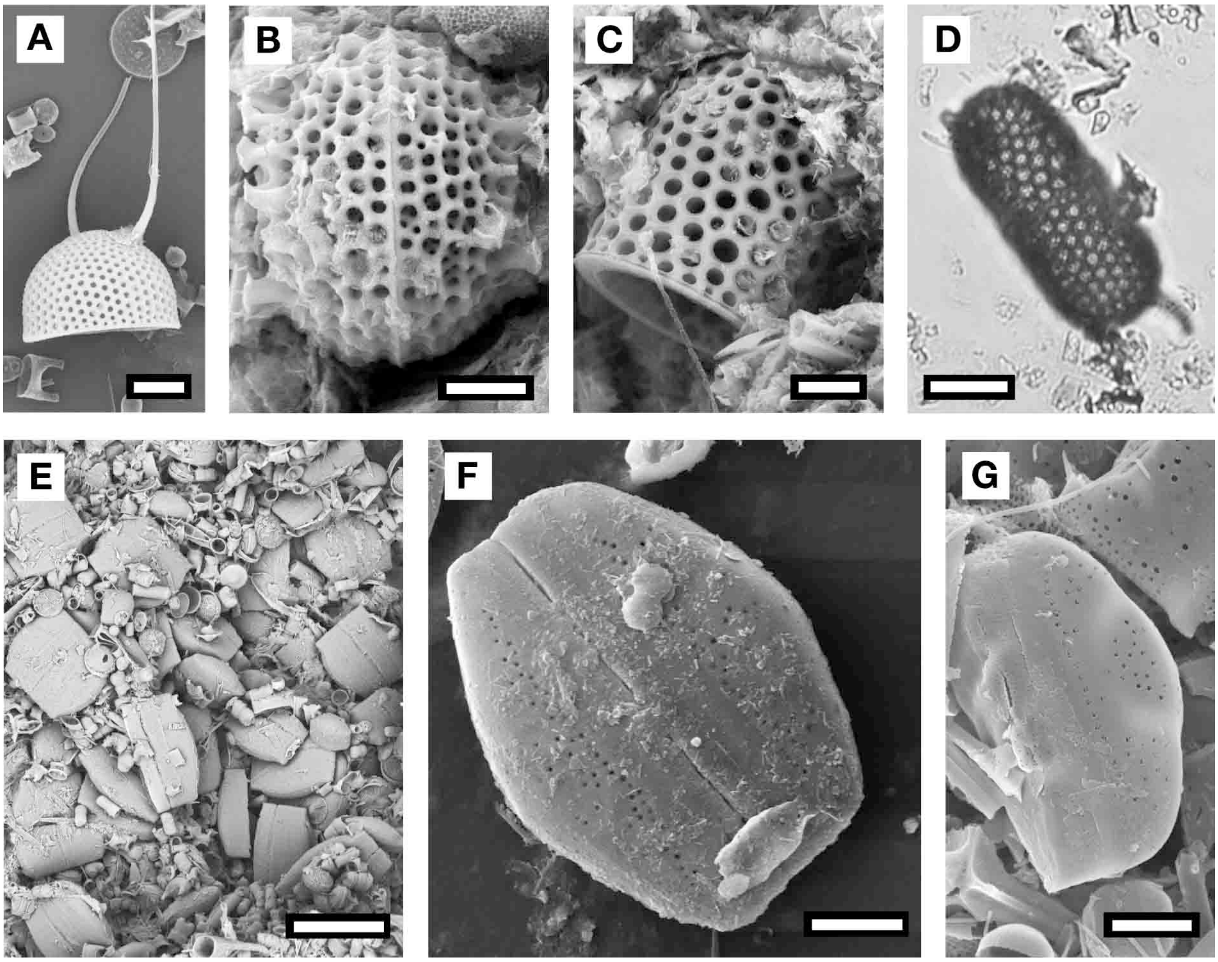

Figure 14

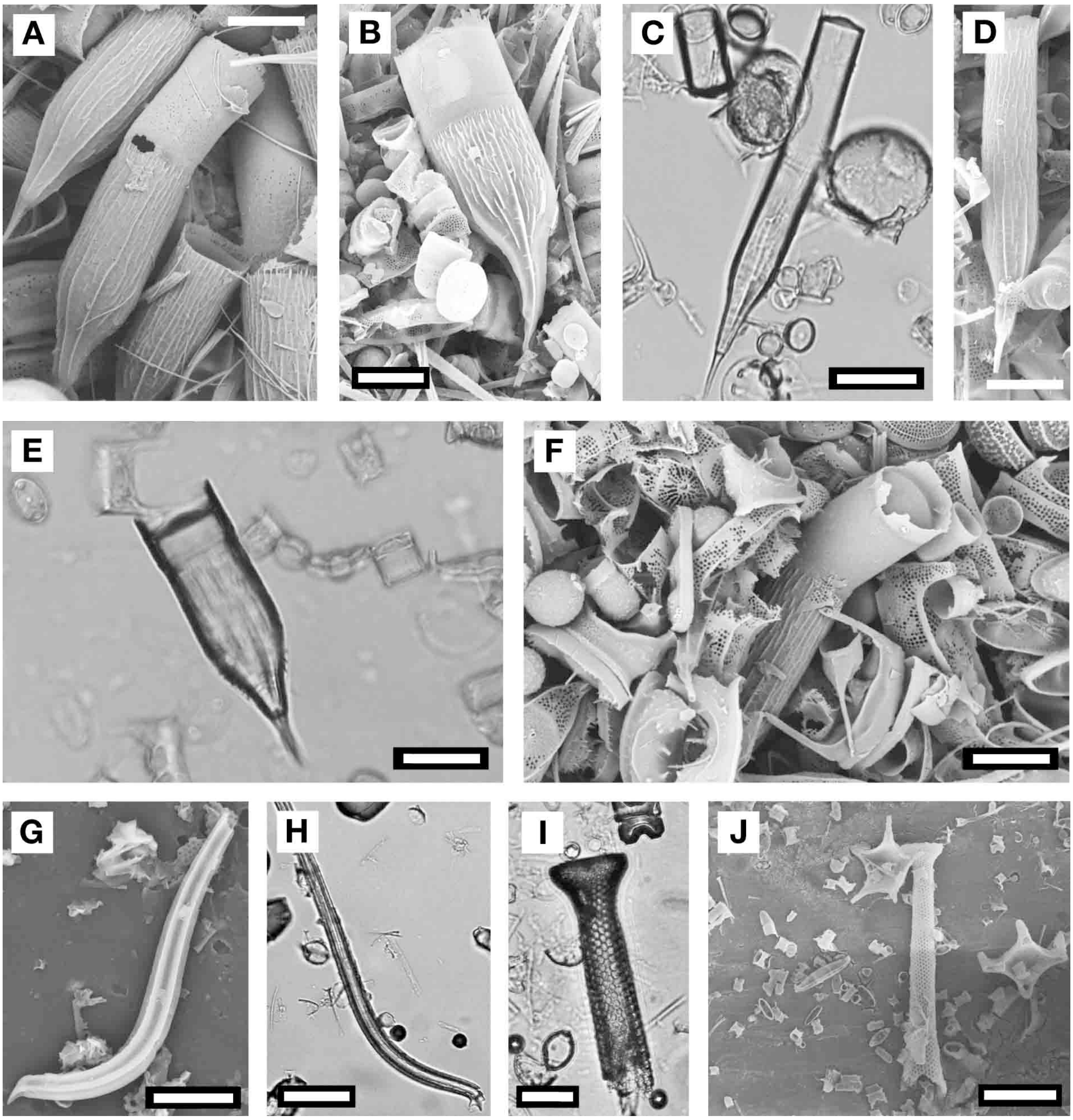

Figure 15

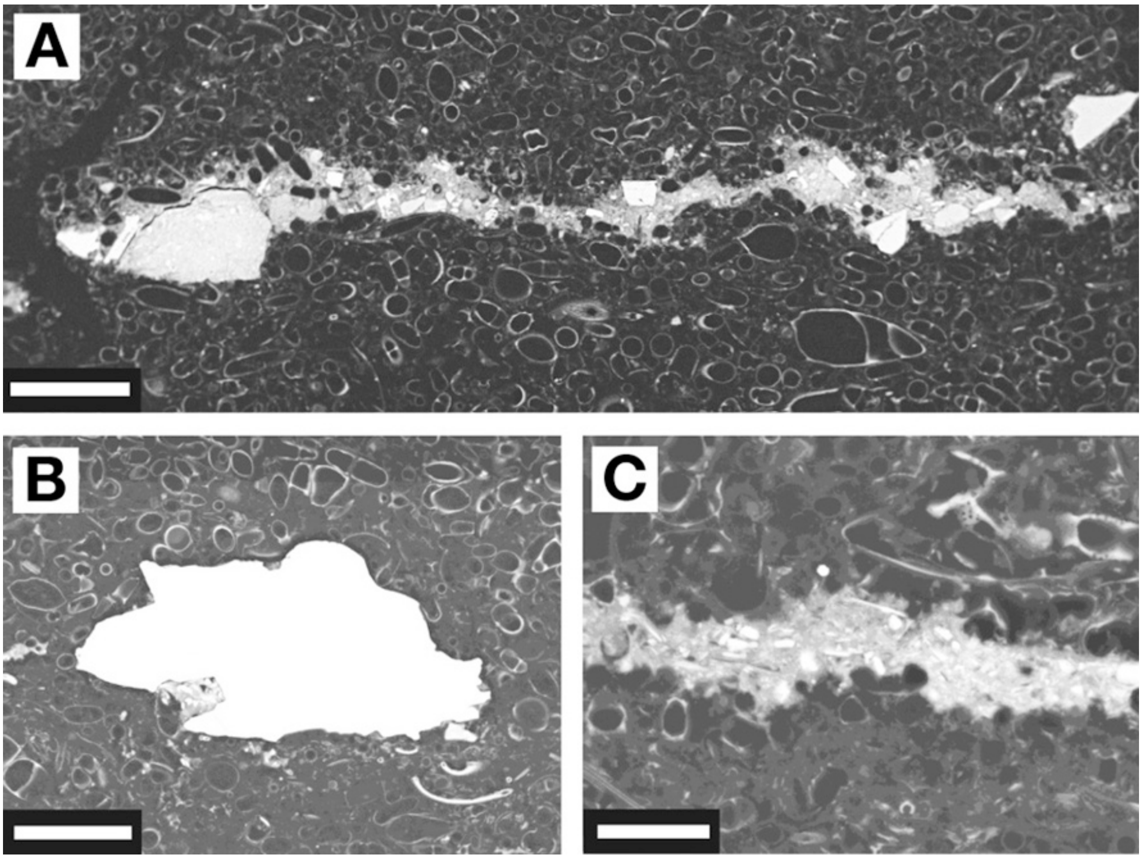

Figure 16

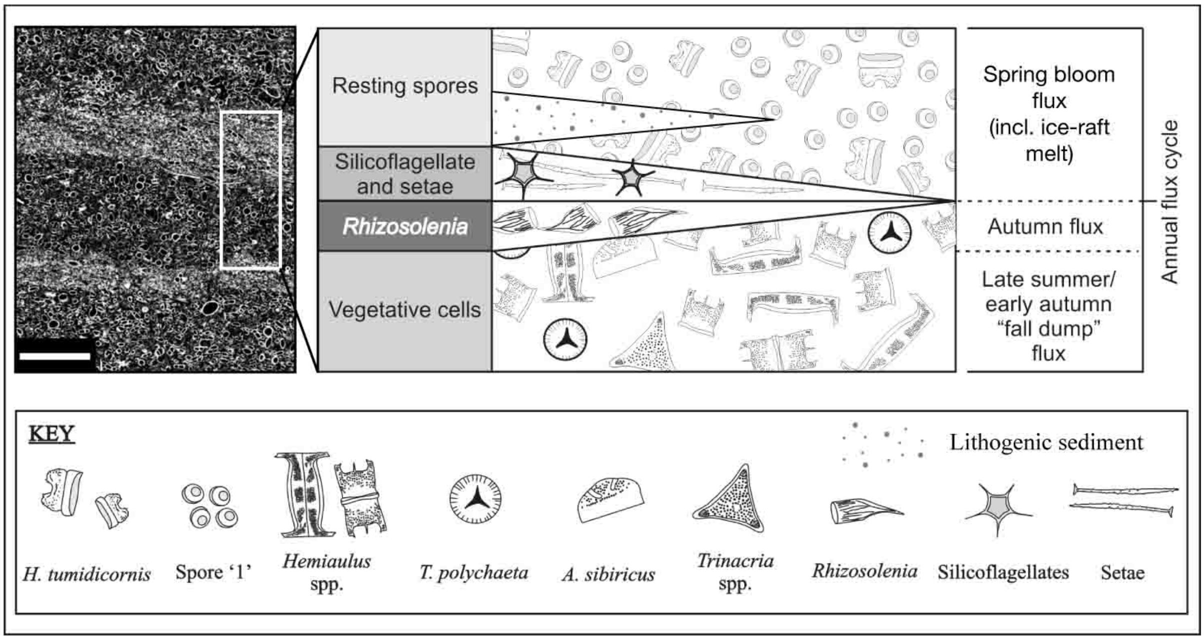

Figure 17

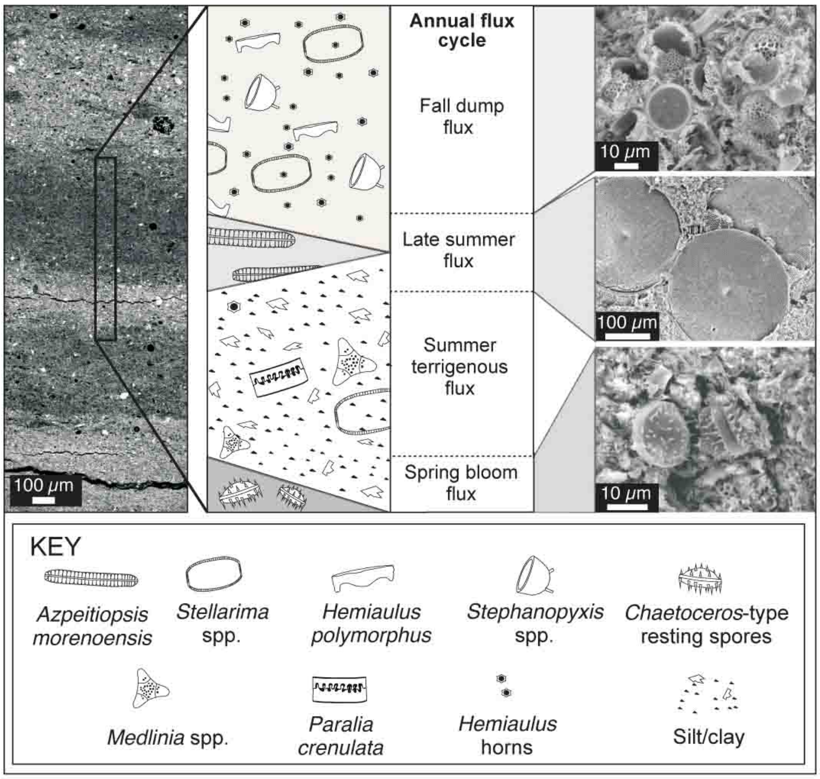
100 μm
Annual flux cycle
Fall dump flux
Late summer flux
Summer terrigenous flux
Spring bloom flux
10 μm
100 μm
10 μm
KEY
Azpeitiopsis morenoensis
Stellarima spp.
Hemiaulus polymorphus
Stephanopyxis spp.
Chaetoceros-type resting spores
Medlinia spp.
Paralia crenulata
Hemiaulus horns
Silt/clay

Figure 18

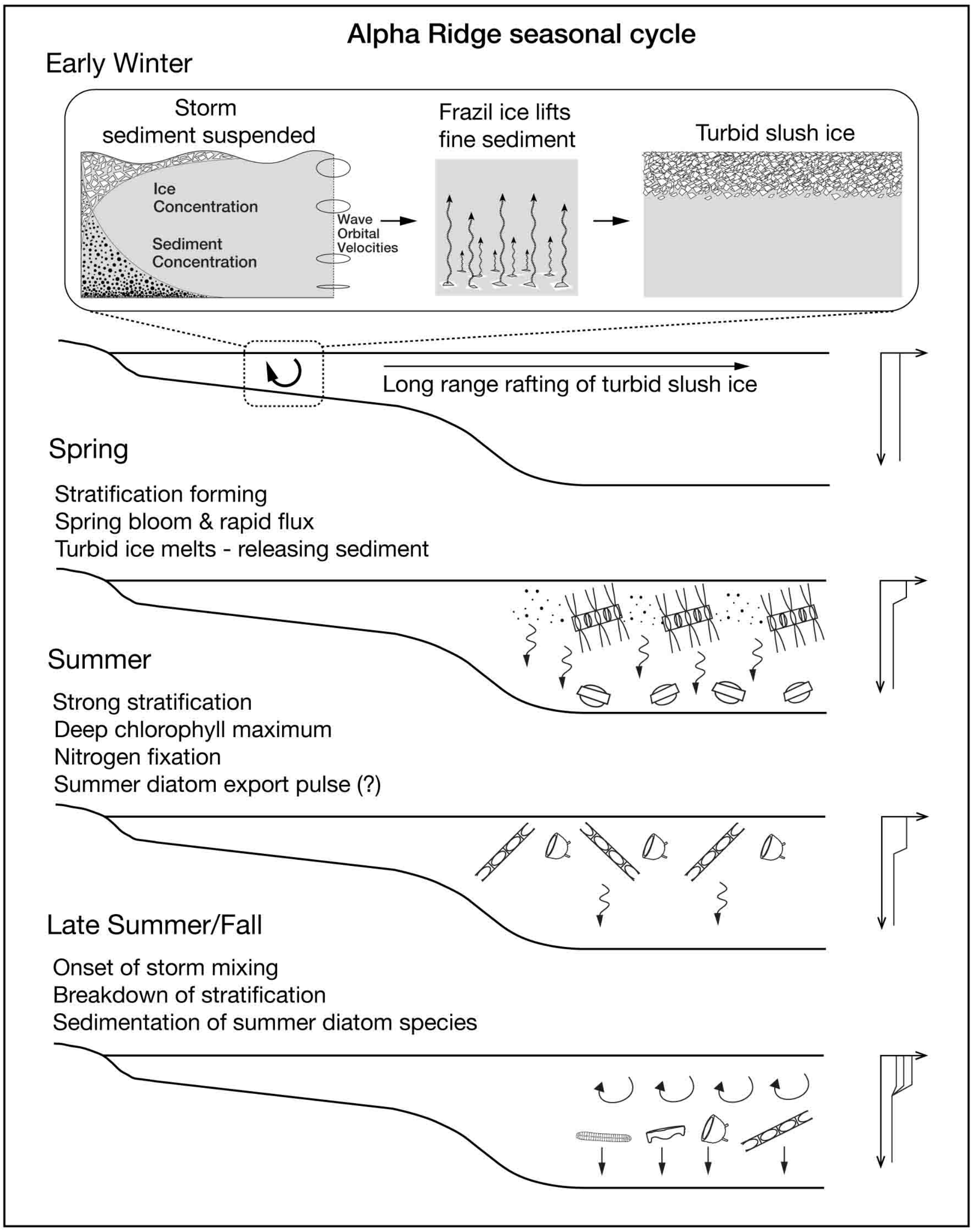
Alpha Ridge seasonal cycle
Early Winter
Storm
sediment suspended
Ice
Concentration
Sediment
Concentration
Wave
Orbital
Velocities
Frazil ice lifts
fine sediment
Turbid slush ice
Long range rafting of turbid slush ice
Spring
Stratification forming
Spring bloom & rapid flux
Turbid ice melts - releasing sediment
Summer
Strong stratification
Deep chlorophyll maximum
Nitrogen fixation
Summer diatom export pulse (?)
Late Summer/Fall
Onset of storm mixing
Breakdown of stratification
Sedimentation of summer diatom species

Figure 19

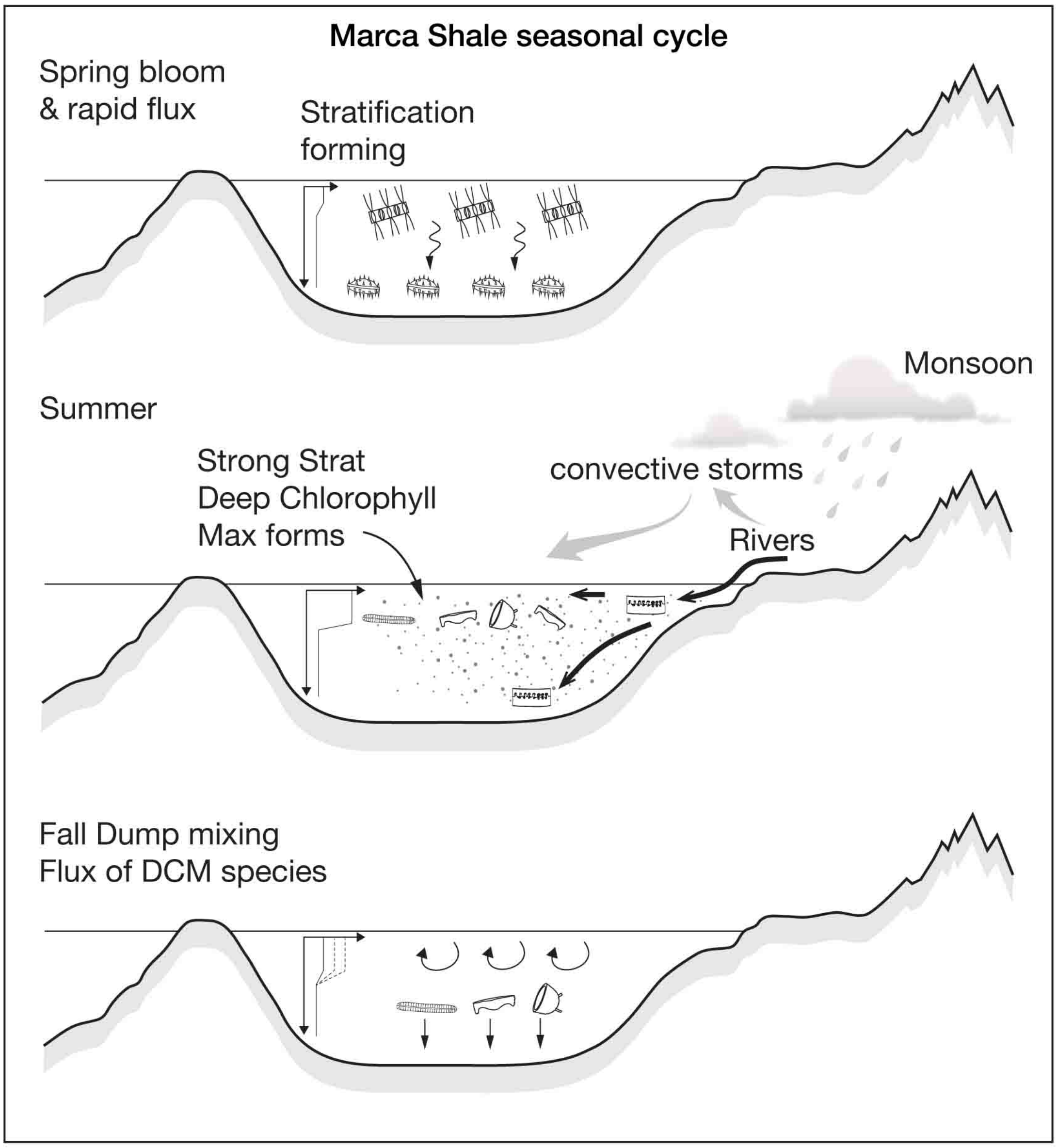
Marca Shale seasonal cycle
Spring bloom
& rapid flux
Stratification
forming
Monsoon
Summer
Strong Strat
Deep Chlorophyll
Max forms
convective storms
Rivers
Fall Dump mixing
Flux of DCM species

SUPPLEMENTARY MATERIAL

Late Cretaceous seasonal palaeoclimatology and diatom palaeoecology from laminated sediments.

Andrew Davies
*Alan E S Kemp

* To whom correspondence should be addressed. E-mail: aesk@noc.soton.ac.uk

Supplementary Figure 1.
Location photograph mosaic of the Dosados Canyon section of the Marca Shale. For overall scale and thickness of subdivisions, see Figure 3 in main paper. Note that the 10 m scale bar shown in the photomosaic applies to the foreground and see overall thicknesses in Figure 3 in the main paper. View is to NE from 36° 39.3' N 120° 42.1' W.

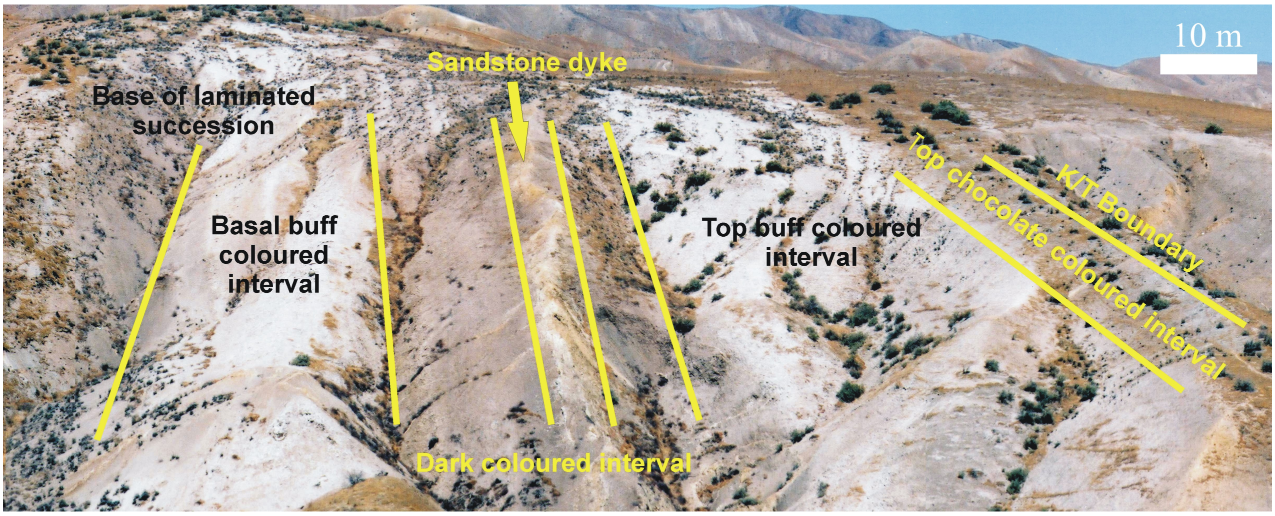

Supplementary Figure 2.

Sampling procedure details. Optical strew slides were prepared following an adapted version (Claire S. Allen, British Antarctic Survey, personal communication) of the method of Scherer (1994). Cartoon showing detail of the method of preparation of settled strew slides (for optical microscopy) and strew stubs (for SEM analysis).

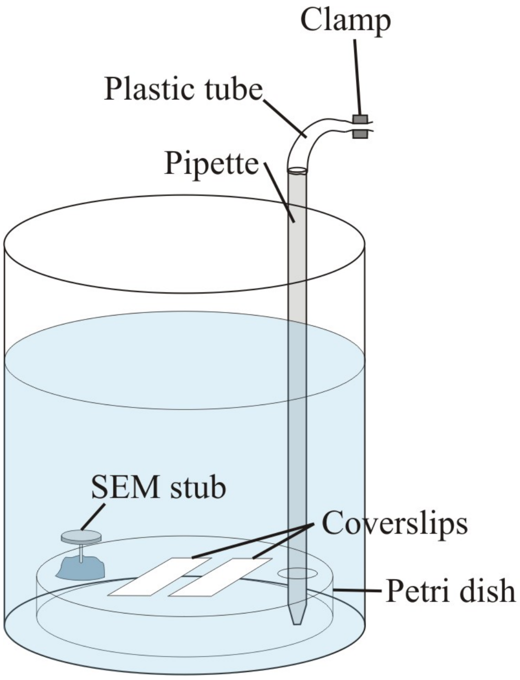

Supplementary Table 1

Sample numbers of material imaged in the Figures. The sample details correspond to the designation in the collection held at the Scanning Electron Microscope Facility of the National Oceanography Centre, Southampton. Note that the samples originally prepared as stubs from the CESAR 6 unconsolidated sediment are now disaggregated and so the interval, only, is designated.

Notes: PTS – polished thin section.

Figure Number	Sample interval	Sample designation
4 A	Marca Shale level – 35.5 m	PTS nodule-2
4 B	Marca Shale level – 35.5 m	PTS nodule-3
4 C	Marca Shale level – 35.5 m	PTS I-3
5 A	CESAR 6 core depth 258 cm	CESAR 6 core depth 258 cm
5 B	Marca Shale level – 68 m	Marca Stub 60
5 C	CESAR 6 core depth 208 cm	CESAR 6 core depth 208 cm
5 D	Marca Shale level – 35.5 m	Marca strew slide Nodule 2
5 E	Marca Shale level – 68 m	Marca Stub 60
5 F	CESAR 6 core depth 278 cm	CESAR 6 core depth 278 cm
6	CESAR 6 core depth 221 cm	CESAR 6 core depth 221 cm
7 A	CESAR 6 core depth 188 cm	CESAR 6 core depth 188 cm
7 B	CESAR 6 core depth 188 cm	CESAR 6 core depth 188 cm
7 C	Marca Shale level – 53 m	Marca Stub 30
7 D	Marca Shale level – 35.5 m	Marca strew slide Nodule 3
7 E	CESAR 6 core depth 248 cm	CESAR 6 core depth 248 cm
7 F	CESAR 6 core depth 248 cm	CESAR 6 core depth 248 cm
7 G	CESAR 6 core depth 188 cm	CESAR 6 core depth 188 cm
7 H	CESAR 6 core depth 288 cm	CESAR 6 core depth 288 cm
8 A	CESAR 6 core depth 188 cm	AR strew stub 6
8 B	CESAR 6 core depth 188 cm	AR strew stub 6
8 C	CESAR 6 core depth 188 cm	CESAR 6 core depth 188 cm
8 D	CESAR 6 core depth 188 cm	CESAR 6 core depth 188 cm
8 E	CESAR 6 core depth 208 cm	CESAR 6 core depth 208 cm
8 F	CESAR 6 core depth 305 cm	CESAR 6 core depth 305 cm
8 G	CESAR 6 core depth 258 cm	AR strew stub 13
8 H	CESAR 6 core depth 258 cm	CESAR 6 core depth 258 cm
8 I	CESAR 6 core depth 178 cm	AR strew stub 5
8 J	CESAR 6 core depth 305 cm	AR strew slide 18
8 K	CESAR 6 core depth 288 cm	AR strew stub 16
9 A	CESAR 6 core depth 288 cm	AR strew stub 16
9 B	CESAR 6 core depth 198 cm	AR strew stub 16
9 C	CESAR 6 core depth 188 cm	AR strew stub 6
9 D	CESAR 6 core depth 288 cm	AR strew stub 16
9 E	CESAR 6 core depth 188 cm	AR strew stub 6
9 F	CESAR 6 core depth 238 cm	AR strew stub 11
9 G	CESAR 6 core depth 208 cm	AR strew stub 8
9 H	CESAR 6 core depth 288 cm	AR strew stub 16
9 I	CESAR 6 core depth 188 cm	AR strew stub 6
9 J	CESAR 6 core depth 278 cm	AR strew slide 15
10 A	CESAR 6 core depth 278 cm	AR strew stub 15
10 B	CESAR 6 core depth 278 cm	AR strew stub 15
10 C	CESAR 6 core depth 278 cm	CESAR 6 core depth 278 cm

10 D	CESAR 6 core depth 278 cm	CESAR 6 core depth 278 cm
10 E	CESAR 6 core depth 278 cm	AR strew stub 15
10 F	CESAR 6 core depth 278 cm	AR strew stub 15
10 G	CESAR 6 core depth 268 cm	AR strew stub 14
10 H	CESAR 6 core depth 228 cm	AR strew stub 10
10 I	CESAR 6 core depth 228 cm	AR strew stub 10
10 J	Marca Shale level – 61 m	Marca strew slide Nodule 2
10 K	Marca Shale level – 61 m	Marca strew slide Nodule 2
10 L	Marca Shale level – 61 m	Marca strew stub B12
10 M	Marca Shale level – 61 m	Marca strew stub B12
11 A	CESAR 6 core depth 278 cm	CESAR 6 core depth 278 cm
11 B	Marca Shale level – 62 m	Marca Stub 71
11 C	CESAR 6 core depth 278 cm	CESAR 6 core depth 278 cm
11 D	Marca Shale level – 60 m	Marca Stub 23
11 E	Marca Shale level – 62 m	Marca Stub 72
11 F	Marca Shale level – 60 m	Marca Stub 15
11 G	Marca Shale level – 68 m	Marca Stub 59
11 H	CESAR 6 core depth 298 cm	AR strew stub 17
11 I	Marca Shale level – 53 m	Marca Stub 39
11 J	CESAR 6 core depth 278 cm	CESAR 6 core depth 278 cm
11 K	CESAR 6 core depth 278 cm	CESAR 6 core depth 278 cm
12 A	CESAR 6 core depth 134 cm	AR strew stub 19
12 B	CESAR 6 core depth 278 cm	CESAR 6 core depth 278 cm
12 C	Marca Shale level – 19 m	Marca Stub 36
12 D	Marca Shale level – 35.5 m	Marca strew slide Nodule 3
12 E	CESAR 6 core depth 178 cm	AR strew stub 5
12 F	CESAR 6 core depth 178 cm	AR strew stub 5
12 G	CESAR 6 core depth 305 cm	AR strew stub 18
12 H	CESAR 6 core depth 305 cm	AR strew slide 18
12 I	Marca Shale level – 35.5 m	Marca strew slide Nodule 3
12 J	Marca Shale level – 35.5 m	Marca strew slide Nodule 3
12 K	Marca Shale level – 35.5 m	Marca strew slide Nodule 2
12 L	Marca Shale level – 61 m	Marca Stub 34
12 M	Marca Shale level – 61 m	Marca Stub 7
13 A	CESAR 6 core depth 188 cm	AR strew stub 6
13 B	Marca Shale level – 68 m	Marca Stub 59
13 C	Marca Shale level – 68 m	Marca Stub 60
13 D	Marca Shale level – 60 m	Marca strew slide B1
13 E	CESAR 6 core depth 278 cm	CESAR 6 core depth 278 cm
13 F	CESAR 6 core depth 188 cm	AR strew stub 6
13 G	CESAR 6 core depth 278 cm	CESAR 6 core depth 278 cm
14 A	CESAR 6 core depth 268 cm	CESAR 6 core depth 268 cm
14 B	CESAR 6 core depth 198 cm	CESAR 6 core depth 198 cm
14 C	CESAR 6 core depth 268 cm	AR strew slide 14
14 D	CESAR 6 core depth 268 cm	CESAR 6 core depth 268 cm
14 E	CESAR 6 core depth 278 cm	AR strew slide 15
14 F	CESAR 6 core depth 278 cm	CESAR 6 core depth 278 cm
14 G	Marca Shale level – 61 m	Marca strew slide Nodule 2
14 H	CESAR 6 core depth 305 cm	AR strew slide 18
14 I	CESAR 6 core depth 305 cm	AR strew slide 18
14 J	CESAR 6 core depth 178 cm	AR peel slide 178 cm

15 A	CESAR 6 core depth 215.7 cm	AR PTS K-3
15 B	CESAR 6 core depth 215.7 cm	AR PTS K-3
15 C	CESAR 6 core depth 215.7 cm	AR PTS K-3

Supplementary Table 2

CESAR-6 diatom strew slide counts inclusive of *Chaetoceros*-type spores and chrysophytes.

sample	CESAR-6 depth in core cm	Chrysophytes	*Chaetoceros*-type spores	Other valves	Total
19	134-135	71	26	409	506
1	137.5-138.5	53	73	350	476
2	147.5-148.5	30	96	378	504
3	157.5-158.5	86	20	336	442
4	167.5-168.5	33	39	343	415
5	177.5-178.5	72	51	362	485
6	187.5-188.5	56	54	236	346
7	197.5-198.5	4	102	290	396
8	207.5-208.5	62	84	213	359
9	217.5-218.5	34	74	216	324
10	227.5-228.5	38	81	278	397
11	237.5-238.5	19	128	228	375
12	247.5-248.5	42	100	198	340
13	257.5-258.5	45	82	224	351
14	267.5-268.5	65	52	360	477
15	277.5-278.5	61	61	210	332
16	287.5-288.5	54	42	475	571
17	297.5-298.5	143	8	200	351
18	304-305	106	10	201	317

Supplementary Table 3

CESAR-6 diatom strew slide counts exclusive of Chaetoceros-type spores and chrysophytes. See Table S2 for sample depth in core. Informal species names are those of this study unless indicated in superscript reference to the footnotes. Note that the nomenclature has been updated from the previously published version of this table as Supplementary Information to Davies et al. (2009).

	Sample number																		
	19	**1**	**2**	**3**	**4**	**5**	**6**	**7**	**8**	**9**	**10**	**11**	**12**	**13**	**14**	**15**	**16**	**17**	**18**
Anaulus sibiricus	171	85	43	100	51	98	27	34	50	27	50	33	37	53	73	49	81	227	201
Trochosira polychaeta	23	46	42	21	8	27	26	30	35	31	51	32	54	45	37	44	27	4	2
Hemiaulus tumidicornis	117	88	125	250	276	261	131	137	120	160	96	170	133	131	218	183	284	26	41
H. cf. antiquus	20	27	16	38	6	23	24	31	25	29	21	5	18	22	21	6	15		2
H. danicus	5	4	2	4	1	1	3	1	4	6	2	4	3		3		3	7	1
H. cf. gleseri	36	34	17	35	17	44	22	25	25	22	37	19	5	15	17	16	11	17	26
H. cf. elegans	2	4				1	1		2	4	1	3		2			3	1	1
H. oonki	1			1	1	2						1	1			1		14	2
H. sp. Barron[1]	3	8	10	17	5	5	2	22	7	14	3	17	13	13	15	15	9		1
H. G[2]				1															
H. kittoni				1			1												
other *Hemiaulus* spp	1	1				1				1	4					2		1	3
H. hostilis		1		2		1				1						1			
H. giganteus										1							1		
H. rossicus	2					1				1				1	1			5	
H. cf. includens																		2	
H. sp. 1	52	43	55	61	32	47	52	76	49	71	139	67	132	82	103	111	64	9	9
H. sp. 2	2			8		1				2							1		
H. sp. 3											1								1
H. sp. 4															1				
H. sp. 5																1	2	1	
H. sp. 6	1			1															
H. sp. 7					1														
Spore 3	17	4	28	15	8	11	17	15	5	11	14	31	28	16	24	28	29	3	1
Coscinodiscus circumspectus		2	1			1			1								1		
Acanthosphaeridium reticulatum	2	4	1	3	3	2	5	1	2	8	4	12	6	23	2	10	7	40	8
Actinoptychus spp.	2	1	1	1			1	1				1	2		1	1		3	6
Skeletonemopsis crawfordii	1			1		1		1			1	1		1				21	5
Rhizosolenia (thick)	1	8	1	6	4	7	1	4	3	2	2	1	1	3		1	1	7	6
Rhizosolenia (thin)	9	13	3	4	3	4	8	10	8	3	9	3	2	7	8	1	2	11	11
Ceratulina cretacea		7		1		1			1	2		3	1		2	1	3	1	
Pseudopyxilla	15	6	7	20	8	10	3	7	10	10	12	10	7	8	10	7	8	9	3
Skeletonema subantarctica	9	3	2	6	5	3	5	3	6	14	10	12	5	6	5	7	8	7	4
Stephanopyxis spp.								1					2		2				
Trinacria tessela	1					3	1												
Cf. Triceratium indefinitum	1	1						1	1									1	
Pennate spp.			1	2		6	4		7	8	1		2	1	3	2	9	1	2
Gladiopsis spp.	1	1	1					1											1

Trinacria acutangulum		2				3		2	1				1		1	1		1	
Pterotheca spp.					2						1		1	1		2			
Pseudopyxilla sp. Strelnikova[3]																		26	53
Stellarima spp.				1	2							1							
Proboscia cretacea		2	3		1	1	5	1	4	6	6	1	2	14	8	4	1	1	3
Goniothecium odontellum				2											2				
Thalassiosiropsis wittiana																			1
Coscinodiscus sibiricus																			1
Anaulus sp. 1				15															
totals	495	395	359	617	434	566	339	404	366	434	465	427	456	444	557	494	570	446	395

[1] Barron (1985) pl. 10.2 fig. 9
[2] Harwood (1988) fig. 14.6
[3] Strelnikova (1974) pl. 54, fig. 16
[4] Strelnikova (1974) pl. 57, fig. 33-34

Supplementary Figure 3.

Graphic showing the range of the main diatom taxa from the CESAR 6 core diatomaceous ooze (Unit 4). (See Fig. 3B in the main paper for the full stratigraphy).

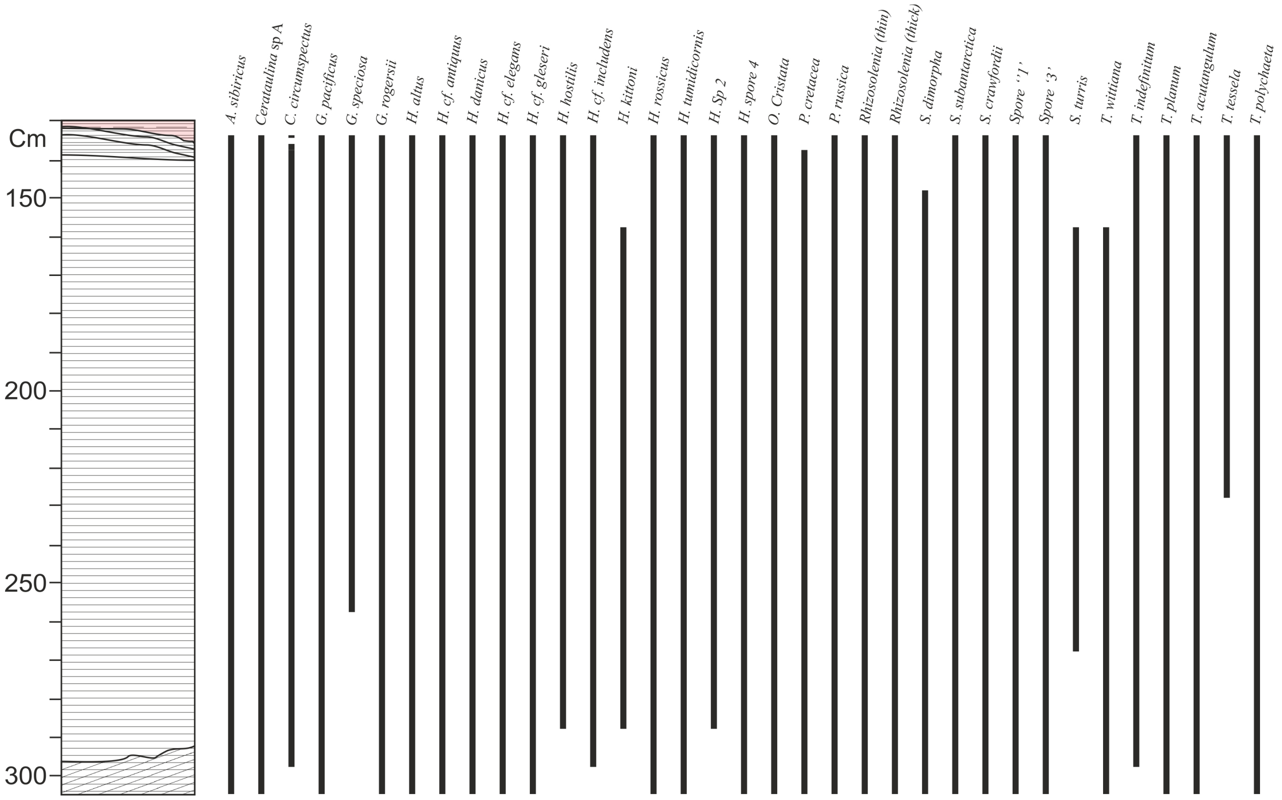

References for Supplementary Material

Barron, J.A., 1985. Diatom Biostratigraphy of the CESAR 6 Core, Alpha Ridge. In H.R. Jackson, P.J. Mudie, S.M. Blasco (Eds.), Initial Geological Report on CESAR-the Canadian Expedition to Study the Alpha Ridge Geological Survey of Canada, Paper 84-22, Report 10. pp. 137-148.

Davies, A., Kemp, A.E.S., Pike, J., 2009. Late Cretaceous seasonal ocean variability from the Arctic. Nature, 460 254-258.

Harwood, D.M., 1988. Upper Cretaceous and lower Paleocene diatom and silicoflagellate biostratigraphy of Seymour Island, eastern Antarctic Peninsula. In M.R. Feldmann, M.E. Woodburne (Eds.), Geology and Paleontology of Seymour Island, Antarctic Peninsula., 169 Geological Society of America Memoir. Boulder. pp. 55-129.

Scherer, R.P., 1994. A new method for the determination of absolute abundance of diatoms and other silt-sized sedimentary particles. Journal of Paleolimnology, 12 171-179.

Strelnikova, N.I., 1974. Late Cretaceous diatoms of western Siberia: Academie Nauk, SSSR, Roy. 8. 202 pp. (In Russian).